Mechanics of Fluid-Saturated Rocks

Yves Guéguen

Ecole Normale Supérieure

and

Maurice Boutéca

Institut Français du Pétrole

Amsterdam Boston Heidelberg London NewYork Oxford Paris
San Diego San Francisco Singapore Sydney Tokyo

Senior Publishing Editor	Frank Cynar
Editorial Coordinator	Jennifer Helé
Project Manager	Troy Lilly
Marketing Manager	Linda Beattie
Marketing Assistant	Clare Fleming
Cover Design	Eric DeCicco
Full-Service Provider	Graphic World Publishing Services
Composition	Integra Software Services Pvt. Ltd.
Interior Printer	The Maple-Vail Book Manufacturing Group
Cover Printer	Phoenix Color Corp.

Elsevier Academic Press
200 Wheeler Road, Burlington, MA 01803, USA
525 B Street, Suite 1900, San Diego, California 92101-4495, USA
84 Theobald's Road, London WC1X 8RR, UK

This book is printed on acid-free paper. ♾

Library of Congress Cataloging-in-Publication Data
Mechanics of fluid saturated rocks / edited by Yves Gueguen and Maurice Bouteca.
p. cm. — (International geophysics series ; v. 89)
Includes bibliographical references and index.
ISBN 0-12-305355-2 (hardcover : alk. paper)
1. Water–rock interaction. 2. Rock mechanics. I. Gueguen, Yves. II. Bouteca, Maurice.
III. Series.

QE431.6.W38M43 1997
552'.06—dc22
2003061665

British Library Cataloguing in Publication Data
A catalogue record for this book is available from the British Library

ISBN: 0-12-305355-2

For all information on all Academic Press publications
visit our website at www.academicpressbooks.com

Printed in the United States of America
04 05 06 07 08 09 9 8 7 6 5 4 3 2 1

Chapter 5 ▶

Localization: Shear Bands and Compaction Bands

Pierre Bésuelle[1]
John W. Rudnicki[2]

5.1 Introduction

Localized deformation is a ubiquitous phenomenon in geomaterials. It occurs over a vast range of size scales, from the microscale level of grains to faults extending over hundreds of kilometers. It occurs in a variety of forms: a concentration or coalescence of cracks, a distinct, planar frictional surface, a gouge zone of finely comminuted material, or simply a region of higher shear strain. In geomaterials, the severe shearing in regions of localized deformation may be accompanied by dilatancy (inelastic volume increase) or compaction (inelastic volume decrease) and by chemical alteration. Localization can even occur purely by compaction without any evident shear. If the material is fluid saturated, as is frequently the case, inelastic volume changes can induce flow of fluid or changes in pore pressure that affect the response. Localization occurs under a variety of conditions. Although most often associated with the formation of shear bands or faults under nominally brittle conditions, localization can also occur by cataclastic flow of rocks at higher mean stresses and by ductile shearing at temperatures and pressures typical of depths of 10 km to 15 km in the Earth's crust.

Sometimes, the occurrence of localization essentially coincides with failure. For example, in the axisymmetric loading of rock specimens, more or less homogeneous deformation is terminated by the sudden appearance of a sharp fault in the sample, rapid loss of strength, and depending on the loading conditions and the

[1]Laboratoire 3S, BP 53, 38041 Grenoble Cedex 09, France. pierre.besuelle@hmg.inpg.fr

[2]Department of Civil and Environmental Engineering and Department of Mechanical Engineering, Northwestern University, 2145 Sheridan Road, Evanston, Illinois 60201, U.S.A. jwrudn@nwu.edu

stiffness of the testing machine, a dynamic or inertial failure. In other instances, incipient localization may be only the first step in a continuing process of slip or deformation that is punctuated by incidents of rapid failure followed by lengthy periods of restrengthening and slow slip or deformation. This is certainly the case for mature fault systems that have undergone large relative displacements over geological time. Incipient localization may have occurred hundreds of thousands of years in the past and been associated with the kinematics of large-scale plate tectonic motion. Even in these cases, however, localization may be significant in the subsequent evolution of the fault system. For example, localization may be important in the reccurrence of failure in regions that have undergone restrengthening over time or in controlling the evolution of the internal structure of the fault zone. In other regions, possibly at the base of fault zones, where temperature and pressure are higher, an alternating sequence of localized and distributed deformation could influence the response at shallower depths.

Obviously, the phenomenon of localization in geological materials is both rich and complex. Its consequences can be important. Seismic activity on large faults is a threat to human life and is of concern for the siting of structures. Shear zones and fractures of a more modest scale can cause problems for foundations and underground structures of all types. Formation of a localized slip surface is often a predecessor to slope failure. More generally, however, localized deformation features control not only mechanical behavior but also transport behavior of the crust. The internal structure of fault zones often inhibits flow of fluids across the fault but facilitates flow parallel to the fault. For example, faults often form impermeable barriers that trap hydrocarbons or bound aquifers. The presence of localized zones of deformation may control hydrocarbon accumulation or disrupt efforts to withdraw or inject fluids into the subsurface. On the other hand, fluids flowing along faults acting as high-permeability channels can propagate much farther and more rapidly than predicted by assuming a homogeneous formation.

Despite the importance of localization and much study of the problem, there exists no detailed understanding of how the occurrence of localization and its subsequent evolution are related to the stress state, deformation history, material properties, and the coupling of deformation with transport of fluid and heat and with chemical alteration. Nevertheless, advances in experimental techniques and computational power, along with different theoretical approaches, have illuminated some aspects of the localization phenomenon. This chapter attempts to review recent observations and discuss the results of theoretical and numerical studies.

5.2 Approaches to Failure

Because of the importance and complexity of localization, there have been a variety of approaches to describing the phenomenon. In this chapter, we will discuss in detail an approach that attempts to describe the onset of localized deformation as

a bifurcation, or nonuniqueness, from homogeneous deformation. Preparatory to doing so, we discuss briefly some other approaches to failure in order to compare and contrast these with the bifurcation approach.

The Mohr-Coulomb criterion is simple, practical, and widely used to predict the failure of rocks and soils in both the field and laboratory. This is one of a class of approaches that attempts to describe failure in terms of the stress state. In particular, failure (in some not precisely defined sense) is assumed to occur when the magnitude of the shear stress on a plane τ_{ns} is equal to a cohesive value τ_0 plus a friction coefficient μ times the compressive normal stress on that plane σ_n (e.g., Jaeger and Cook, 1969; Paterson, 1978; Scholz, 1990). If the friction coefficient is constant, then the plane on which this condition is first met is given by a simple graphical construction. This criterion provides a very good first-order description of the plane on which failure occurs and of the orientations of faults in different tectonic regimes.

In the Mohr-Coulomb criterion, the dependence of failure on material properties is minimal and includes only the cohesion and the friction coefficient, parameters that are associated with the failure surface, not the material before the formation of the surface. This simplicity is advantageous in many geological applications in which material properties are not well known, but it is likely to be an oversimplification. Parameters describing the deformation of the material, e.g., whether it dilates or compacts, are completely absent. The Mohr-Coulomb criterion predicts that failure is completely independent of the intermediate principal stress. Note that this dependence can enter in two ways, through the mean stress or through the intermediate principal value of the deviatoric stress. Thus, the Mohr-Coulomb criterion predicts that the failure plane makes the same angle with the most compressive principal stress in both axisymmetric compression and extension. In contrast, the angle observed in experiments tends to be smaller for axisymmetric extension (e.g., Brace, 1964; Mogi, 1967; Bésuelle et al., 2000) and in addition, the angle depends on whether the volume deformation is dilatant or compactant (Bésuelle, 2001a). (The data of Mogi [1967] is discussed in Section 5.7.2.)

Another approach to describing failure is fracture mechanics: failure is predicted to occur because the high local stress due to an acute geometry, in particular, a crack, causes the crack to grow. In contrast to the Mohr-Coulomb approach, which essentially assumes a uniform stress field, the condition for fracture growth is dominated by the concentration of stress at the flaw tip. Fracture mechanics has been successful when initial growth of a crack continues with small or no increase in load and leads immediately to failure. This is often the case in nominally brittle materials under tensile loadings. Typically, in applications to geomaterials, all of the principal stresses are compressive. Consequently, the tensile stress fields driving crack growth are limited to the vicinity of the crack tips and flaw propagation is inherently stable. Failure does not occur by the growth of a single dominant flaw but, instead, by the coalescence and linking of many flaws that extend under local tensile fields (although joints, which often extend kilometers as a single rupture plane, are an exception [Pollard and Aydin 1988]).

Many microstructural observations have revealed that the details of the process of localization in rocks are very complicated (e.g., Wong, 1982; Wong and Beigel, 1985; Fredrich et al., 1989). Micrographs of specimens at various stages of deformation have shown that the process occurs by crack growth, interaction, and coalescence. The microstructural observations inevitably reveal that the geometry of cracks on this scale is quite different from the ideal geometries assumed in calculations, that growth is influenced by grain boundaries and the different strengths and crystallographic properties of the constituent minerals. Furthermore, in many rocks at low temperatures and pressures, in particular, those containing a significant fraction of calcite, and most rocks at higher temperature and pressure, brittle mechanisms of crack growth and cataclasis interact with mechanisms of plasticity such as dislocation motion and interaction and twinning. At a larger size scale associated with seismic events in mines (McGarr et al., 1979), shear zones form a pattern of en echelon, interacting, and cross-cutting fractures. At the still larger scale of major fault systems (with significant relative displacement), the fault zone exhibits a complex structure of comminuted material, interacting shear surfaces of different orientations, and often, chemical alteration (Chester et al., 1993).

Attempts to simulate the process of localization have generally focused on a single mechanism, mainly growth and interaction of brittle cracks. Even the problem of growth of a single crack out of plane is difficult, and attempting to consider the interaction with more than a few cracks becomes prohibitively complex. Consequently, these attempts to simulate localization have often used ad hoc approximations that mimic the behavior of a single crack and adopted simple rules for their interaction. The success achieved by these simulations (Lockner and Madden, 1991a,b) suggests that, at least to some extent, the macroscopic behavior does not depend on all the details of the microscale processes. Of course, it is not easy to decide which of these details are the dominant ones. In highly porous compacting rocks, microcrack growth and linking is still an important deformation mechanism, but collapse of pores and indentation of hard grains also play an important role (Menéndez et al., 1996; Wong and Baud, 1999). Consequently, the response depends on the angularity of grains and strength of the cement between grains (DiGiovanni et al., 2000).

Obviously, it is not possible to model all the microstructural processes involved in localization. Here we mainly focus on an approach to localization that includes the detailed microscale mechanisms of deformation only as they enter the macroscopic constitutive relation for homogeneous deformation. The analysis of localization then poses the following question: If the loading is such that further homogeneous deformation is a possible solution, under what conditions does the constitutive response permit an alternative solution corresponding to localized deformation? Many important aspects of this approach are revealed by considering a simple one-dimensional example. Hence, before proceding to formulate this approach in general, we examine its application to the simple shear of a layer.

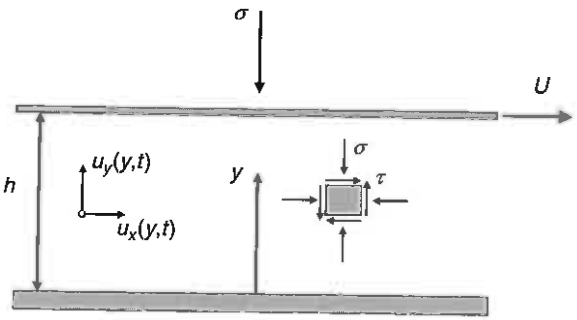

Figure 5.1 ▶ Layer with width h subjected to a boundary displacement U in the x direction and normal stress σ in the y direction. The layer extends indefinitely in the x and z directions.

5.3 Localization of a Layer

5.3.1 Rate-Independent Material Model

Figure 5.1 shows a layer of homogeneous material of thickness h. The layer is loaded at its upper surface by a prescribed displacement U and a normal stress σ. The stress state in the layer is a shear stress τ, a normal stress, σ, in the y direction and whatever normal stresses in the x and z directions are required to maintain one-dimensional deformation. The only nonzero displacements are in the x and y directions, u_x and u_y. Because the layer extends infinitely in the x and z directions, the only spatial variation is in the y direction. Consequently, the only nonzero strains, a shear strain γ and a normal strain ε, are related to the displacements by

$$\gamma = \frac{\partial u_x}{\partial y} \qquad \varepsilon = \frac{\partial u_y}{\partial y} \tag{5.1}$$

Because the normal strains in the x and z directions are zero, the volume strain is equal to ε. The nontrivial equilibrium equations

$$\frac{\partial \tau}{\partial y} = 0 \qquad \frac{\partial \sigma}{\partial y} = 0 \tag{5.2}$$

require that τ and σ be uniform through the layer.

If the material response (constitutive relation) of the layer is described (for constant normal stress) in terms of the shear stress as a simple function of the shear strain,

$$\tau = \mathrm{F}(\gamma), \tag{5.3}$$

increments of shear stress are related to increments of shear strain by

$$d\tau = H_{\tan}(\gamma)d\gamma, \tag{5.4}$$

where $H_{\tan} = F'(\gamma)$ is the slope of the τ versus γ curve (at constant σ). Obviously, one solution for the response of the layer is homogeneous deformation, $\gamma = U/h$ and the shear stress is given by equation (5.3). The condition of Hill (1958; 1961a,c) guarantees that the incremental solution is unique if

$$\int_0^h \Delta d\tau \Delta d\gamma dy > 0, \tag{5.5}$$

where $\Delta(a)$ denotes the differences of quantity a between two possible solutions satisfying equilibrium and the boundary conditions. Using equation (5.4), the integrand in this expression becomes

$$\Delta d\tau \Delta d\gamma = H_{\tan}(\gamma)(\Delta d\gamma)^2. \tag{5.6}$$

Because equation (5.6) is positive as long as $H_{\tan} > 0$, Hill's sufficient condition ensures that the homogeneous solution is the only one (Hill, 1958; 1961a,c). For $H_{\tan} \leq 0$, a unique solution is not guaranteed but neither is it ruled out. The homogeneous solution continues to furnish a possible solution if the displacement of the boundary is specified, but it may not be the only one. If the shear traction is specified, quasi-static deformation cannot be maintained for increasing traction beyond the point where $H_{\tan} = 0$ and inertia terms should be included on the right sides of equation (5.2).

Assume that the layer has been homogeneously deformed to a shear strain $\gamma = \gamma_0$. Now consider the possibility of a nonhomogeneous solution for the next increment of deformation. In particular, consider nonuniform deformation in a band:

$$d\gamma^{\text{band}} = d\gamma^{\text{out}} + \Delta d\gamma, \tag{5.7}$$

where $d\gamma^{\text{band}}$ is the increment of shear strain in the band and $d\gamma^{\text{out}}$ is the increment outside the band. Because of equation (5.2), the increments of shear stress in the band and outside must be equal:

$$d\tau^{\text{band}} = d\tau^{\text{out}}. \tag{5.8}$$

If the incremental constitutive relation has the form of equation (5.4), then substituting into equation (5.8) yields

$$H_{\tan}(\gamma_0) d\gamma^{\text{band}} = H_{\tan}(\gamma_0) d\gamma^{\text{out}}, \tag{5.9}$$

where $H_{\tan}$ is evaluated at γ_0 both inside and outside the band. Using equation (5.7) then yields the condition for the existence of a nonuniform solution in the layer

$$H_{\tan}(\gamma_0) \Delta d\gamma = 0. \tag{5.10}$$

For $H_{\tan} > 0$, the difference in strain increments $\Delta d\gamma$ must vanish, confirming the result of Hill's condition that a nonuniform solution is not possible. The first possibility for a nonuniform increment of shear strain to exist occurs when

$$H_{\tan}(\gamma_0) = 0 \tag{5.11}$$

or when the τ versus γ relation has a peak. Thus, not only is the sufficient condition violated, but it is also possible to construct a solution corresponding to nonuniform deformation in a planar band. This nonuniform solution is not, however, unique. Other solutions for nonuniformities in bands of different widths or with multiple bands could also be constructed. The continuum mechanics formulation of the problem gives no guidance as to which of these is appropriate. Numerical solutions will pick out one of these nonuniform solutions depending on the discretization, algorithm, and accuracy (Needleman, 1987).

The constitutive relation (5.3) is a special one appropriate for nonlinear elastic materials in which the stress follows the same curve for decreasing and increasing strain (Figure 5.2). Nevertheless, the condition (5.11) for the first possible occurrence of a nonuniform solution is identical to that for a much wider class of material models. For many materials deformed into the nonelastic range, including most geomaterials, the response differs for increasing and decreasing increments of strain. Typically, the total shear strain increment is the sum of the elastic portion and a nonelastic portion

$$d\gamma = d\tau/G + d\gamma^p, \tag{5.12}$$

where G is the (incremental) elastic unloading modulus and the second term is dropped for elastic unloading. In the simplest case, the increment of inelastic shear strain is proportional to the increment of shear stress

$$d\gamma^p = d\tau/H(\gamma^p), \tag{5.13}$$

where $H(\gamma^p)$, the inelastic hardening modulus, is the slope of a curve of τ versus γ^p. For continued inelastic loading, the tangent modulus of the τ versus γ curve is related to H by

$$H_{\text{tan}} = H/(1 + H/G) \tag{5.14}$$

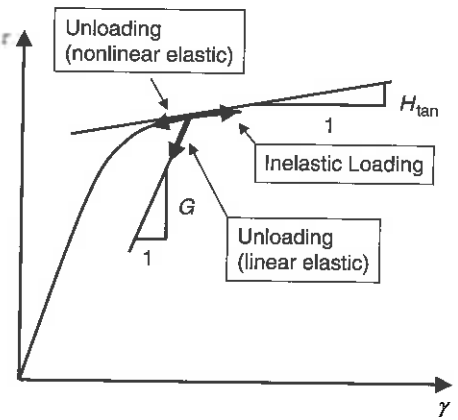

Figure 5.2 ▶ Schematic stress-strain curve illustrating different unloading responses for a nonlinear elastic and a linear elastic-plastic material.

and thus, $H_{\tan} \approx H$ when $H \ll G$. For elastic unloading $H_{\tan} = G$. If the material outside the band is assumed to be unloading then equation (5.10) becomes

$$H_{\tan}(\gamma_0)\Delta d\gamma = \left[G - H_{\tan}(\gamma_0)\right] d\gamma^{\text{out}}. \tag{5.15}$$

Because $H_{\tan}(\gamma_0)$ is less than or equal to G, is initially positive, and decreases with increasing strain, equation (5.15) is first met when equation (5.11) is satisfied. This requires that $d\gamma^{\text{out}} = 0$, corresponding to the onset of elastic unloading in the material outside the band. This example is a special case of a more general result of Hill (1958; 1961a,c) that bifurcation (nonuniqueness) in the actual elastic-plastic solid cannot precede loss of uniqueness in a *comparison solid* defined to always follow the constitutive branch yielding the softest (most compliant) response. In the simple example considered here, the branch for continued nonelastic loading is more compliant than elastic unloading and the result is analogous to that of Shanley (1947) for buckling of an elastic-plastic column. For more general deformation states, the ratio $d\gamma^{band}/d\gamma^{out}$ becomes infinite at the onset of localization (Chambon, 1986). Thus, at the onset of localization, the material outside the incipient band is essentially rigid with respect to the material inside the band.

The condition for the inception of localization, equation (5.11), is identical for an elastic-plastic material, which has different constitutive branches for loading and unloading, and for a nonlinear elastic material, for which the stress retraces the loading curve for decreasing strain, as long as both have the same stress–strain relation for monotonically increasing strain. The subsequent evolution of the strain in the localized zone will, however, be much different for the two types of material models. Softer unloading response of the nonlinearly elastic solid causes the strain to decrease more rapidly outside the localized zone than for the elastic-plastic material; consequently, the strain in the localized zone will increase more rapidly to yield the same boundary displacement (assuming the same width of the localized zone in both materials).

Although this analysis identifies $H_{\tan} = 0$ as the first point at which bifurcation from a homogeneous deformation is possible, it does not yield any information about the width of the zone of inhomogeneous deformation or whether one or more zones of inhomogeneous deformation exist. Beyond this point, the boundary value problem is nonunique. Information about the width or number of localized zones cannot be obtained from a continuum analysis using a constitutive relation that does not contain a characteristic length scale (see Section 5.8). Constitutive relations that do introduce a length scale, such as nonlocal or gradient formulations (Mühlhaus and Vardoulakis, 1987; Bažant and Pijaudier-Cabot, 1988), can predict the width of the zone of localized deformation. Physically, the width of the localized zone is likely controlled by the microstructure of the material; for example, a well-established rule of thumb in granular materials is that the width of the localized zone is approximately 5 to 10 grain sizes (Roscoe, 1970; Mühlhaus and Vardoulakis, 1987). In rocks the width of the localized zone appears to decrease with increasing mean stress. Consequently, the accuracy with which gradient or nonlocal theories

are able to predict the width of the zone is likely to depend on the extent to which they reflect the actual microscale mechanisms in the material.

The preceding analysis has discussed the case of simple shear loading and conditions for the formation of a pure shear (no dilation or compaction) band. A completely analogous analysis (Olsson, 1999) for uniaxial compression leads to the conclusion that formation of a compaction band is first possible at the peak of the stress-strain curve for uniaxial deformation.

5.3.2 Imperfection Approach

The analysis leading to condition (5.11) assumes that the localized zone appears instantaneously, i.e., bifurcates, from the solution for homogeneous deformation. In any real material, the deformation is not perfectly homogeneous because of material heterogeneity or slight imperfections in application of boundary conditions. In granular materials a region may be weaker because of a slightly different packing density or grain arrangement; in rock, a weaker region may be due to a higher density of microcracks or the presence of a weakened mineral phase. Consequently, it is of interest to compare the preceding analysis with one that assumes the existence of an initially weakened zone. This approach was introduced for the study of localized necking in thin sheets by Marciniak and Kuczynski (1967) and extended to a more general analysis of localization by Rice (1976)

For the simple geometry shown in Figure 5.1, the imperfection is assumed to be a sublayer of width ϵh, where $\epsilon \ll 1$. The increment of boundary displacement dU must be the sum of displacement increments across the weakened sublayer and the surrounding material:

$$dU = \epsilon h d\gamma^{\text{band}} + (1-\epsilon) h d\gamma^{\text{out}}, \tag{5.16}$$

where $d\gamma^{\text{band}}$ refers to the strain increment in the sublayer and $d\gamma^{\text{out}}$ to that outside. Both $d\gamma^{\text{band}}$ and $d\gamma^{\text{out}}$ are assumed to be related to the stress increments by equation (5.4) with $H_{\text{tan}}^{\text{band}} \leq H_{\text{tan}}^{\text{out}}$ because the sublayer is weaker. Because of equilibrium, the stress increments must satisfy equation (5.8). The solution for the strain increments in terms of the imposed displacement increment can be obtained by substituting equation (5.4) into equation (5.8) and using equation (5.16). The result is

$$d\gamma^{\text{band}} = \frac{dU}{h} \frac{H_{\text{tan}}^{\text{out}}}{\epsilon H_{\text{tan}}^{\text{out}} + (1-\epsilon) H_{\text{tan}}^{\text{band}}} \tag{5.17a}$$

$$d\gamma^{\text{out}} = \frac{dU}{h} \frac{H_{\text{tan}}^{\text{band}}}{\epsilon H_{\text{tan}}^{\text{out}} + (1-\epsilon) H_{\text{tan}}^{\text{band}}} \tag{5.17b}$$

and is depicted graphically in Figure 5.3. When the condition for localization in the weakened imperfection is met, $H_{\text{tan}}^{\text{band}} = 0$ and the ratio of the strain increments $d\gamma^{\text{band}}/d\gamma^{\text{out}}$ becomes unbounded. Significantly, this may occur well before the condition for localization is met in terms of the response outside the weakened imperfection, $H_{\text{tan}}^{\text{out}} = 0$.

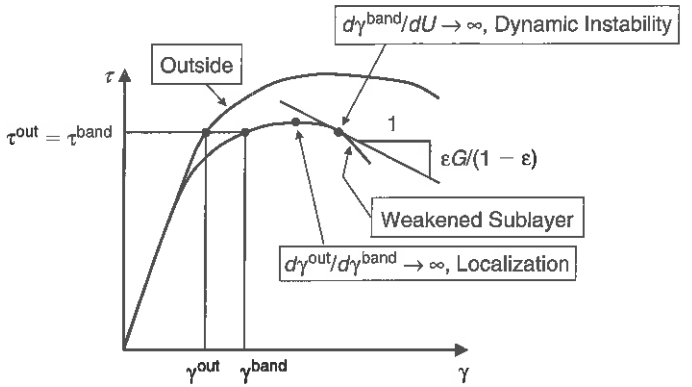

Figure 5.3 ▶ Graphical solution for a layer of width h with a weakened sublayer of width ϵh, with $\varepsilon \ll 1$.

If the weakened sublayer is regarded as representing an already localized zone and the constitutive relation in the band is assumed to be appropriate for the postlocalized material response, equation (5.17) gives the solution for further evolution of the strain. (For the reasons stated earlier, the solution in the sublayer is nonunique beyond this point.) It is, however, necessary to replace H_{tan}^{out} by G for the elastic-plastic material because $d\gamma^{out} = 0$ at $H_{tan}^{band} = 0$, signaling the onset of elastic unloading. A quasi-static solution is not possible beyond the point where $H_{tan}^{band} = -\epsilon G/(1-\epsilon)$, at which the ratio of the strain increment in the localized sublayer to the nominal strain rate $d\gamma^{band}/(dU/h)$ becomes unbounded. This corresponds to a dynamic, "runaway" instability (Rudnicki, 1977b) that results from the assumption of equilibrium and the neglect of inertia terms in the momentum balance (5.2). This instability is analogous to what occurs in a compliant testing machine if the sample strength decreases more rapidly than the machine can unload (Jaeger and Cook, 1969). As the localized layer becomes thinner, $\epsilon \to 0$, the condition for the dynamic instability approaches that for localization.

5.3.3 Rate-Dependent Material

The examples in the preceding discussion assumed that the material response was independent of the rate of loading. This rate-independent idealization is reasonable for many granular materials and for rocks at relatively low temperatures and pressures, at least if the time scale of interest is sufficiently short. In other circumstances rate dependence cannot be neglected. Rate dependence can arise, even in nominally brittle materials, from the presence of fluids that cause subcritical growth of microcracks or time-dependent surface chemical effects at contact points of grains or on microcrack surfaces. Indeed, the rate-and state-dependent effects in frictional sliding of rock surfaces, although small in magnitude, have been demonstrated to control the stability of sliding (Dieterich, 1979a,b; Rice and Ruina,

1983; Ruina, 1983). At higher temperatures and pressures, for example, those typical of midcrustal depths or greater, rate dependence can arise from mechanisms of dislocation creep, chemical reactions, and diffusive mass flux. Rate-dependent effects are likely to be significant in localizing deformation at the roots of shear or seismogenic zones where there is a transition from more brittle behavior at shallower depths to more viscous at greater.

Even when magnitude of rate sensitivity is small, it dramatically affects the character of localization and alters the nature of the localization analysis. Because only the moduli governing the instantaneous response enter the bifurcation analysis of localization, this analysis is inadequate for predicting localization in rate-sensitive materials and it is necessary to consider the growth of initial imperfections. On the other hand, inclusion of rate sensitivity removes the nonuniqueness and mesh sensitivity that is associated with the rate-independent limit (Pan and Rice, 1983; Needleman, 1987). To explore the effects of rate sensitivity on localization within the simple shear problem, consider the inelastic strain rate to be given by

$$\dot{\gamma}^p = \dot{a} f(\tau, \gamma^p), \tag{5.18}$$

where $\dot{a}$ is a reference strain rate. The shear stress τ is equal to the product of the elastic shear modulus G and the elastic shear strain, that is, the difference between the total shear strain γ and the inelastic shear strain,

$$\tau = G(\gamma - \gamma^p). \tag{5.19}$$

An important difference between equation (5.18) and the rate-independent description (5.13) is the absence of the stress rate on the right side of equation (5.18). A consequence, discussed by Needleman (1987), is that the incremental solution is unique: unless bifurcation is permitted by the instantaneous, elastic moduli, the condition (5.5) guarantees uniqueness of the solution (Hill, 1958; 1961a,c). Using equation (5.19) in this expression (now written in terms of rates rather than increments) gives

$$\Delta\dot{\tau}\Delta\dot{\gamma} = G(\Delta\dot{\gamma} - \Delta\dot{\gamma}^p)\Delta\dot{\gamma} \tag{5.20}$$

for the integrand. Because only the current values (not rates or increments) of τ and γ^p enter the right side of equation (5.18), $\Delta\dot{\gamma}^p = 0$ and $\Delta\dot{\tau}\Delta\dot{\gamma} > 0$ as long as the elastic shear modulus is positive. Consequently, the problem for a rate-dependent solid is unique and the possibility of localization requires assuming an initial nonuniformity of properties or strain.

Both Pan (1983) and Needleman (1987) have discussed the development of localization for the simple shear of the layer using a power law rate-dependent constitutive relation of the form

$$\dot{\gamma}^p = \dot{a}\left(\frac{\tau}{g(\gamma^p)}\right)^{1/m}, \tag{5.21}$$

where $g(\gamma^p)$ is a hardening function that is equal to the shear stress τ when $\dot{\gamma}^p = \dot{a}$, a reference plastic strain rate, and m is the plastic strain-rate sensitivity, defined by

$$m = \frac{\partial \ln(\tau)}{\partial \ln(\dot{\gamma}^p)}. \tag{5.22}$$

As discussed by Needleman (1987), relation (5.21) has no explicit yield stress, but for small values of m, typical of many materials, the stress-strain curve has a rapid transition at a value of the stress equal to $g(0) = \tau_0$. Figure 5.4 shows stress-strain curves for $m = 0.02$, for constant imposed strain rates equal to 10^0, 10^3, and 10^6 times the reference strain rate and $g(\gamma^p)$ taken as

$$g(\gamma^p) = \tau_{\text{peak}} - \frac{1}{2}\kappa G(\gamma^p - \gamma^p_{\text{peak}})^2, \tag{5.23}$$

where τ_{peak} is the maximum stress and γ^p_{peak} is the plastic strain at which it occurs. For $g(0) = \tau_0$, κ, the curvature, is given by $2(\tau_{\text{peak}} - \tau_0)/G(\gamma^p_{\text{peak}})^2$. The rate-independent limit of $m = 0$, for which equation (5.23) gives the stress, is identical to the curve for $\dot{\gamma} = \dot{a}$. As illustrated by Figure 5.4, the stress–strain relation depends only weakly on the strain rate over several orders of magnitude.

Pan (1983) gives the linearized perturbation of equation (5.21)

$$\tilde{\dot{\gamma}}^p = \frac{\dot{\gamma}^p}{m\tau}\left(\tilde{T} + \tilde{\tau} - \tau\frac{g'(\gamma^p)}{g(\gamma^p)}\tilde{\gamma}^p\right), \tag{5.24}$$

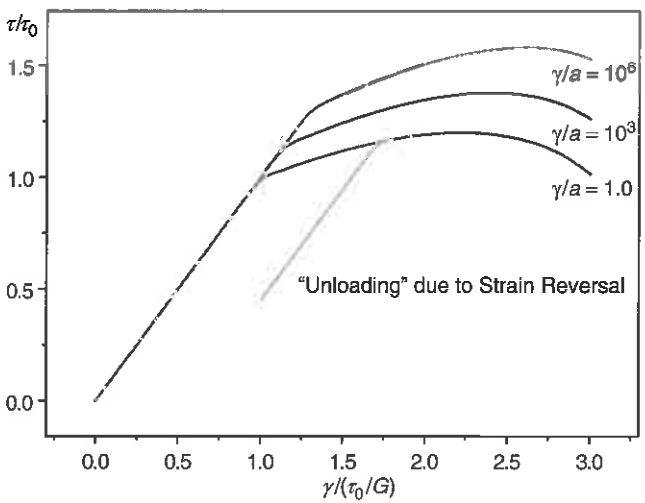

Figure 5.4 ▶ Response of the rate-dependent material model (5.21) with $m = 0.02$ and three values of strain rate. Although the model contains no explicit yield stress, the response is similar to that of a rate-independent elastic-plastic material with yield stress τ_0.

where $(\sim)$ denotes a perturbation, g' is the derivative of g with respect to its argument, and T is linear in the perturbations of the material properties $\tilde{\dot{a}}$, $\tilde{g}$, and $\tilde{m}$:

$$\tilde{T} = m\tau \left\{ \frac{\tilde{\dot{a}}}{\dot{a}} - \frac{1}{m}\frac{\tilde{g}(\gamma^p)}{g(\gamma^p)} - \frac{\tilde{m}}{m^2} \ln\left(\frac{\tau}{g(\gamma^p)}\right) \right\}. \tag{5.25}$$

If the traction is specified at the boundary, equilibrium (5.2) requires that $\tilde{\tau} = 0$ and equation (5.24) can be expressed as a linear ordinary differential equation for $\tilde{\gamma}^p$:

$$\frac{d\tilde{\gamma}^p}{d\gamma^p} + \frac{1}{m}\frac{g'(\gamma^p)}{g(\gamma^p)}\tilde{\gamma}^p = \frac{\tilde{T}}{m\tau(\gamma^p)}. \tag{5.26}$$

Solutions of the homogeneous equation ($\tilde{T} = 0$) change from exponentially decaying to exponentially increasing as $g'(\gamma^p)$ changes from positive to negative. Because $g'(\gamma^p) = 0$ corresponds to the peak of the stress-strain curve in the rate-independent limit, this result connects the growth of perturbations in the rate-dependent material with the localization condition for the rate-independent material. Using numerical calculations for the growth of strain in a slightly weakened sublayer, Pan (1983) shows, however, that the condition $g'(\gamma^p) = 0$ considerably underestimates the strain at which localization (corresponding to an unbounded ratio of an increment of strain in the sublayer to that the strain outside) occurs in the rate-dependent material. Localization is increasingly delayed beyond its occurrence in the rate-independent material for increasing values of rate sensitivity m.

As previously noted and emphasized by Needleman (1987), uniqueness is not lost for the rate-dependent problem. Consequently, the pathological mesh sensitivity that occurs in numerical solutions of the rate-independent problem is eliminated. The material relation does not contain a length scale, but one is introduced in the problem by the requirement of an initial imperfection. Although the mesh sensitivity is eliminated by the introduction of (even small amounts of) rate dependence, stable numerical integration of the equations for small m can require extremely small time steps. Pierce et al. (1984) have, however, introduced an efficient method for these types of solids (also Needleman [1987]). Needleman (1987) also discussed numerical solutions of the simple shear problem under dynamic loading conditions when inertia must be included. Dynamic loading for a rate-independent solid can lead to "wave trapping" in simple shear (Wu and Freund, 1984). Again, this undesirable feature is eliminated in the rate-dependent solid.

At higher rates of loading or low thermal conductivities, the increase in temperature due to heat generated by inelastic shear can have a significant effect on the evolution of localization. Basically, weakening due to increasing temperature tends to enhance localization and compete against retardation due to strain hardening and increasing strain-rate sensitivity. There has been considerable study of the

development of localization in thermal, viscoplastic materials, particularly in the simple shear configuration, for a variety of constitutive relations (e.g., Shawki and Clifton, 1989). The results tend to indicate that the linear perturbation analysis, although suggestive of the role of various effects, is a poor indicator of the ultimate strain at which localization has occurred. Most of the studies have been in the context of engineering materials for which significant shear heating results from rapid loading, but in the geological problems, particularly for deep fault zones, the high normal stress and low thermal conductivities may lead to significant shear heating even at low strain rates.

A more complete constitutive description than equation (5.18) would include dependence on temperature and, possibly, one or more state variables. The latter are internal variables, not directly measurable at the macroscopic level and in addition to the inelastic strain. Their current values reflect the past history of inelastic deformation, and they are typically in the form of concentrations per unit volume of reference state, e.g., of numbers of dislocation loops or masses of mobile chemical species. Rice (unpublished notes, 1981) has given a general formulation for simple shear of a layer that includes diffusive transport of the state variables. He gives a linearized perturbation analysis for both specified velocity and traction boundary conditions. This treatment includes as a special case the analysis of Ruina (1980) for the stability of shear for a rate- and state-dependent material description analogous to the form widely used to model rock friction (Dieterich, 1979a,b; Ruina, 1983). This framework of rate and state friction has been very successful at describing a variety of phenomena, e.g., stable sliding, stick slip, and oscillatory slip, observed in laboratory rock friction experiments and in simulating aspects of earthquake occurrence (e.g., Tse and Rice, 1986). Although the magnitude of the rate- and state-dependent effects is small compared with the first-order Coulomb description of friction, these effects have been shown to control the stability of steady sliding. The possible connection of rate and state description of friction with localization arises from the observation that this description has been used not only for experiments in which slip occurs on (nominally) flat, cut rock surfaces but also for the net relative displacement that occurs across simulated gouge zone layers in experiments. The analyses of Ruina (1980) and Rice (unpublished notes, 1981) indicate that steady state strain-rate weakening, analogous to velocity weakening, which is necessary for unstable frictional slip, tends to lead to localization, in the sense that spatial nonuniformities grow with time. A variety of localized substructures typically observed within the gouge layer (Mandl et al., 1977; Marone et al., 1990; Logan et al., 1992; Chester et al., 1993) may indicate evolving processes of localization. Thus, the evolution of the gouge zone layer and its response may be related to processes of localization within it.

5.3.4 Pore Fluid Effects

Geomaterials in shallow environments are usually saturated with ground water or other mobile fluids. In addition, mobile fluid has been observed at surprisingly

large depths in drill holes. There are suggestions that sources of fluid exist deep at the root of ductile fault zones (Rice, 1992) and that dewatering of subducting slabs may supply fluid to the lower crust (Nur and Walder, 1990). The effects of fluids on the mechanical response of granular materials has been recognized since the pioneering investigations of Reynolds (1901) and von Terzaghi (1936). The weakening effect of high pore fluid pressure on crustal fault systems was pointed out by Hubbert and Rubey (1959) and supported by observations of Raleigh et al. (1976) in the Rangely oil field. Consequently, it is not surprising that the mechanical interaction of pore fluid and deformation can also significantly affect the occurrence and evolution of localization. A seminal study of the effects of coupling of deformation and pore fluid diffusion on the development of localization is that of Rice (1975), and the treatment here is a modified version of his. Further studies have been done by Rudnicki (1984b; 2000), Han and Vardoulakis (1991), and Benallal and Comi (2002).

The interaction of fluid diffusion with inelastic deformation is related to dependence of inelasticity on the mean stress and inelastic volume changes, features that are absent from the simple constitutive relations (5.3), (5.13), and (5.18). For most geomaterials, at least at relatively low temperatures and pressures, the shear stress needed to cause inelastic deformation depends on the mean stress. Following Rice (1975), we amend equation (5.13) to include dependence of $d\gamma^p$ on not only the increment of shear stress $d\tau$ but also on the increment of normal stress $d\sigma$:

$$d\gamma^p = \frac{1}{H}(d\tau - \mu d\sigma), \tag{5.27}$$

where H is the slope of the τ versus γ^p curve at constant normal stress. The coefficient μ is the local slope of the yield surface in the plane of the stresses τ and σ. For medium and densely packed granular materials and low porosity rocks, increasing normal compression tends to inhibit inelastic shear strain related to mechanisms of frictional sliding on fissure surfaces or at grain contacts and to microcracking caused by local tensile stress. Consequently, $\mu > 0$ and μ can be interpreted as a "friction coefficient." For low-porosity rock or granular materials, the pure normal stress needed to cause inelastic deformation is often so high, at least by comparison with the range of interest, that the yield surface is depicted as open for high values of σ (Figure 5.5a).

On the other hand, for high-porosity rock or loosely consolidated granular materials, or high normal stress, increasing normal stress may contribute to inelastic deformation by the crushing of porosity or grains. In this case, the yield surface is closed for high σ (Figure 5.5c). Closure is often accomplished by a separate surface, referred to as a "cap" (DiMaggio and Sandler, 1971), that intersects the "shear" surface at a corner or by a continuation of the shear surface (Figure 5.5b). In either case, the local slope of the surface in the τ versus σ plane is negative. We continue to denote this local slope by μ even though the interpretation of a friction coefficient is not appropriate for $\mu < 0$. Note that because τ denotes the *magnitude* of the shear stress, symmetry requires that the surface intersect the σ

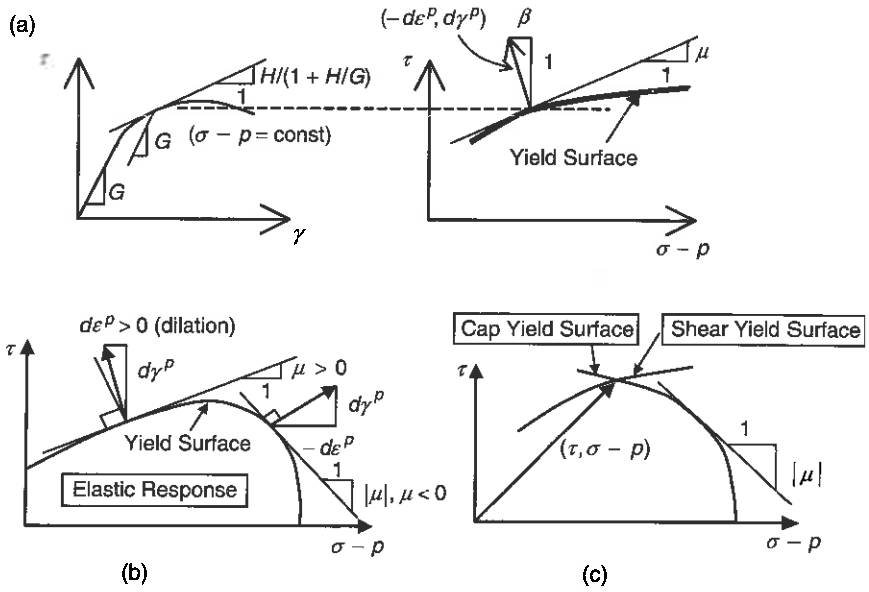

Figure 5.5 ▶ Yield surfaces for low-porosity, dilatant material (a) and for high-porosity material (b and c). Yield surface may be a single surface (b) or different surfaces for shear and compaction (c).

axis either with a vertical tangent or at a corner. If the intersection is smooth, then $\mu \to -\infty$ there.

The analysis of Rice (1975) focused on low-porosity rocks for which $\mu \geq 0$, but here we include the possibility of high-porosity rock or soil by allowing μ to be negative (Rudnicki, 2000; Issen and Rudnicki, 2000; 2001). This implicitly assumes that the surface or intersection of the surfaces is smooth and a more detailed treatment is needed for stress states at a corner (Issen, 2002).

For low-porosity rocks and densely packed granular materials, inelastic increments of shear typically induce an inelastic volume strain increase, dilatancy. In rocks, dilatancy can be caused by microcracking due to local tensile stresses induced at the tips of sliding fissures, or resulting from indentation of hard phases, mismatch of constituent grains, and uplift in sliding along frictional surfaces. In soils and granular materials, dilatancy results from grain movement causing a less compact structure. Thus, Rice (1975) expresses the increment of inelastic volumetric strain as

$$d\varepsilon^p = \beta d\gamma^p, \tag{5.28}$$

where $\beta > 0$ corresponds to dilation (Figure 5.5). The coefficient β may, however, be negative. Inelastic shearing can enhance compaction of very porous rock

(Menéndez et al., 1996; Wong and Baud, 1999) and can cause lightly compacted granular materials to assume a more dense structure. On the shear yield surface, where $\mu > 0$, experiments indicate that $\beta < \mu$ and, consequently, the inelastic increment of strain $(-d\varepsilon^p, d\gamma^p)$, when plotted as a vector in the τ–σ plane, is not normal to the yield surface. On the portion of the surface where $\mu < 0$, there is no clear evidence indicating that $\beta \neq \mu$, hence the strain increment is often assumed to be normal to the yield surface.

When elastic increments of strain are included, the incremental constitutive relations are

$$d\gamma = \frac{d\tau}{G} + \frac{1}{H}(d\tau - \mu d\sigma) \tag{5.29a}$$

$$d\varepsilon = -\frac{d\sigma}{M} + \frac{\beta}{H}(d\tau - \mu d\sigma), \tag{5.29b}$$

where G is again the shear modulus and M is an elastic modulus for one-dimensional compression (equal to $2G(1-\nu)/(1-2\nu)$ for isotropic elasticity). The second terms in equation (5.29) are the inelastic portions. When $H > 0$, deformation increments tending to make $d\tau \leq \mu d\sigma$ are purely elastic and the second terms in equation (5.29) are dropped. (When $H < 0$, elastic unloading corresponds to $d\tau \geq \mu d\sigma$.)

When the pore pressure is not constant, the constitutive relations (5.29) are modified by replacing the increment of normal stress by an increment of the effective normal stress, a linear combination of $d\sigma$ and dp. Experiments on failure of rocks (e.g., Paterson, 1978) suggest that $\sigma - p$ is the appropriate form for the effective stress for inelastic response. In addition, Rice (1977) has argued on theoretical grounds that this is the appropriate form for inelasticity due to microcracking from the tips of sharp fissures and to frictional sliding on surfaces with small real contact areas. Generally, a different form is needed for elastic deformation (Nur and Byerlee , 1971; Rice and Cleary, 1976) but, when the solid and fluid constituents are much less compressible than the porous matrix, $\sigma - p$ is also the appropriate form of the effective stress for elastic straining. Rice (1975) gives expressions for fully compressible consituents but for simplicity we use $\sigma - p$ as the effective stress for both elastic and inelastic increments. In this case, equations (5.29a and b) become

$$d\gamma = \frac{d\tau}{G} + \frac{1}{H}\left[d\tau - \mu d(\sigma - p)\right] \tag{5.30a}$$

$$d\varepsilon = -\frac{d(\sigma - p)}{M} + \frac{\beta}{H}\left[d\tau - \mu d(\sigma - p)\right]. \tag{5.30b}$$

An additional constitutive relation is Darcy's law that, in the absence of body forces, has the following form:

$$q = -\kappa \frac{\partial p}{\partial y}, \tag{5.31}$$

where q is fluid volume flow rate per unit area in the y direction and κ is a permeability that is more commonly expressed as $\kappa = K/\eta$, where K is the intrinsic permeability (with dimensions of length squared) and η is the fluid viscosity. If the solid phase is incompressible, the equation expressing conservation of fluid mass is

$$\frac{\partial q}{\partial y} + \frac{\partial \varepsilon}{\partial t} = 0. \tag{5.32}$$

Substituting equation (5.31) into equation (5.32) yields an equation relating gradients in pore pressure to changes in volumetric strain:

$$\frac{\partial}{\partial y}\left[\kappa \frac{\partial p}{\partial y}\right] = \frac{\partial \varepsilon}{\partial t}. \tag{5.33}$$

If drainage from the boundaries of the layer is prevented and the deformation and properties are uniform, equation (5.31) yields $q = 0$ throughout the layer and, from equation (5.32), increments in volume strain are zero. Setting $d\varepsilon = 0$ in equation (5.30b) yields the following expression for the change in effective normal stress:

$$d(\sigma - p) = \frac{\beta M}{H + \mu\beta M} d\tau. \tag{5.34}$$

Because M is an elastic modulus and positive, the pore pressure decreases for dilation ($\beta > 0$) and increases for compaction ($\beta < 0$) at fixed normal stress. Substitution of equation (5.34) into equation (5.30a) reveals that the slope of the shear stress versus shear strain curve (no longer at constant effective normal stress) is still given by equation (5.14) but with the hardening modulus H replaced by

$$H_{\text{undrained}} = H + \mu\beta M. \tag{5.35}$$

If both μ and β have the same sign, either positive or negative, then $H_{\text{undrained}} \geq H$ and the undrained response is stiffer than the drained. For dilatancy, $\beta > 0$, an increase in pore space (without fluid mass influx) reduces the pore pressure, shown in equation (5.34), and increases the effective compressive stress. For $\mu > 0$, the increase in effective compressive stress inhibits further inelastic shear deformation, shown in equation (5.27). This increase in effective stiffness is called *dilatant hardening*. For compaction, $\beta < 0$, a decrease in pore space (without fluid mass influx) increases the pore pressure, shown in equation (5.34), and decreases the effective compressive stress. If, however, $\mu < 0$, the decrease in effective compressive stress inhibits further inelastic shear deformation. equation (5.27). Thus, for stress states on a portion of the yield surface with $\mu < 0$, inelastic compaction causes a strengthening.

If μ and β have different signs, then $H_{\text{undrained}} \leq H$ and the undrained response is softer than the drained. This seems most likely to occur when β is negative, during compaction, and when μ is positive though perhaps small and approaching the stress states where it changes sign.

Rice (1975) proceeds to show, however, that even when the undrained solution is stiffer than the drained, homogeneous deformation is unstable with respect to small spatial perturbations in the strain or pore pressure. In particular, linearization of the governing equations about the undrained homogeneous solution yields the homogeneous diffusion equation for the perturbations in pore pressure $\tilde{p}$:

$$\frac{\partial^2 \tilde{p}}{\partial y^2} = \frac{1}{c}\frac{\partial \tilde{p}}{\partial t}, \tag{5.36}$$

where the effective diffusivity c is given by

$$c = \frac{\kappa M H}{H + \mu\beta M} \tag{5.37}$$

and the constitutive parameters are to be evaluated at homogeneous undrained deformation. Perturbations of the form

$$\tilde{p} = \tilde{p}(0)e^{rt}\cos(2\pi y/\lambda) \tag{5.38}$$

satisfy the no-flux boundary conditions at $y = 0, h$, and substitution into equation (5.36) reveals that components with a Fourier wavelength λ grow exponentially at a rate

$$r = -4\pi^2 c/\lambda^2. \tag{5.39}$$

Thus, if the diffusivity is positive, $c > 0$, perturbations decay exponentially, but if the diffusivity is negative, $c < 0$, they grow.

If both β and μ have the same sign, then $H_{\text{undrained}} > H$ and the homogeneous, undrained response is hardened. But, because H is generally a decreasing function of inelastic deformation, c of equation (5.37) passes through zero from positive to negative when $H = 0$, corresponding to a peak in the drained τ versus γ curve (at constant $\sigma - p$). Thus, the homogeneous response becomes unstable when the *underlying drained response* passes through a peak. Perturbation components with the smallest wavelengths will grow the fastest, indicating localization of deformation. Thus, the onset of instability in the fluid-infiltrated material, due to rapid growth of small spatial perturbations, coincides with the prediction of localization for the underlying drained solid. This suggests that homogeneous undrained deformation will not be observed beyond the point corresponding to the peak in the drained response curve (which, for dilatant materials, will correspond to prepeak, hardening response of the undrained material). Of course, the possible wavelengths of perturbations are bounded from below by some microstructural length, perhaps several times the grain size. Consequently, the growth rate of even the smallest wavelength perturbations is finite and it is possible, for sufficiently rapid imposed strain rate or small enough permeability κ that the material can be driven to the peak of the undrained response curve, $H_{\text{undrained}} = 0$, before significant growth of perturbations occurs.

If the signs of β and μ are different, then $H_{\text{undrained}} < H$ and the peak of the undrained response curve will occur at a smaller strain than the drained. Thus, the denominator of equation (5.37) passes through zero before the numerator and the growth rate equation (5.39) changes from unbounded negative to unbounded positive. This singular jump in diffusivity suggests the need for a more elaborate perturbation analysis. Vardoulakis (1996) has applied Rice's analysis to study the stability of biaxial deformation of water-saturated sand and noted that the instability at $H_{\text{undrained}} = 0$ can be mitigated by the introduction of rate dependence in the material constitutive behavior. By including the variation of constitutive parameters with the uniform background deformation in the perturbation solution, Garagash and Rudnicki (2000) show that undrained deformation of compacting material is stable as $H_{\text{undrained}}$ passes through zero if the ratio of the diffusion length to the maximum perturbation wavelength (defined by the layer width) is larger than a critical value defined by the dependence of the inelastic moduli on the deformation state. This result suggests that the maximum perturbation wavelengths are most unstable and that, for inelastic compaction, failure will occur by a diffuse rather than a localized mode, as for dilatant hardening. In addition, the stability criterion implies that compaction softening is stable near the peak shear stress ($H_{\text{undrained}} = 0$) if the specimen size is small enough (to sufficiently limit the maximum perturbation wavelength). This result is consistent with the small-scale laboratory results of Han and Vardoulakis (1991) and Finno et al. (1997).

For arbitrarily compressible solid and fluid constituents, Rice (1975) showed that the effect on the stability analysis is to replace the elastic modulus M in equations (5.34), (5.35), and (5.37) by a modified value

$$M' = \left\{ \frac{1}{M} + \frac{\phi}{K_f} - \frac{1}{M_s} - \frac{\phi}{N_s} \right\}^{-1}, \tag{5.40}$$

where ϕ is the apparent void volume fraction, K_f is the bulk modulus of the pore fluid, and M_s and N_s are additional moduli associated with the solid constituents. When both the solid and fluid constituents are effectively incompressible, $M' = M$. If the solid constituents are incompressible, i.e., $M_s, N_s \gg M$,

$$M' = \frac{M}{1 + M\phi/K_f}. \tag{5.41}$$

If the fluid is very compressible, $K_f/\phi \gg M$ and $M' \approx K_f/\phi$. Thus, the hardening or softening effect diminishes with reduction of the pore fluid bulk modulus and vanishes in the limit $K_f \to 0$. If dilatant hardening causes a sufficient reduction of the pore fluid pressure, exsolution of dissolved gases or cavitation of the fluid may occur and the pore fluid bulk modulus will be dramatically reduced. Rudnicki and Chen (1988) have proposed that cavitation is a limit to strong dilatant hardening associated with slip on a weakening frictional surface and suggest that this effect is consistent with observations by Martin (1980) of pore fluid stabilization of rock

failure. In addition, in undrained biaxial experiments on a quartz sand, Mokni and Desrues (1999) have observed that the formation of shear bands in dilatant specimens does not occur until cavitation of the pore fluid. The numerical simulations of Schrefler et al. (1996) also indicate the importance of cavitation in the formation of shear bands.

Rudnicki (1984b) examined the effect of an initial nonuniformity on dilatant hardening by considering the shear of a weakened layer embedded in an infinite body. Both the layer and the surrounding material deform nonelastically, but the peak stress in the layer is slightly less than that in the surrounding material. The pore pressure is assumed to be uniform in both the layer and the surrounding material and the fluid mass exchange is assumed to be proportional to the difference. The development of instability in time depends on the ratio of the rate of imposed far-field strain rate $\dot{\gamma}_\infty$ to the rate of exchange of fluid mass with the layer, r_d. In the limit $\dot{\gamma}_\infty / r_d \to 0$, the pore pressure in the layer is the same as in the surrounding material and instability occurs at the peak of the drained stress-strain curve. For finite $\dot{\gamma}_\infty / r_d$, instability is delayed until the weakened layer reaches the peak of its dilatantly hardened stress-strain curve. For small $\dot{\gamma}_\infty / r_d$, as appropriate for most applications, an asymptotic analysis predicts that the time delay is given by $(\alpha r_d)^{2/3}(\Lambda / \dot{\gamma}_\infty)^{1/3}(\Delta\tau_{\text{peak}})^{-1/6}$, where Λ is the half-width of the peak of the stress-strain curve, $\Delta\tau_{\text{peak}}$ is the difference in the peak stresses of the weakened layer and the surrounding material divided by Λ times the elastic shear modulus, and α is a nondimensional measure of the strength of dilatant hardening. These delay times are less than a few hours for tectonic strain rates and less than a few tens of seconds for typical laboratory strain rates.

Relation (5.28) assumes that all inelastic volumetric deformation arises from inelastic shearing. This will be a good approximation for low-porosity rock or dense soils for which hydrostatic or uniaxial compression causes little inelastic volume change. To include the possibility of inelastic volume decrease resulting from normal compressive stress, as expected for high-porosity rock or loose soil, we append a term to equation (5.28),

$$d\varepsilon^p = \beta d\gamma^p - \frac{1}{k} d\sigma, \tag{5.42}$$

where k is an inelastic modulus that is the slope of the σ versus ε^p curve at constant shear stress ($d\tau = 0$). Aydin and Johnson (1983) have included such a term in their modification of the constitutive relations used by Rudnicki and Rice (1975). Inclusion of this term causes the ratio of the inelastic strain increments to depend on the direction of the stress increment rather than being fixed by the current state of stress and inelasticity. Consequently, as noted by Issen (2002), equation (5.42) corresponds to the response at a yield surface vertex formed by the intersection of the shear yield surface and a vertical cap in the τ versus σ plane. Similar to the approximate analysis of the response at a vertex by Rudnicki and Rice (1975), the effect of including this term is to modify the elastic contribution

to the volumetric strain in equation (5.29b) and in the stability analysis to replace the elastic modulus M (or M') by the effective value

$$M'' = \frac{k}{1 + k/M}. \tag{5.43}$$

For typical cases, $k \geq 0$ but $k \ll M$. Decreasing k will reduce the difference between the drained and undrained hardening moduli.

Many geomaterials exhibit both compaction and dilation depending on the initial confining stress, initial porosity, and load path. Examples include simulated fault gouge (Marone et al., 1990), loose sand (Finno et al., 1997), and limestone (Baud et al., 2000). When these materials are fluid saturated and deformed without allowing fluid flow from the boundaries, the evolution of localized zones depends on the local rate of fluid flow, the imposed rate of straining, and the transition from contraction to dilation. A simple analysis (Rudnicki et al., 1996) shows that small variations in the evolution of porosity with shear strain can dramatically alter the undrained response. Rudnicki et al. (1996) have suggested that compaction softening followed by dilatant hardening may be an explanation for the evanescent shear band structures observed in some experiments of Finno et al. (1997). If compaction softening causes the onset of localized deformation in a narrow zone but gives way to dilatant hardening before full development of the band, formation of a shear band in another orientation may occur when the dilatant hardening response becomes unstable.

5.4 Bifurcation Theory

The preceding section examined the conditions for localization for the simple deformation state of shear and uniaxial deformation. Although that analysis suffices to illustrate several aspects of the bifurcation approach to localization, this deformation state is a special one. In particular, the onset of localization for this deformation state is associated with a peak in the stress-strain curve. More generally, the onset of localization, as predicted by the bifurcation analysis, does not correspond to the peak in the stress-strain curve as observed in any simple test. As will be explained in more detail later, localization may be predicted to occur before the peak for favorable conditions but not until well after the peak for unfavorable ones. These differences depend on the nature of the constitutive relation and the deformation state. In this section we develop the bifurcation approach for arbitrary deformation states and for a wide class of constitutive relations.

Again, we consider a homogeneous body subjected to boundary conditions such that one possible solution for the next increment is additional homogeneous deformation. The bifurcation approach seeks conditions for which an alternative solution, corresponding to localized deformation in a planar band, is possible. If so, then the solution to the boundary value problem is not unique and, as for the

layer, the onset of localization is connected with loss of uniqueness. Conversely, this approach cannot predict localized deformation when uniqueness is assured (Hill, 1958; Hueckel and Maier, 1977; Raniecki and Bruhns, 1981; Chambon and Caillerie, 1999). Because the onset of localization corresponds to a particular type of nonuniqueness, localized deformation in a planar band, the occurrence of other nonunique, inhomogeneous deformation fields may, and in general will, precede localization. These *diffuse* or *geometric* modes are associated with the specification of tractions on some portion of the boundary and depend on the geometry of the body (e.g., Hill and Hutchinson, 1975). By extending an argument of Hill (1962), Rice (1976) has shown that the localization condition is a limiting nonuniqueness in the following sense: once the condition for localization is met, it is possible to construct a localized deformation field that violates the sufficient condition for uniqueness even for all-round velocity boundary conditions, although in this case the width of the band must be vanishingly thin.

5.4.1 Constitutive Relation

Consider the class of materials without rate or time dependence (no viscosity) for which the stress rate can be expressed as a function of the rate of deformation:

$$\dot{\sigma}_{ij} = \mathcal{L}_{ij}(D_{kl}), \tag{5.44}$$

where $D_{ij} = (\partial v_i/\partial x_j + \partial v_j/\partial x_i)/2$ is the rate of deformation (i.e., the symmetric part of the velocity gradient $l_{ij} = \partial v_i/\partial x_j$), x_i is the spatial (Eulerian) coordinate, and $\mathcal{L}$ is a function of $\mathbf{D}$ that depends on the state of the material (the stress, the history of the deformation, etc.). For the material behavior to be independent of rate, the relation (5.44) must be positively homogeneous of degree one:

$$\lambda\ \mathcal{L}_{ij}(D_{kl}) = \mathcal{L}_{ij}(\lambda\ D_{kl}) \qquad \text{if} \qquad \lambda \geq 0. \tag{5.45}$$

If deformation or rotation in the solid is large or the stress level is comparable to the tangent moduli of the constitutive law, a derivative of the stress that is invariant to rigid spin, unlike the ordinary material rate used in equation (5.44), should be used in the constitutive relation. One possibility is the Jaumann rate of stress, defined by (e.g., Prager, 1973),

$$\overset{\Delta}{\sigma}_{ij} = \dot{\sigma}_{ij} - \sigma_{il}\, l_{jl} + \sigma_{ik}\, l_{kj} - \sigma_{lj}\, l_{il} + \sigma_{kj}\, l_{ki}. \tag{5.46}$$

There are other possibilities for corotational rates (Mandel, 1966b) but all differ from $\dot{\sigma}_{ij}$ by terms that are linear in the product of stress and velocity gradient. For simplicity, we neglect here the effect of material rotation on the stress time derivative, although this does not introduce any fundamental difficulties. The consequence of this simplification on the localization predictions will be discussed later in Section 5.5.

First, we derive the bifurcation condition for the general relation (5.44). Then we will apply the bifurcation condition to particular cases of different types of constitutive laws: linear, bilinear, multilinear, and thoroughly nonlinear rate laws. A more detailed analysis will be presented for elasto-plastic laws in section 5.5.

5.4.2 Kinematic Condition

The nonhomogeneous solution is assumed to have the form of a planar band with unit normal **n**. Inside the band, the rate of deformation depends only on the position across the band; outside the band, the rate of deformation, denoted by D^0_{ij}, is assumed to remain homogeneous (Figure. 5.6). If the velocity field remains continuous at the instant of band formation, then the rate of deformation inside the band D^1_{ij} must have the form

$$D^1_{ij} = D^0_{ij} + \frac{1}{2}(g_i n_j + g_j n_i), \tag{5.47}$$

where $g = g(x_i n_i)$ is an arbitrary vector, depending in direction and intensity on the position across the band (Hill, 1961b). The form of equation (5.47) requires that the difference field $D^1_{ij} - D^0_{ij}$ has a vanishing intermediate principal value and, thus, contains a plane of zero extension rates. In other words, the deformation in the band is the superposition simple shear and uniaxial deformation and the homogeneous deformation mode. This turns out to be a strong restriction. Consequently, as will be shown later, localization is favored when the prebifurcation, homogeneous field contains a plane of zero extension rates, as in plane strain, and inhibited when it does not, as in axisymmetric deformation.

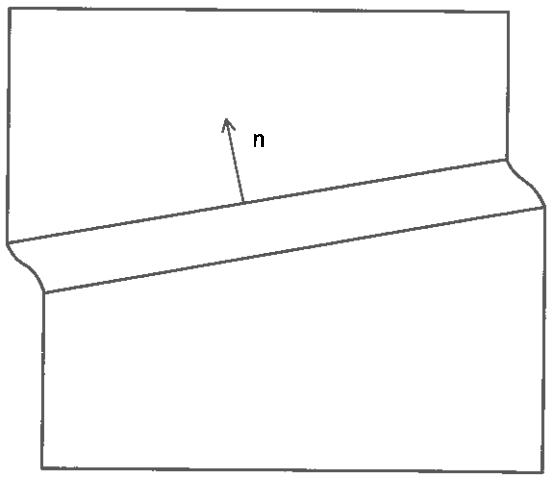

Figure 5.6 ▶ Kinematic condition: planar localization band.

5.4.3 Equilibrium Condition

In each point of the body, the stress field satisfies conditions of quasi-static equilibrium:

$$\sigma_{ij,i} = 0. \tag{5.48}$$

Because the prebifurcation stress field is presumed to be uniform (Rudnicki and Rice, 1975; Rice, 1976), the stress rate at the onset of localization satisfies

$$\dot{\sigma}_{ij,i} = 0. \tag{5.49}$$

This condition is satisfied outside the band because the velocity gradient and, consequently, the stress rate field is homogeneous. Because of equations (5.44) and (5.47), the stress rate in the band depends at most on distance across the band. Therefore equation (5.49) is satisfied inside the band (Rudnicki and Rice, 1975) if the tractions at the interface of the band are continuous:

$$\dot{\sigma}^1_{ij} n_j = \dot{\sigma}^0_{ij} n_j, \tag{5.50}$$

where $\dot{\sigma}^0$ and $\dot{\sigma}^1$ are the stress rates outside and inside the band, respectively.

5.4.4 Bifurcation Condition

Using the constitutive expression (5.44) to replace of the stress rate in the equilibrium condition (5.50) and the kinematic relation yields the bifurcation condition

$$\mathcal{L}_{ij}\left(D^0_{kl} + (1/2)\left(g_k n_l + g_l n_k\right)\right) n_j = \mathcal{L}_{ij}\left(D^0_{kl}\right) n_j. \tag{5.51}$$

An obvious solution of this equation is the trivial one, $\mathbf{g} = 0$, which corresponds to continued homogeneous deformation. Strain localization is possible if there exists a vector $\mathbf{g} \neq 0$ and a unit vector $\mathbf{n}$ (an orientation of the band) that satisfy the relation (5.51). In this case, the vector $\mathbf{g}$ has a physical significance in terms of the difference of the strain rates inside and outside the band. If $\mathbf{g}$ is normal to $\mathbf{n}$, the jump of the rate of deformation is a pure shearing. Otherwise, there is also a volumetric component and, in the limiting case that $\mathbf{g}$ is in the same (or opposite) direction from $\mathbf{n}$, no shearing.

The localization criterion (5.51) clearly depends on the constitutive relation. Consequently, the prediction of localization is strongly dependent on the selection of the mathematical expression of the function $\mathcal{L}$. In the following subsections, the bifurcation condition is examined for several particular types of constitutive laws.

5.4.5 Bifurcation Condition: Particular Cases of Constitutive Laws

The constitutive relation (5.44) is assumed to be a linear relation between the stress rate $\dot{\sigma}$ and the rate of deformation $\mathbf{D}$:

$$\dot{\sigma}_{ij} = L_{ijkl}\, D_{kl}, \tag{5.52}$$

where L_{ijkl} is a fourth-order tensor that may depend on the stress, the accumulated deformation, or history of deformation. If L_{ijkl} is completely independent of the direction $\mathbf{D}$, then the response is incrementally linear (which includes elastic and hypo-elastic laws) (e.g., Truesdell, 1955; Prager, 1973). Then equation (5.52) is a generalization of the one-dimensional nonlinear elastic relation (5.3) or (5.4) in Section 5.3.1 and illustrated in Figure 5.2. More generally, L_{ijkl} may be different for different directions of $\mathbf{D}$ (piecewise linear rate law). For a standard elastic-plastic material, the L_{ijkl} will have one form for $\mathbf{D}$ in directions tending to cause inelastic deformation and another form for directions tending to cause elastic unloading. Thus, the space of rate of deformation $\mathbf{D}$ is divided into two regions by a plane and the response can be described as bilinear. Again, this is illustrated for the one-dimensional case in Figure 5.2, and the sign of the shear-strain increment $d\gamma$ determines whether the response is elastic unloading or further plastic deformation.

Fundamental considerations of the microstructure of materials (e.g., Hill, 1967) suggest that the material response depends continuously on the direction of $\mathbf{D}$. But, because of the complexity of this type of constitutive model, the space of rate of deformation $\mathbf{D}$ is usually regarded as composed of several cones, centered on the origin (Koiter, 1953; Mandel, 1965; Hill, 1967). In each cone, the constitutive relation is incrementally linear:

$$\dot{\sigma}_{ij} = L^{\alpha}_{ijkl}\, D_{kl} \tag{5.53}$$

if $\mathbf{D}$ is contained in a cone $\mathcal{D}^{\alpha}$. Continuous dependence on the direction of $\mathbf{D}$ is the limit of an infinity of cones. Because of the symmetry of σ and $\mathbf{D}$, the tensors L^{α}_{ijkl} satisfy the relations $L^{\alpha}_{ijkl} = L^{\alpha}_{jikl} = L^{\alpha}_{ijlk}$. If, in addition, the relation (5.53) is expressed in work conjugate variables and a rate potential for the material exists (Hill, 1959), the L^{α}_{ijkl} are also symmetric with respect to interchange of the first- and last-pair indices. This last condition is, however, generally too restrictive for geomaterials. For a deformation increment D_{ij} in the interface of two adjacent cones $\mathcal{D}^{\alpha}$ and $\mathcal{D}^{\beta}$, the condition that the stress rate be the same as the interface is approached from either cone requires that

$$L^{\alpha}_{ijkl}\, D_{kl} = L^{\beta}_{ijkl}\, D_{kl}. \tag{5.54}$$

Linear Rate Laws

For an incrementally linear law, the constitutive relation is given by equation (5.52). Then, the bifurcation condition equation (5.51) reduces to:

$$L_{ijkl}\, n_j\, n_l\, g_k = 0. \tag{5.55}$$

A nontrivial solution for $\mathbf{g}$ is possible only if

$$\det[L_{ijkl}\, n_j\, n_l] = 0 \tag{5.56}$$

or, without components,

$$\det[\mathbf{n} \cdot \mathbf{L} \cdot \mathbf{n}] = 0. \tag{5.57}$$

The tensor $\mathbf{n} \cdot \mathbf{L} \cdot \mathbf{n}$ is often called the *acoustic tensor*, because of its connection with the analysis of the propagation of acceleration waves in solids. The condition of localization (5.57) corresponds to the existence of an acceleration wave of vanishing speed of propagation (Hadamard, 1903).

Bilinear Rate Laws

For the incrementally bilinear laws, there exist two cones in the $\mathbf{D}$-space. One of the cones corresponds to the domain of elastic behavior (either because the material is below yield or is unloading) and the other to elasto-plastic behavior (loading of the material). The locus of stress states that forms the boundary between the two domains is the *yield surface*. In general, the yield surface depends on the history of inelastic deformation of the material, which may be expressed in terms of current values of state variables. Implicit in the assumption of two domains of behavior is that the yield surface is smooth and has a uniquely defined normal at each point. An example of a yield surface is shown in Figure 5.7. In this example, the size of elastic domain perpendicular to the axis $\sigma_1 = \sigma_2 = \sigma_3$ increases linearly with the mean stress and can evolve with the loading of the material. A more detailed example is presented in a later section.

Inside the elastic $\mathbf{D}$-domain, the constitutive relation is

$$\dot{\sigma}_{ij} = L^e_{ijkl}\, D_{kl} \tag{5.58}$$

and outside

$$\dot{\sigma}_{ij} = L^{ep}_{ijkl}\, D_{kl}. \tag{5.59}$$

These relations generalize the simple one-dimensional elastic-plastic relation for the layer, as shown in equations (5.12) and (5.13). If an elastic strain energy function exists, $\mathbf{L}^e$ is symmetric with respect to interchange of the first and last pair of indices (in addition to interchange of the first two and last two indices).

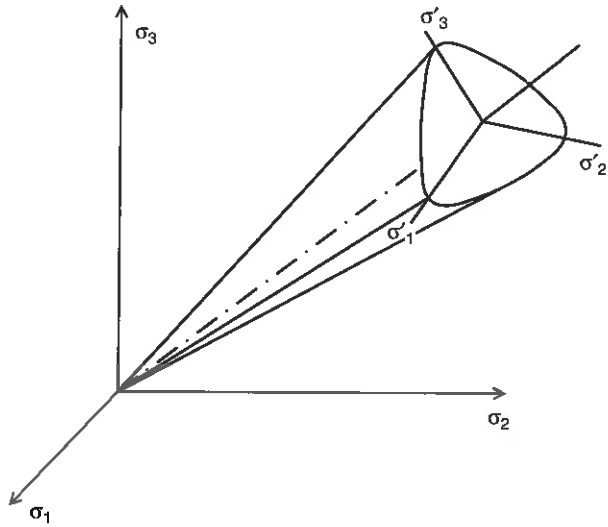

Figure 5.7 ▶ Example of an elastic domain delimited by a smooth surface in the principal stress space. Axes σ_i' are the projections of the principal stress axes on the plane normal to the trisectri x $\sigma_1 = \sigma_2 = \sigma_3$.

If a rate potential for the elastic-plastic response exists, $\mathbf{L}^{ep}$ will satisfy the same symmetries (at least when the constitutive relation is expressed in terms of work conjugate measures of stress and strain). A rate potential will exist if the plastic potential, the gradient of which gives the inelastic portion of the strain rates, is identical with the yield surface (an associated flow law) or, in other words, if the inelastic strain-rate vector is normal to the yield surface (normality). This assumption is generally too restrictive for geological materials and, consequently, their constitutive tensor typically does not satisfy the symmetry $L^{ep}_{ijkl} = L^{ep}_{klij}$. As will be shown later for particular constitutive models, this symmetry has an important effect on predictions for localization.

Comment: If D^+_{ij} is a loading strain increment and $\dot{\sigma}^+_{ij} = L^{ep}_{ijkl}\, D^+_{kl}$ the corresponding stress increment, then for the unloading strain increment $D^-_{ij} = -D^+_{ij}$ the stress increment $\dot{\sigma}^-_{ij} = L^e_{ijkl}\, D^-_{kl}$ is not equal to $-\dot{\sigma}^+_{ij}$ (see Figure 5.2).

The bifurcation condition (5.51) is expressed by

$$L^1_{ijkl}\, n_j\, n_l\, g_k = (L^0_{ijkl} - L^1_{ijkl})\, D^0_{kl}\, n_j, \tag{5.60}$$

where $\mathbf{L}^0$ and $\mathbf{L}^1$ are the constitutive tensors outside and inside the band. Each of these can be equal to $\mathbf{L}^e$ or to $\mathbf{L}^{ep}$ depending on whether the behavior is plastic or elastic.

Comment: In general, the velocity gradient inside the band $\mathbf{D}^1$ may vary with position across the band because of its dependence on $\mathbf{g}$ (see Section 5.4.2). However, the vector $\mathbf{g}$ must be such that $\mathbf{D}^1$ is in the same constitutive cone for any position.

Generally the material deformation inside the band is assumed to be plastic, and the deformation outside the band may be plastic or elastic. If the behavior is plastic on both sides of the band interface (i.e., $\mathbf{L}^0 = \mathbf{L}^1 = \mathbf{L}^{ep}$), the bifurcation is called continuous (Rice and Rudnicki, 1980). In this case equation (5.60) reduces to equation (5.55) and the localization condition becomes identical to equation (5.56) with $\mathbf{L}$ replaced by $\mathbf{L}^{ep}$. Consequently, for plastic loading both inside and outside the band, the conditions for localization in the incrementally bilinear (elastic plastic) solid are identical to those for an incrementally linear solid with moduli equal to those of the elastic-plastic solid for loading.

If elastic unloading occurs outside the band, the bifurcation is discontinuous and equation (5.60) becomes:

$$L^{ep}_{ijkl}\, n_j\, n_l\, g_k = (L^{e}_{ijkl} - L^{ep}_{ijkl})\, D^0_{kl}\, n_j. \tag{5.61}$$

If the tensor $\mathbf{L}^{ep}$ possesses the symmetry $L^{ep}_{ijkl} = L^{ep}_{klij}$, that is, for an associated elasto-plastic model, the discontinuous bifurcation cannot precede the continuous bifurcation. This is an instance of Hill's (1961a) more general result that loss of uniqueness in an actual elastic-plastic solid cannot precede that in a *comparison solid* defined to have the incremental moduli of the actual solid for loading regardless of the direction of $\mathbf{D}$, i.e., a linear rate law (see also Bigoni and Hueckel, 1991, Figure 1), for the detailed relationships between the sufficient condition of uniqueness and localization criteria). If the tensor $\mathbf{L}^{ep}$ is not symmetric, $L^{ep}_{ijkl} \neq L^{ep}_{klij}$, then this result is not guaranteed. Nevertheless, Rice and Rudnicki (1980) and Ottosen and Runesson (1991) have shown that the continuous bifurcation is the lower limit of a range of discontinuous bifurcations for particular classes of nonassociated models. Consequently, only the condition (5.56), with $\mathbf{L}$ replaced by $\mathbf{L}^{ep}$, needs to be analyzed.

Chambon (1986) has shown a related result that does not depend on the symmetry of $\mathbf{L}^{ep}$. He shows that the bifurcation condition for general incrementally bilinear laws is equivalent to the double condition

$$\det[L^{ep}_{ijkl}\, n_j\, n_l] = 0 \qquad \text{or} \qquad \det[L^{e}_{ijkl}\, n_j\, n_l] = 0. \tag{5.62}$$

Because the elasticity tensor is generally positive definite, the second condition on the elastic tensor is never met. Consequently, only the first condition needs to be analyzed, corresponding to continuous bifurcation.

Comment: For constitutive models that are not incrementally continuous in the sense of condition (5.54), the sign of the determinant (5.56, 5.57) may change

from positive to negative without passing through zero. In this case, the bifurcation condition becomes (Borre and Maier, 1989)

$$\det[L^{ep}_{ijkl}\, n_j\, n_l] \leq 0. \tag{5.63}$$

In addition, the predicted orientation of the localization band is not unique, but there exists a range of possible orientations (Larsson and Axelsson, 1994).

Four-Linear Rate Laws

As shown in the preceding subsection, the bifurcation analysis for an incrementally bilinear model reduces, in most practical cases, to that for an incrementally linear model. For incrementally four-linear models, the analysis is more complex. These models are, however, useful for describing the behavior of very porous rocks and soils. In the bilinear, elastic-plastic model, the boundary of the stress states causing elastic deformation, i.e., the yield surface, is a single, smooth surface. In the four-linear models, the elastic domain is bounded by two surfaces that, in general, intersect at a corner. Each surface is often interpreted to reflect the activation of a specific mechanism, for example, shearing and compaction. From the phenomenological point of view, the two surfaces then reflect the observation that inelastic deformation can be caused by purely deviatoric stress (at fixed mean stress) and by purely hydrostatic stress. From a microscopic point of view, the shearing of the material generates sliding and microcracking of grains and can be associated with either dilatancy or compaction. Increasing compressive mean stress can induce plastic deformation by alteration of the asperities of grains and by grain crushing and pore collapse (see Chapter 2). The surface associated with the inelastic compaction causing compressive mean stress is typically called a cap (DiMaggio and Sandler, 1971; Lade, 1977).

If the stress path intersects only one of the two yield surfaces, the bifurcation analysis reduces to that for the bilinear case. Although it might be thought unlikely that the stress path will hit the intersection of the two surfaces, this will, in fact, be typical because of the evolution of the two surfaces. Figure 5.8 shows a stress path that first intersects the shear yield surface. As loading continues along the same path, the shear yield surface moves outward and, eventually, the stress point coincides with the intersection of the shear and the cap surfaces. Hereafter, the stress point will remain at the corner if the stress path has a component in the direction of the outward normal of both surfaces. This example assumes that motion of the two surfaces is independent, but if they are coupled, the evolution will be more complex.

Figure 5.9 illustrates the different response sectors for a four-linear model. The **D**-space is composed of four cones. The first cone $\mathcal{D}^1$ corresponds to the elastic domain (neither of the two plasticity mechanisms is active), the second cone $\mathcal{D}^2$ to one active mechanism, the third cone $\mathcal{D}^3$ to a second active mechanism, and the last cone $\mathcal{D}^4$ to the case for which both inelastic mechanisms are active.

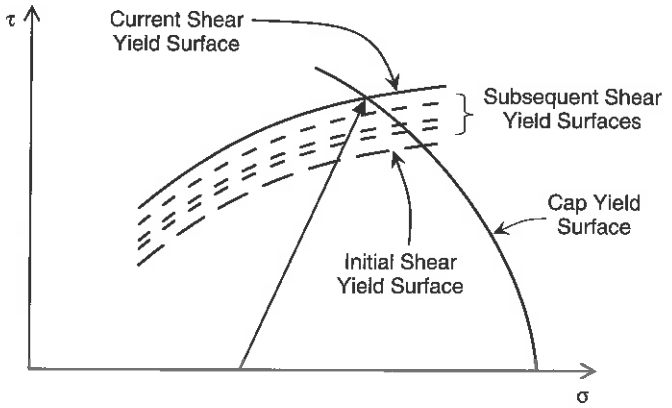

Figure 5.8 ▶ Example of the evolution of the shear yield surface with the loading path (shear hardening) in the τ-σ plane for a two-independent-mechanisms law. σ is the mean stress and τ is the shear stress $|\sigma_{max} - \sigma_{min}|/2$.

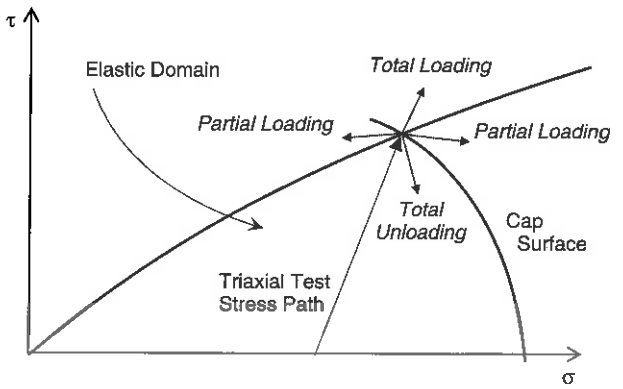

Figure 5.9 ▶ When the stress state is both on the shear yield surface and on the cap yield surface, the rate law is four linear.

The four-linear model and the multilinear models, to be discussed in the next subsection, are examples of the singular yield surfaces examined by Koiter (1953). As noted there, only when the stress point is at the intersection of two or more surfaces does the analysis differ from that for a standard (bilinear) elastic-plastic model. If the tensors $\mathbf{L}^{\alpha}(\alpha \in \{1, .., 4\})$ possess the symmetry $L^{\alpha}_{ijkl} = L^{\alpha}_{klij}$, a variation of the argument used by Koiter (1953) to extend the sufficient condition for uniqueness to the case of singular yield surfaces can be used to demonstrate Hill's (1961a) result that bifurcation in the actual (multilinear) elastic-plastic solid cannot precede that in the comparison solid (also see Sewell, 1973). Here, the comparison solid is defined to have the incremental moduli of the actual solid for $\mathbf{D}$ directed into the most compliant cone, regardless of the actual direction of $\mathbf{D}$.

Of course, failure of the sufficient condition for uniqueness for the comparison solid does not necessarily mean that a bifurcation of any type, not just localization, will actually occur. The occurrence of such a bifurcation requires that a sufficient increment of the homogeneous field $\mathbf{D^0}$ be added so that the resulting $\mathbf{D}$ is directed into the most compliant cone. This is analogous to the result for the buckling of an elastic-plastic column (Shanley, 1947).

When the $\mathbf{L}^\alpha$ are not symmetric ($L^\alpha_{ijkl} \neq L^\alpha_{klij}$), this result is not available and it is necessary to examine all the possibilities for continuous and discontinuous localization to determine which, if any, occurs. Similar to the analysis of the bilinear rate models, Chambon (1986) has shown that for four-linear rate laws, the bifurcation condition can be stated in terms of six problems. The rate of deformation $\mathbf{D^0}$ outside the band is assumed to be in the cone $\mathcal{D}^4$. The condition for a continuous bifurcation is

$$\det[L^4_{ijkl}\, n_j\, n_l] = 0. \tag{5.64}$$

The conditions for a discontinuous bifurcation are the following three:

$$\det[L^\alpha_{ijkl}\, n_j\, n_l] = 0 \qquad \text{with} \qquad \alpha \in \{1, 2, 3\}, \tag{5.65}$$

which imply that it is necessary to check that $(g^c_i\, n_j + g^c_j\, n_i) \in \mathcal{D}^\alpha$, where $\mathbf{g^c}$ is an eigenvector of $\mathbf{n} \cdot \mathbf{L}^\alpha \cdot \mathbf{n}$ associated with the zero eigenvalue. The two remaining problems correspond to the case where $\mathbf{D^1}$ is on the interface of two neighboring cones (e.g., $\mathcal{D}^\alpha$ and $\mathcal{D}^\beta$) with $\{\alpha, \beta\} = \{1, 2\}$ or $\{1, 3\}$:

$$L^\alpha_{ijkl}\, n_j\, n_l\, g_k = (L^4_{ijkl} - L^\alpha_{ijkl})\, D^0_{kl}\, n_j \qquad \text{for} \qquad i \in \{1, 2, 3\}. \tag{5.66}$$

In addition to these three equations for g_i, they must also satisfy the constraint that $[D^0_{ij} + (1/2)\,(g_i\, n_j + g_j\, n_i)]$ has to be on the interface $\mathcal{D}^\alpha \cap \mathcal{D}^\beta$ (i.e., $a^{\alpha/\beta}_{ij}\,(D^0_{ij} + g_i\, n_j) = 0$, where $a^{\alpha/\beta}$ is the tensor that defines the limit between the two cones). This system of four equations for the three unknown g_i reduces to the condition that a fourth-order determinant be zero (as discussed by Chambon [1986], this determinant can be easily reduced to a third-order determinant).

The cases for which $\mathbf{D^0}$ belongs to another cone also need to be examined, although the possibility of elastic behavior can be ruled out. Each of these conditions is no more complicated than the condition for a linear law.

Multilinear Rate Laws and Nonlinear Rate Laws

Incrementally multilinear models have been developed for a better description of geological material. For example, Darve and Labanieh (1982) developed an incrementally eight-linear model for soils. The complete bifurcation analysis requires checking multiple problems, as for the previous case; otherwise, some hypothesis on the magnitude of $g_i\, n_j$ with respect to D^0_{ij} is necessary.

On the other hand, most microstructure-based models of material behavior (e.g., Hill, 1967; Rice, 1976) imply a thoroughly nonlinear incremental response.

Generally, nonlinear models require numerical computation to find the critical onset of bifurcation, but an analytical condition can be derived that by assuming that the magnitude of $g_i\, n_j$ is small enough so that the response law can be linearized about the direction of D^0_{ij}. In this case, deformation theories (Budiansky, 1959; Christoffersen and Hutchinson, 1979) can provide a good approximation of the response. Alternatively, the magnitude of $g_i\, n_j$ can be assumed to be much larger than that of D^0_{ij}. For some particular formulations of nonlinear models, it is possible to treat the complete problem without simplifying hypotheses (Chambon et al., 2000). An interesting result of this type of analysis is that the bifurcation of the complete problem generally occurs earlier in the loading process than predicted for the linearized problem. Here, we describe an example of such a formalism, the so-called hypoplastic models (Chambon, 1989; Kolymbas, 1991).

The relation between the stress rate and the rate of deformation (there is no distinction between elastic and plastic deformation) is expressed by

$$\dot{\sigma}_{ij} = h_{ij}(\sigma_{mn}, D_{kl}). \tag{5.67}$$

The function **h** can be represented according to the general representation theorem (Wang, 1970). This decomposition, after simplifications (Kolymbas, 1991), is rearranged as the sum of terms that are linear and nonlinear with respect to **D**:

$$\dot{\sigma}_{ij} = L_{ijkl} D_{kl} + N_{ij} \|\mathbf{D}\|, \tag{5.68}$$

where $\|\mathbf{D}\| = \sqrt{D_{mn}\, D_{mn}}$ is the Euclidean norm of the rate of deformation, **L** and **N** are a fourth-order tensor and second-order tensor that depend on the state of the material (including the stress σ_{mn}), respectively. The incremental nonlinearity of the law comes from the last term on the right side and the relation (5.68) is valid for any direction of **D**. Recall that for the incrementally bilinear law (see page 246) the sum of the stress rates due to oppositely directed deformation rates $D^-_{kl} = -D^+_{kl}$ is $(L^{ep}_{ijkl} - L^{e}_{ijkl})\, D^+_{kl}$. For the relation (5.68), this sum is $2\, N_{ij} \|\mathbf{D}^+\|$.

We apply the bifurcation condition to this class of hypoplastic model, following the development of Chambon et al. (1994; 2000). The rate of deformation inside the band $\mathbf{D^1}$ is assumed to be linked to the rate of deformation outside the band $\mathbf{D^0}$ by the relation (5.47). For convenience, the intensity of the rate of deformation inside the band is defined by

$$\|\mathbf{D^1}\| = \|\mathbf{D^0}\|(1 + r), \tag{5.69}$$

where r is a scalar. Consequently, the bifurcation condition (5.51) becomes

$$(L_{ijkl}\, n_j\, n_l)\, g_k + r\, N_{ij}\, n_j\, \|\mathbf{D^0}\| = 0, \tag{5.70}$$

with the additional constraint on g_k from equation (5.69)

$$\|D^0_{kl} + \frac{1}{2}(g_k\, n_l + g_l\, n_k)\| = \|\mathbf{D^0}\|\,(1 + r). \tag{5.71}$$

Bifurcation is possible if there exist a vector $\mathbf{g} \neq 0$, a unit normal vector $\mathbf{n}$, and a scalar $r \geq -1$ for which the previous equations (5.70) and (5.71) are satisfied.

Two cases are possible depending on whether the matrix $\mathcal{L}_{ik} = L_{ijkl}\, n_j\, n_l$ is invertible.

i) If $\mathcal{L}_{ik}$ is invertible, then

$$g_k = -r\mathcal{L}_{ki}^{-1} N_{ij} n_j \tag{5.72}$$

is the solution of equation (5.70). Substitution into equation (5.71) reveals that bifurcation is possible if there exist a nonvanishing unit vector $\mathbf{n}$ and a scalar $r \geq -1$ such that

$$\|D_{kl}^0 - \frac{1}{2}(r\mathcal{L}_{ki}^{-1} N_{ij} n_j n_l + r\mathcal{L}_{li}^{-1} N_{ij} n_j n_k)\| = \|\mathbf{D^0}\|\,(1+r). \tag{5.73}$$

One bifurcation condition is

$$\|\frac{1}{2}(\mathcal{L}_{ki}^{-1} N_{ij} n_j n_l + \mathcal{L}_{li}^{-1} N_{ij} n_j n_k)\| = 1. \tag{5.74}$$

If this condition is met, the solution r is unbounded. This means that the ratio of the intensity of the rate of deformation inside the band to that outside is infinite, or in other words, the material outside the band responds rigidly compared with the material inside the band.

ii) If $\mathcal{L}_{ik}$ is not invertible, then there exists a vector direction $\mathbf{g}$ such that $\mathcal{L}_{ik}\, g_k = 0$, and so equations (5.70) and (5.71) are satisfied if $r = 0$. Thus, the other bifurcation condition is

$$\det[L_{ijkl}\, n_j\, n_l] = 0 \tag{5.75}$$

and the norm of the rate of deformation inside the band is equal to that outside the band.

The condition (5.74) is generally met before equation (5.75) during a loading process (Chambon et al., 1994). Note that if the evolution of constitutive tensors $\mathbf{L}$ and $\mathbf{N}$ is not continuous, the norm in the bifurcation condition (5.74) should be greater than one.

It is also interesting to analyze the bifurcation condition (5.74) for the nonlinear rate law (5.68) in the case of a directional linearization. If one considers that a thoroughly nonlinear relation corresponds to a rate law with an infinity of cones (i.e., some cones in the space of the rate of deformation are reduced to a single direction), it is possible to express the law for each cone (each direction) by a

linear relation. For any rate of deformation such that $D_{ij} = u_{ij} \|\mathbf{D}\|$, where u_{ij} is considered as a given direction of the rate of deformation ($\|\mathbf{u}\| = 1$), the previous nonlinear relation (5.68) can be replaced by the linear relation

$$\begin{aligned} \dot{\sigma}_{ij} &= \ell_{ijkl}(u_{mn})\, D_{kl} \\ &= [L_{ijkl} + N_{ij} u_{kl}]\, D_{kl}. \end{aligned} \tag{5.76}$$

The bifurcation condition (5.74) is equivalent to the existence of a direction u_{ij} of rate of deformation such that (Chambon et al., 2000)

$$\det[\ell_{ijkl}(u_{mn})\, n_j\, n_l] = 0. \tag{5.77}$$

5.5 Constitutive Models

5.5.1 Elasto-Plastic Models

We develop here a class of nonassociated elasto-plastic models. The yield surface is the boundary of the domain of elastic behavior and can evolve during the loading process. This yield surface is assumed to be smooth (incremental bilinearity assumption). The constitutive equations are presented and the bifurcation analysis is applied to these models.

Constitutive Equations

The rate of deformation is the sum of reversible (elastic) and irreversible (plastic) contributions:

$$D_{ij} = D^e_{ij} + D^p_{ij}. \tag{5.78}$$

The reversible rate of deformation and the stress rate are related by a linear rate law:

$$D^e_{ij} = M_{ijkl}\, \dot{\sigma}_{kl}, \tag{5.79}$$

where $\mathbf{M}$ is the elastic compliance tensor that has the symmetries

$$M_{ijkl} = M_{jikl} = M_{ijlk} = M_{klij}. \tag{5.80}$$

The last applies for a hyperelastic relation (assuming the existence of an elastic potential).

The yield surface is defined by the following equation (see Chapter 1):

$$F(\sigma_{ij}, q^{(n)}) = 0, \tag{5.81}$$

where σ_{ij} is the effective stress and $q^{(n)}$ are state variables that keep track of the history of the deformation. Similarly, the plastic potential is defined by

$$G(\sigma_{ij}, q^{(n)}) = 0. \tag{5.82}$$

During a loading process, a plastic strain rate exists if the state of stress is on the yield surface (i.e., $F = 0$) and if, in case of plastic hardening, the stress rate is directed to the outside of the yield surface. The latter condition is expressed as $d\sigma_{ij}\,(\partial F/\partial\sigma_{ij}) > 0$, where $\partial F/\partial\sigma_{ij}$ is the outward normal to the yield surface. Consequently, the yield surface can follow the current stress point (i.e., $\dot{F} = 0$).

Following Hill (1950), Mròz (1963), and Mandel (1966a), the direction of the plastic rate of deformation is given by the normal to the plastic potential, $\partial G/\partial\sigma_{ij}$ and is proportional to the product of the stress rate and the normal to the yield surface:

$$D_{ij}^{p} = \frac{1}{H}\left(\frac{\partial F}{\partial\sigma_{kl}}\,\dot{\sigma}_{kl}\right)\frac{\partial G}{\partial\sigma_{ij}}, \tag{5.83}$$

where H is a plastic coefficient[3]. For hardening, perfect or softening plasticity, H is positive, zero, or negative, respectively. Generally H decreases with inelastic deformation.

If F (equation [5.81]) and G (equation [5.82]) are assumed to be isotropic functions of the stress tensor, they depend only on the three invariants of the stress tensor and scalar measures of the hardening or inelastic deformation. In this case, the plastic rate of deformation is coaxial with the stress; that is, the principal directions of the plastic rate of deformation and the stress tensor are identical. The relation of the rate of deformation, plastic potential, and yield surface is illustrated in Figure 5.10.

If $F = G$, the plastic strain rate is normal to the yield surface and the model is said to be *associated* or to obey *normality*. Associated models are widely used for metals, but for geological materials, experimental evidence shows that, in general, $F \neq G$.

Comment: Anisotropic hardening, corresponding to an anisotropic plastic behavior of the material, is possible if either F or G depends on a tensor hardening parameter, α_{ij}, rather than only a scalar. In this case, the plastic rate of deformation is not coaxial with the stress. One possibility is kinematic hardening that depends only on the difference $\sigma_{ij} - \alpha_{ij}$. In this case, α_{ij} defines the center of the yield surface in stress space, and its evolution expresses the translation of the yield surface.

Substituting equations (5.79) and (5.83) into equation (5.78) yields an expression for the total rate of deformation

$$D_{ij} = M_{ijkl}\,\dot{\sigma}_{kl} + \frac{\alpha}{H}\,(Q_{kl}\,\dot{\sigma}_{kl})\,P_{ij}, \tag{5.84}$$

where $\mathbf{P}$ and $\mathbf{Q}$ are defined by

$$P_{ij} = \frac{\partial G}{\partial\sigma_{ij}} \quad \text{and} \quad Q_{ij} = \frac{\partial F}{\partial\sigma_{ij}}, \tag{5.85}$$

[3]A more detailed description of the flow rule is given in Chapter 1.

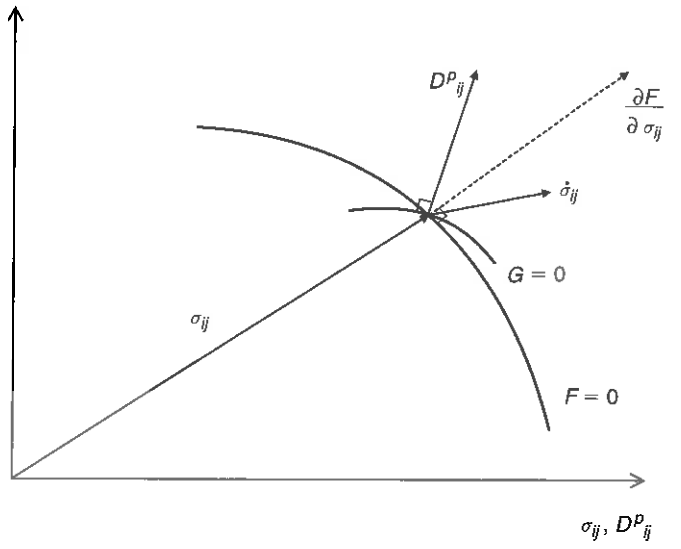

Figure 5.10 ▶ The plastic rate of deformation is normal to the plastic potential ($G = 0$) when the stress rate is directed to the outside of the yield surface ($F = 0$).

and α takes on different values for plastic loading

$$\alpha = 1 \quad \text{if} \quad F = 0 \quad \text{and} \quad \dot{F} = 0 \tag{5.86}$$

and elastic unloading

$$\alpha = 0 \quad \text{if} \quad F < 0 \quad \text{or} \quad F = 0 \quad \text{and} \quad \dot{F} < 0. \tag{5.87}$$

Inverting the expression (5.84) yields the stress rate in terms of the rate of deformation

$$\dot{\sigma}_{ij} = E_{ijkl}\, D_{kl} - \frac{\alpha'}{h}\,(Q_{mn}\, E_{mnkl}\, D_{kl})\, E_{ijuv}\, P_{uv}, \tag{5.88}$$

where $h = H + Q_{ij}\, E_{ijkl}\, P_{kl}$ (assumed to be positive for no snap-back [Nguyen and Bui, 1974]), $\mathbf{E}$ is the elastic stiffness tensor having the same symmetry properties as $\mathbf{M}$ in equation (5.80), and α' is one for plastic loading and zero for elastic unloading:

$$\begin{aligned} \alpha' = 1 \quad &\text{if} \quad F = 0 \quad \text{and} \quad Q_{mn}\, E_{mnkl}\, D_{kl} \geq 0 \\ \alpha' = 0 \quad &\text{if} \quad F < 0 \quad \text{or} \quad F = 0 \quad \text{and} \quad Q_{mn}\, E_{mnkl}\, D_{kl} < 0. \end{aligned} \tag{5.89}$$

Thus, the constitutive tensor that gives the stress rate in terms of the rate of deformation is

$$L_{ijkl} = E_{ijkl} - \frac{\alpha'}{h}\, E_{ijuv}\, P_{uv}\, Q_{mn}\, E_{mnkl}. \tag{5.90}$$

Note that, in general, the constitutive tensor $\mathbf{L}$ is symmetric (i.e., $L_{ijkl} = L_{klij}$) only for the associated models.

Bifurcation Analysis

The bifurcation analysis reduces to a condition that the determinant of the acoustic tensor must vanish. This requires finding a hardening modulus H and an orientation of the band that satisfy the condition (5.55) in Section 5.4.5.

Substituting the constitutive tensor (5.90) into equation (5.55) yields

$$n_j\, E_{ijkl}\, n_l\, g_k - (1/h)\, n_j\, E_{ijuv}\, P_{uv}\, Q_{mn}\, E_{mnkl}\, n_l\, g_k = 0 \tag{5.91}$$

or more concisely,

$$(\mathbf{n}\cdot\mathbf{E}\cdot\mathbf{n})_{ik}\, g_k - (1/h)\, (\mathbf{n}\cdot\mathbf{E}:\mathbf{P})_i\, (\mathbf{Q}:\mathbf{E}\cdot\mathbf{n})_k\, g_k = 0, \tag{5.92}$$

where $(\mathbf{E}:\mathbf{P})_{ij} = E_{ijkl}\, P_{kl}$ and $(\mathbf{Q}:\mathbf{E})_{ij} = Q_{kl}\, E_{klij}$.

Ottosen and Runesson (1991) solved equation (5.92) by examining the spectral properties of the characteristic tensor and considering the related eigenvalue problem: $(\mathbf{n}\cdot\mathbf{L}\cdot\mathbf{n})\cdot\mathbf{y} = \lambda\,(\mathbf{n}\cdot\mathbf{E}\cdot\mathbf{n})\cdot\mathbf{y}$. Two eigenvalues $\lambda = 1$ correspond to a bifurcation in the elastic regime, which is generally excluded for the materials studied here. The third eigenvalue (which is the smallest) corresponds to the case exhibited by Rice (1976). If $(\mathbf{n}\cdot\mathbf{E}\cdot\mathbf{n})$ is invertible, then equation (5.92) can be rewritten as

$$g_s = (1/h)(\mathbf{n}\cdot\mathbf{E}\cdot\mathbf{n})^{-1}_{si}\, (\mathbf{n}\cdot\mathbf{E}:\mathbf{P})_i\, (\mathbf{Q}:\mathbf{E}\cdot\mathbf{n})_k : g_k = 0. \tag{5.93}$$

The nontrivial solution is

$$g_s = \gamma\, [(\mathbf{n}\cdot\mathbf{E}\cdot\mathbf{n})^{-1}\cdot(\mathbf{n}\cdot\mathbf{E}:\mathbf{P})]_s, \tag{5.94}$$

where γ is an arbitrary value. Substituting equation (5.94) into equation (5.93) yields an expression for h and then

$$H = -(\mathbf{Q}:\mathbf{E}:\mathbf{P}) + (\mathbf{Q}:\mathbf{E}\cdot\mathbf{n})_k\, (\mathbf{n}\cdot\mathbf{E}\cdot\mathbf{n})^{-1}_{ki}\, (\mathbf{n}\cdot\mathbf{E}:\mathbf{P})_i. \tag{5.95}$$

If there exists a vector $\mathbf{n}$ for which equation (5.95) is satisfied, localization is possible. Because the hardening modulus generally decreases with the plastic strain, and localization is generally not possible in the elastic regime, Rudnicki and Rice (1975) argued that the first possible localization during a loading process corresponds to the greatest plastic modulus H satisfying this condition, denoted here by H^c. Finding H^c requires determining the vector $\mathbf{n}^c$ that maximizes the expression (5.95).

Comment: For isotropic elasticity and associated plasticity, Rice (1976) showed that the localization is possible only in the softening regime (i.e., H^c is necessarily negative), at least when the effect of material rotation on the stress rate is neglected. In the general case, the absolute value of the hardening modulus at the incipient localization is small. Consequently, at localization the tangent moduli in the constitutive relation (5.44) are also small and the terms entering from use of the corotational stress rate in equation (5.46) can be significant. Analyses including these terms made for particular models (e.g., Hill and Hutchinson, 1975; Rudnicki and Rice, 1975) suggest that they cause localization to occur slightly earlier than predicted when neglecting them.

Rudnicki and Rice (1975) used Lagrange's multiplier method to determine H^c by maximizing (equation [5.95]) for a particular model (to be described in detail later). Perrin and Leblond (1993) determined H^c for the same model by using Mohr circles, in the spirit of the geometrical analysis of Benallal and Comi (1996). To treat the general model presented previously, Ottosen and Runesson (1991) and also Bigoni and Hueckel (1991) used Lagrange's multiplier method (with the assumption that **P** and **Q** have identical principal directions).

The expression for H^c depends on the type of the yield surface and plastic potential, and also on the stress state. Several typical surfaces are presented next.

Common Yield Surfaces

The yield surfaces to be discussed here are all isotropic and, hence, can be expressed in terms of the stress invariants. The first invariant[4] is defined by

$$I_1 = tr(\sigma_{ij}) = \sigma_{ii}, \tag{5.96}$$

where we adopt the convention that tensile stress is positive. This invariant corresponds physically to 3 times the mean stress. The second invariant is defined by

$$\begin{aligned} I_2^2 &= 3\,\bar{\sigma}_{ij}\,\bar{\sigma}_{ij} \\ &= (\sigma_1 - \sigma_2)^2 + (\sigma_2 - \sigma_3)^2 + (\sigma_3 - \sigma_1)^2, \end{aligned} \tag{5.97}$$

where σ_k are the principal stresses such that $\sigma_1 > \sigma_2 > \sigma_3$, $\bar{\sigma}_{ij}$ is the deviatoric stress tensor defined by $\bar{\sigma}_{ij} = \sigma_{ij} - (I_1/3)\delta_{ij}$, and δ_{ij} is the Kronecker delta ($\delta_{ij} = 1$ if $i = j$; if not, $\delta_{ij} = 0$). The trace of the deviatoric tensor is of course zero. The second stress invariant physically represents the shear stress intensity. The third invariant is defined by

$$I_3 = \det(\sigma_{ij}). \tag{5.98}$$

[4]Several expressions of the three invariants exist. We present a possible expression for each one.

This third invariant physically represents, among other things, the type of stress state (axisymmetric stress state, plane stress state, etc.).

Coulomb Surface This yield surface is defined by

$$F(\sigma_{ij}) \equiv \sigma_1 - \sigma_3 + (\sigma_1 + \sigma_3)\,\sin\varphi - 2\,C\cos\varphi = 0, \tag{5.99}$$

where φ is the so-called friction angle and C is the cohesion. (Although it is possible to express the condition in terms of the invariants [e.g., Lubliner 1990], the result is cumbersome.) The friction angle is constant for any stress state. The surface is not smooth because it has corners for the axisymmetric stress states. The intersection of the surface with a plane Π normal to the trisectrix of the principal stress axes (i.e., $\sigma_1 = \sigma_2 = \sigma_3$) is shown in Figure 5.11.

Drucker-Prager Surface The Drucker-Prager surface (Drucker and Prager, 1952) is a simple smooth surface given by

$$F(\sigma_{ij}) \equiv I_2 + I_1 \tan\phi - C_{DP} = 0, \tag{5.100}$$

where ϕ an alternative friction angle and C_{DP} represents a cohesive component. Because the surface does not depend on the third invariant, its shape is a right circular cone with axis $\sigma_1 = \sigma_2 = \sigma_3$ (see Figure 5.11) and apex semi-angle ϕ. For cohesionless materials, the Drucker-Prager and Coulomb surfaces will agree in axisymmetric compression stress state ($\sigma_1 = \sigma_2 > \sigma_3$) if

$$\sin\varphi^C = \frac{\sigma_3 - \sigma_1}{\sigma_1 + \sigma_3} = \frac{3\tan\phi}{2\sqrt{2} + \tan\phi}$$

and for an axisymmetric extension stress state ($\sigma_1 > \sigma_2 = \sigma_3$) if

$$\sin\varphi^E = \frac{\sigma_3 - \sigma_1}{\sigma_1 + \sigma_3} = \frac{3\tan\phi}{2\sqrt{2} - \tan\phi}.$$

These equations suggest that for a Drucker-Prager surface, the friction angle for extension stress state φ^E is higher than the friction angle for compression stress state φ^C. In addition, the second of them indicates that $\tan\phi$ has to be smaller than $\sqrt{2}/2$ for cohesionless materials. The Drucker-Prager surface generally overestimates the extension friction angle with respect to the compression friction angle (e.g., Matsuoka and Nakai, 1982, from experimental measurements in a sand at failure).

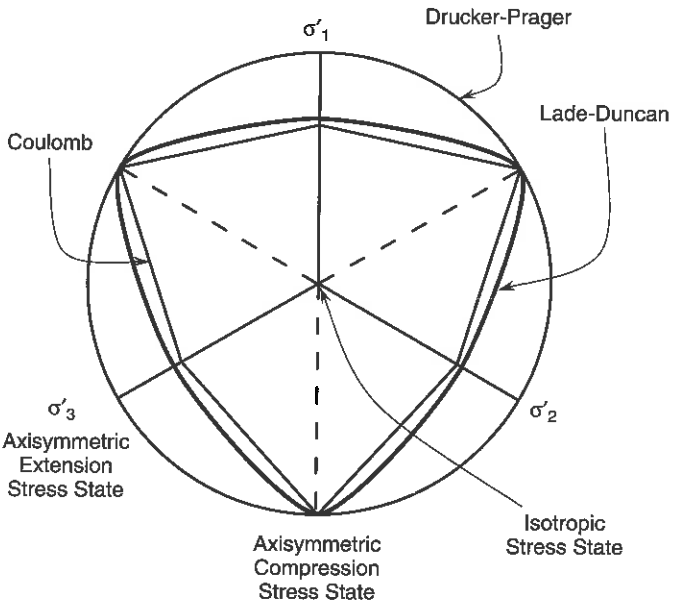

Figure 5.11 ▶ Traces of yield surfaces in a plane Π normal to the trisectrix to the principal stress axes. Axes σ_i' are the projections of the principal stress directions on the plane Π. They represent the axisymmetric extension stress states. The dotted axes represent the axisymmetric compression stress states.

Other smooth yield surfaces that include dependence on the third invariant include those of Lade and Duncan (1975) and Van Eekelen (1980).

Lade-Duncan Surface The yield surface and plastic potential used by Lade and Duncan (1975) for noncohesive soils are expressed by the relation

$$F(\sigma_{ij}) \equiv I_1^3 - \kappa\, I_3 = 0, \tag{5.101}$$

where κ defines the aperture of the cone and is larger than 27 (which corresponds to the isotropic stress state). The trace of the cone in a plane Π normal to the trisectrix of the principal stresses frame is presented in Figure 5.11. In a subsequent paper, Lade (1977) adopted a nonconic yield surface, with a similar trace in the plane Π:

$$F(\sigma_{ij}) \equiv \left(\frac{I_1^3}{I_3} - 27\right)(I_1/p_a)^m = 0, \tag{5.102}$$

where p_a is the atmospheric pressure. In addition, he used a spherical cap surface to describe the compaction induced by the mean stress increase. Such a combination of two yield surfaces constitutes an incrementally four-linear model.

Van Eekelen Surface Van Eekelen (1980) proposed a surface similar to that used by Lade and Duncan (1975):

$$F(\sigma_{ij}) \equiv a\, I_1 \left(1 + b\, \frac{I_3}{I_2^3}\right)^n - I_2 = 0, \tag{5.103}$$

where a, b, and n control the shape of the surface in plane Π (the shape can be made more or less close to the Coulomb or the Drucker-Prager surfaces). This surface has the additional advantage that the friction angles in axisymmetric compression and extension stress states can be expressed independently.

5.5.2 A Drucker-Prager Model for Porous Rocks

To illustrate the previous bifurcation analysis applied to the nonassociated elasto-plastic models, we present here in detail the model used in Rudnicki and Rice (1975). This model is the most general type with a smooth yield surface and dependence of the yield and plastic potential surfaces on the first and second stress invariants. Although the model was originally focused on applications to low-porosity rocks, more recently it has been interpreted for high-porosity rocks. We discuss also in detail the predictions of the analysis with respect to some physical parameters of the model.

The yield surface and the plastic potential are Drucker-Prager type of surfaces that are coaxial and nonassociated with respect to the mean stress:

$$tr(\mathbf{P}) \neq tr(\mathbf{Q}) \qquad \text{but} \qquad \bar{\mathbf{P}} = \bar{\mathbf{Q}}, \tag{5.104}$$

where $\bar{\mathbf{P}}$ and $\bar{\mathbf{Q}}$ are the deviatoric tensors of $\mathbf{P}$ and $\mathbf{Q}$ defined in equation (5.84). The yield surface can be expressed by

$$F(\sigma_{ij}, q^{(n)}) \equiv \bar{\tau} + m(\sigma, q^{(n)}) - C_{DP} + f(q^{(n)}) = 0, \tag{5.105}$$

where $\bar{\tau}$ is the von Mises equivalent stress defined as $\bar{\tau} = I_2/\sqrt{6}$, $\sigma = I_1/3$ is the mean stress, and the $q^{(n)}$ are a collection of internal variables that keep track of the history of the plastic deformation. The expression for $\mathbf{Q}$ in equation (5.85) is then

$$Q_{ij} = \frac{\bar{\sigma}_{ij}}{2\bar{\tau}} + \frac{1}{3}\,\mu\,\delta_{ij}, \tag{5.106}$$

where $\mu = \partial m(\sigma, q^{(n)})/\partial\sigma$ is the local slope of the yield surface in the $\bar{\tau}$ versus σ plane. The plastic potential can be expressed in a similar form:

$$G(\sigma_{ij}, q^{(n)}) \equiv \bar{\tau} + b(\sigma, q^{(n)}) - C'_{DP} + g(q^{(n)}) = 0. \tag{5.107}$$

The expression for $\mathbf{P}$ in equation (5.85) then yields

$$P_{ij} = \frac{\bar{\sigma}_{ij}}{2\bar{\tau}} + \frac{1}{3}\,\beta\,\delta_{ij}, \tag{5.108}$$

where $\beta = \partial b(\sigma, q^{(n)})/\partial\sigma$. If $\beta = \mu$, the model is associated because, in this case, $\mathbf{P} = \mathbf{Q}$. The factor β can be recognized as the ratio between the volumetric part of the rate of deformation (D^p_{kk}) and the shearing intensity ($2\,\bar{D}^p_{ij}\,\bar{D}^p_{ij}$)$^{1/2}$.

In their original presentation, Rudnicki and Rice (1975) focused on low-porosity rocks. In this case, μ can be interpreted as a friction coefficient and β as a dilatancy factor. There is, however, nothing in the formulation that restricts μ and β to be positive. Olsson (1999) and Issen and Rudnicki (2000) have shown that negative values can be appropriate for high-porosity rocks. For such rocks, it is appropriate introduce a cap that closes the yield surface on the hydrostatic stress axis in order to describe the compacting behavior. As explained in more detail by Rudnicki (2000; 2001) and as shown in Figure 5.12, values of μ and β are negative for stress states on the cap.

The elastic stiffness tensor for isotropic behavior (see Chapter 1) is given by

$$E_{ijkl} = G(\delta_{ik}\,\delta_{jl} + \delta_{il}\,\delta_{jk}) + \left(K - \frac{2\,G}{3}\right)\delta_{ij}\,\delta_{kl}, \tag{5.109}$$

where $K = 2G(1+\nu)/3(1-2\nu)$ is the (drained) bulk modulus, G is the shear modulus, and ν the Poisson coefficient. The constitutive tensor given in equation (5.90) that links the stress rate and the rate of deformation can then be expressed as

$$L_{ijkl} = G(\delta_{ik}\delta_{jl} + \delta_{il}\delta_{jk}) + \left(K - \frac{2}{3}G\right)\delta_{ij}\delta_{kl} - \frac{\left(GN_{ij} + K\beta\delta_{ij}\right)\left(GN_{kl} + K\mu\delta_{kl}\right)}{H + G + \mu\beta K}, \tag{5.110}$$

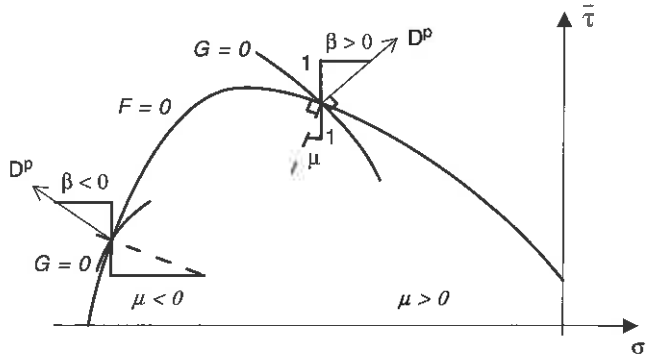

Figure 5.12 ▸ Yield surface for a porous rock. For low mean stress, the behavior is frictional and dilatant (plastic deformation), μ and β are positive. For higher mean stress, the behavior is compacting, μ and β are negative.

where $N_{ij} = \bar{\sigma}_{ij}/\bar{\tau}$ is a normalized deviatoric stress tensor ($1/2\, N_{ij}\, N_{ij} = 1$). Of course, the rightmost term of equation (5.110) is dropped for elastic unloading. With equations (5.109), (5.106), and (5.108), the general expression for the hardening modulus satisfying the bifurcation condition (5.95) becomes

$$H = \frac{(G\, n_i N_{ij} n_j + \mu K)(G\, n_k N_{kl} n_l + \beta K)}{(\frac{4}{3}G + K)} + G\,[(n_i N_{ij} n_k N_{kj}) - (n_i N_{ij} n_j)^2] - (G + \mu\beta K). \tag{5.111}$$

The expression for the critical hardening modulus H^c that maximizes equation (5.111) is different depending on whether the normal to the plane of localization is perpendicular to one or two of the principal stress axes. (Although there is a stationary value of equation [5.111] for which the normal has nonzero components in all the principal stress directions, it occurs only when the stress state is hydrostatic and the resulting value of the hardening modulus is so negative as to be practically improbable.) If the band normal is perpendicular to the intermediate principal stress direction (so that the plane of the band contains the maximum shear stress), the critical value of the hardening modulus is given by (Rudnicki and Rice, 1975)

$$\frac{H^c}{G} = \frac{1+\nu}{9(1+\nu)}(\beta - \mu)^2 - \frac{1+\nu}{2}\left[N + \frac{1}{3}(\beta + \mu)\right]^2, \tag{5.112}$$

where N is the intermediate principal value of N_{ij} and varies from $-1/\sqrt{3}$ for axisymmetric extension ($\sigma_1 = \sigma_2 > \sigma_3$) to $1/\sqrt{3}$ for axisymmetric compression ($\sigma_1 > \sigma_2 = \sigma_3$). The value $N = 0$ corresponds to deviatoric pure shear ($\sigma_1 = -\sigma_3, \sigma_2 = 0$). The expression (5.112) would include additional terms of order, $\bar{\tau}/G$, if the constitutive relation had used a stress rate invariant to rigid spins. Rudnicki and Rice (1975) give the first-order correction for the Jaumann stress rate. The angle between the band normal and σ_3 direction (the most compressive stress direction), can be expressed as (Rudnicki and Olsson, 1998)

$$\theta^c = \frac{\pi}{4} + \frac{1}{2}\arcsin\alpha, \tag{5.113}$$

where

$$\alpha = \frac{(2/3)(1+\nu)(\beta+\mu) - N(1-2\nu)}{\sqrt{4 - 3N^2}}. \tag{5.114}$$

Figure 5.13 shows a typical variation of the hardening modulus satisfying $\det(\mathbf{n}\cdot\mathbf{L}\cdot\mathbf{n}) = 0$ with respect to the orientation of the band.

The solution of equations (5.112) and (5.113) gives the largest critical value of the hardening modulus and band angle when the magnitude of the sum $\mu + \beta$ is relatively small and, in particular, when

$$(1-2\nu)N - \sqrt{4-3N^2} \le \frac{2}{3}(1+\nu)(\beta+\mu) \le (1-2\nu)N + \sqrt{4-3N^2}. \tag{5.115}$$

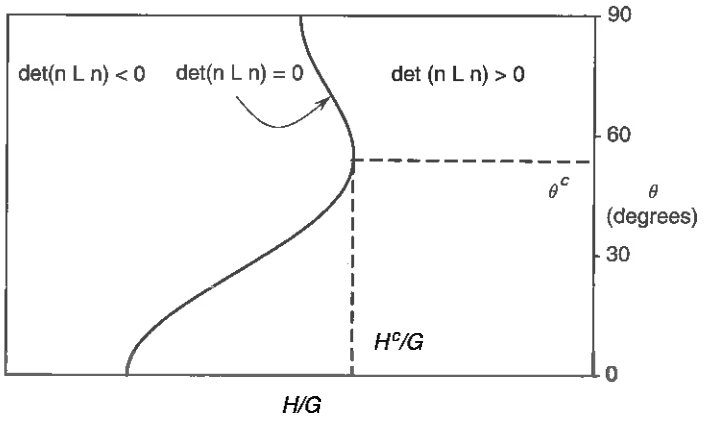

Figure 5.13 ▶ Typical evolution of the hardening modulus satisfying $\det(\mathbf{n}\cdot\mathbf{L}\cdot\mathbf{n}) = 0$ with respect to the band orientation angle θ. The localization in the domain of $\det(\mathbf{n}\cdot\mathbf{L}\cdot\mathbf{n}) > 0$ is not possible. When H decreases with the plastic strain, the first possible localization corresponds to H^c. The example is valid in the range of $\mu+\beta$ defined in equation (5.115). The value of θ^c depends on μ and β, and outside the previous range, θ^c is equal to 0 or $\pi/2$.

Values of $\mu+\beta$ satisfying equation (5.115) correspond to values of the critical angle in the range $0 \le \theta^c \le \pi/2$. Although Rudnicki and Rice (1975) focused on low-porosity rocks with values satisfying equation (5.115), they did not correctly identify this constraint. Perrin and Leblond (1993) have noted this correction and given expressions for H^c outside the range of equation (5.115). These results can also be inferred from Ottosen and Runesson (1991) and have been discussed in detail by Issen and Rudnicki (2000).

If the right inequality of equation (5.115) is violated, the normal to the band is in the direction of the least compressive principal stress, $\theta^c = \pi/2$, or if the left inequality is violated, the most compressive principal stress, $\theta^c = 0$. The former has been called a split mode by Bigoni and Hueckel (1991) or a dilation mode by Issen and Rudnicki (2000) and the latter a compaction band by Issen and Rudnicki (2000). Because the solution for a compaction band requires the sum $\mu+\beta$ to be negative and relatively large in magnitude, it can be applicable to high-porosity rock (Olsson, 1999; Issen and Rudnicki, 2000). In either of these cases, the critical hardening modulus has the form

$$\frac{H_k^c}{G} = \frac{1+\nu}{9(1-\nu)}(\beta-\mu)^2 - \frac{1+\nu}{1-\nu}\left(\frac{1}{2}N_k - \frac{\beta+\mu}{3}\right)^2 - \left(1-\frac{3}{4}N_k^2\right), \quad (5.116)$$

where $k = 1$ for the split mode and $k = 3$ for the compaction band and N_1 and N_3 are the least and the most compressive principal values of $\mathbf{N}$, i.e., $N_1 \ge N \ge N_3$, respectively. As noted by Perrin and Leblond (1993), the hardening modulus and

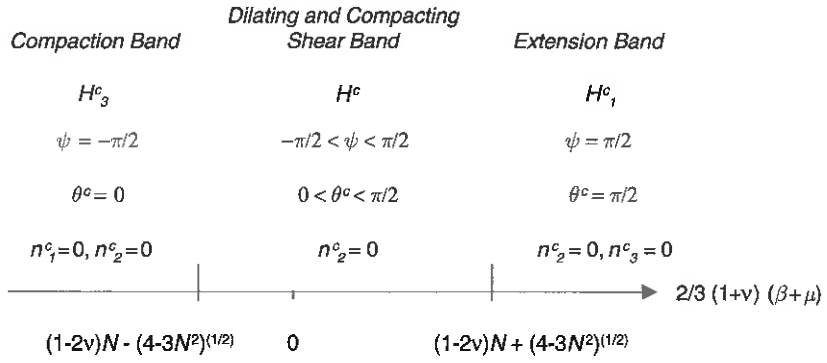

Figure 5.14 ▶ Range of validity of the different expressions for the critical hardening modulus. The three domains correspond to three modes of localization: extension band, shear band, and compaction band.

band orientation angle are continuous over the limits expressed in equation (5.115). The solutions in the different ranges are summarized in Figure 5.14.

In general, the difference between deformation in the band and the homogeneous field is expressed by equation (5.47). The components of the vector **g** characterizing this difference are given by

$$g_s = \gamma \left\{ \frac{\beta K - (K + \frac{1}{3}G)(n_i^c N_{ij} n_j^c)}{(K + \frac{4}{3}G)} n_s^c + n_k^c N_{ks} \right\}, \tag{5.117}$$

where γ is an arbitrary constant and n_i^c are components of the unit normal to the critical band orientation. The volumetric part of the difference in the rate of deformation is

$$\begin{aligned} \Delta D^{\text{vol}} &= g_s n_s^c = \frac{\gamma}{K + \frac{4}{3}G} \left[\beta K + G\,(n_i^c N_{ij} n_j^c)\right] \\ &= \frac{\gamma}{(1-\nu)} \left\{ \frac{\beta}{3}(1+\nu) - \frac{(1-2\nu)}{4}(N + \sqrt{4 - 3N^2}\cos 2\theta^c) \right\} \end{aligned} \tag{5.118}$$

and the shear intensity is

$$\begin{aligned} \Delta D^{\text{shear}} &= \| \frac{1}{2}(g_k n_s^c + g_s n_k^c)\, n_k^c - D^{\text{vol}} n_s^c \| \\ &= \| \frac{\gamma}{2} \left[(n_k^c N_{ks} - (n_i^c N_{ij} n_j^c)\, n_s^c \right] \| \\ &= | \frac{\gamma}{4} \sqrt{4 - 3N^2} \sin 2\theta^c |. \end{aligned} \tag{5.119}$$

Because the localization band is characterized by $n_{II} = 0$, the difference field is a plane strain state in the plane of the major and minor principal stress directions.

There is no shearing in the direction of the intermediate principal stress direction. The ratio of the volumetric to shear deformation rate can be expressed by the band dilatancy angle ψ, defined by Bésuelle (2001a) as (Figure 5.15)

$$\tan\psi = D^{\text{vol}}/D^{\text{shear}}. \tag{5.120}$$

The (pure) extension band corresponds to $\psi = \pi/2$, the dilating shear band to $0 < \psi < \pi/2$, the compacting shear band to $-\pi/2 < \psi < 0$, and the (pure) compaction band to $\psi = -\pi/2$. Pure extension and pure compaction bands correspond to $\theta^c = \pi/2$ and $\theta^c = 0$, respectively; they occur in the domain defined by violation of the right and left inequalities in equation (5.115), respectively. The limit between the compacting shear band and the dilating shear band is the case of the pure shear band, with no volume change inside the band. It occurs at the value of N satisfying

$$3(1-2\nu)(1-\nu)N = (1+\nu)\left[(1-2\nu)(\beta+\mu)+2\beta\right]. \tag{5.121}$$

For an associated model (i.e., $\beta = \mu$), the condition (5.121) corresponds to a band orientation angle $\theta^c = \pi/4$ (i.e., $\alpha = 0$ in equation [5.114]). The relation, for the associated case, between the type of the band (i.e., the band dilatancy angle ψ) and the orientation of the band is plotted in Figure 5.16a when μ changes.

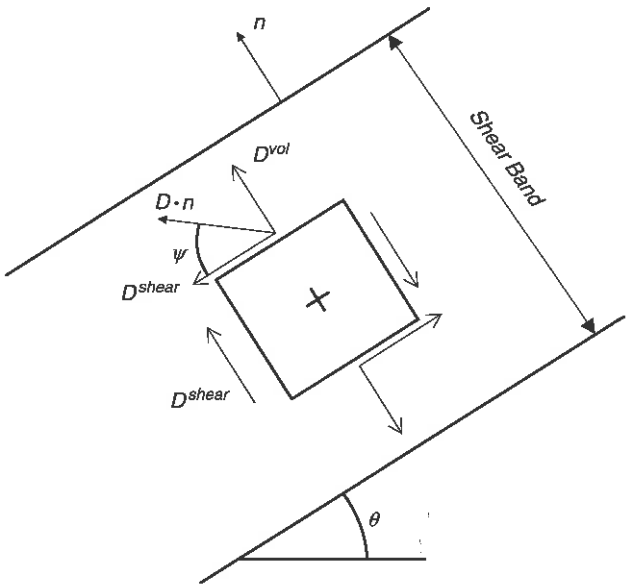

Figure 5.15 ▶ The difference between the rates of deformation in the incipient localization band and the homogeneous field, in the plane of the major and minor principal stress directions. ψ is a band dilatancy angle.

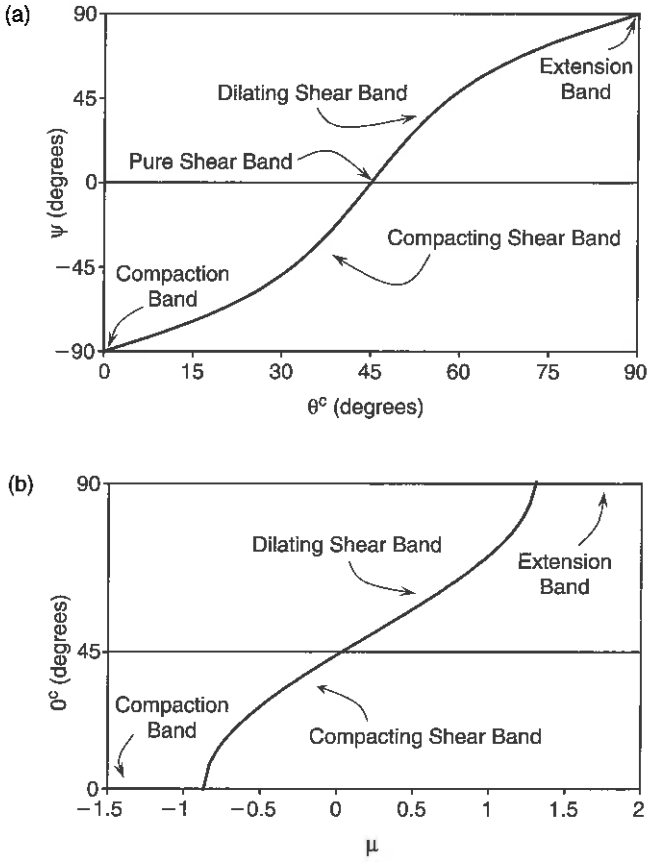

Figure 5.16 ▶ Variation for an associated model (i.e., $\beta = \mu$) (a) of the band dilatancy angle ψ with respect to the band orientation angle θ^c, when μ changes, and (b) of the band orientation angle θ^c with respect to the coefficient μ, in an axisymmetric compression stress state (i.e., $N = 1/\sqrt{3}$), with $\nu = 0.2$.

The variation of the band orientation angle θ^c with respect to the coefficient μ is plotted in Figure 5.16b. Around the transition value of μ between the extension band and dilating shear band (compaction band and compacting shear band, respectively), there is an abrupt evolution of the deformation band orientation. One can expect that for a small increase of the mean stress, inducing a small decrease of μ, the localization mode changes abruptly. This is effectively observed experimentally for specimens of high-porosity rock for small confining pressure (e.g., Paterson, 1978; Bésuelle et al., 2000). The cylindrical specimen confined with a very small confining pressure failed by axial splitting, and a specimen stressed with a slightly higher confining pressure failed by inclined shear localization. Despite

this apparent agreement, another possible explanation for axial splitting, which is different from the bifurcation approach, is unstable flaw propagation enhanced by a low value of the confining pressure.

The variations of ψ and θ^c with respect to μ and β for the nonassociated case are plotted in Figure 5.17 for an axisymmetric compression stress state. The curves in Figure5.16 correspond to the evolution along the line $\beta = \mu$ in Figure 5.17. The band dilatancy angle ψ is continuous with respect to μ and β, except for particular combinations of μ and β not represented in the figure and that seem physically improbable (where the isocurve $\psi = 0$ joins the isocurves $\psi = \pm\pi/2$) (Bésuelle, 2001a).

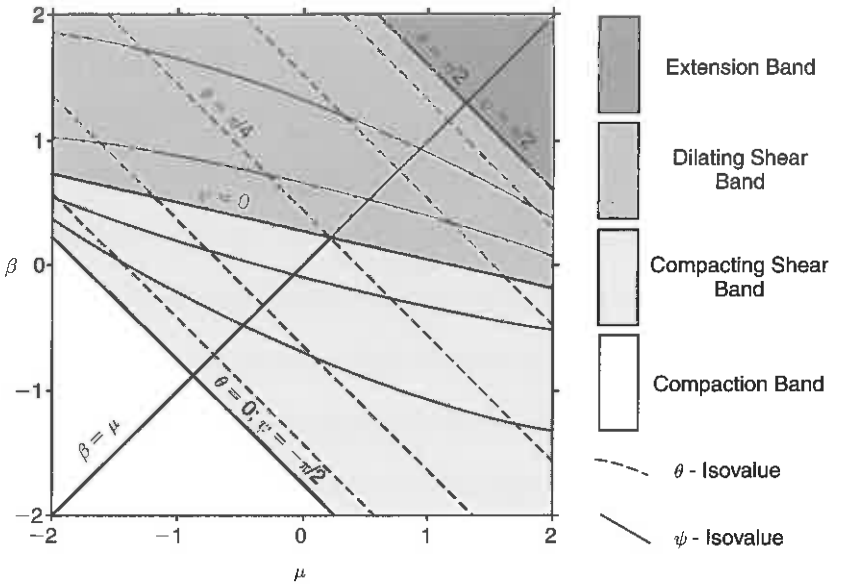

Figure 5.17 ▶ Evolution of the band dilatancy angle ψ and the band orientation angle θ^c, with respect to coefficients μ and β, in an axisymmetric compression stress state (i.e., $N = 1/\sqrt{3}$), with $\nu = 0.2$.

Equations (5.112) and (5.116) predict that the critical hardening modulus for the associated model (i.e., $\beta = \mu$) is always negative and, thus, that localization is possible only in the softening regime (i.e., $H^c < 0$). The evolution of H^c with respect to μ and β is plotted in Figure 5.18 for an axisymmetric compression stress state. The critical hardening modulus increases with an increase in the difference between β and μ (i.e., the more the model is nonassociated). The localization is possible in the hardening regime in some cases (i.e., $H^c > 0$).

The critical hardening modulus also depends strongly on the deviatoric stress state. Typical variation of H^c with respect to N is plotted in Figure 5.19, for

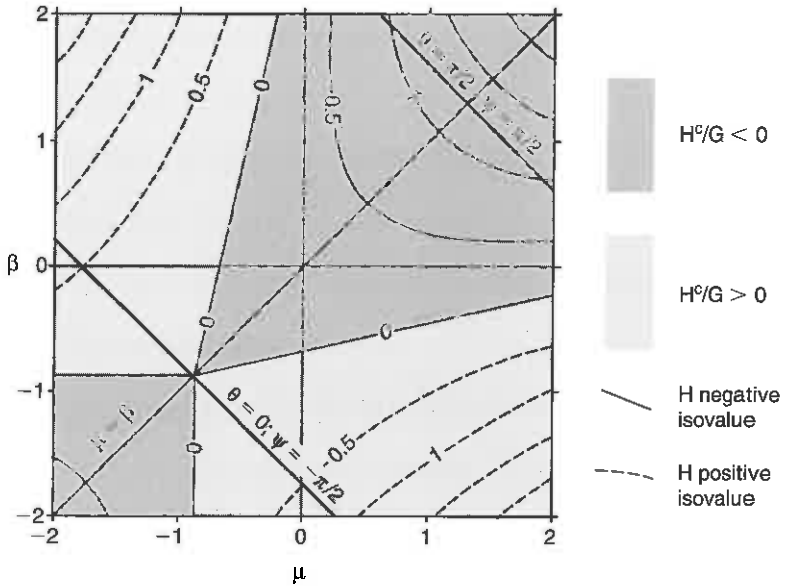

Figure 5.18 ▶ Evolution of the critical hardening modulus H^c/G with respect to coefficients μ an β, in an axisymmetric compression stress state (i.e., $N = 1/\sqrt{3}$), with $\nu = 0.2$.

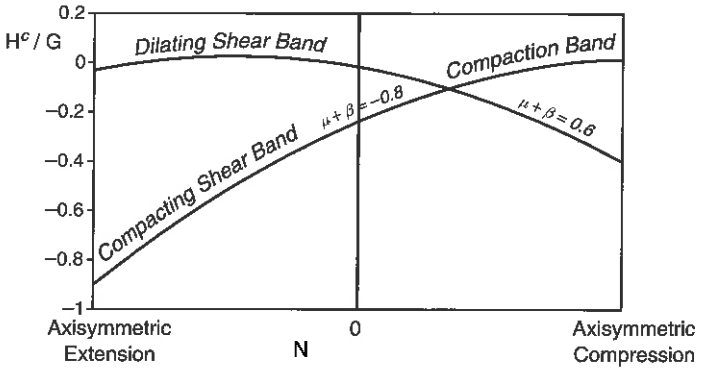

Figure 5.19 ▶ Evolution of the critical hardening modulus H^c/G with respect to the deviatoric stress state (i.e., N), for two pairs of values of (μ, β) in an arbitrary nonassociated case ($|\beta - \mu| = 0, 4$).

two pairs of values of μ and β, for a slightly nonassociated case. For frictional behavior, the hardening modulus is negative close to axisymmetric stress states and is positive in the intermediate range. This means that a frictional material is more inclined to localization when the stress state is far from axisymmetric. For a compacting behavior, the hardening modulus is highest near the axisymmetric

compression stress state. Consequently, a compaction band is more likely in such a stress state.

5.5.3 Influence of the Shape of the Yield Surface

The predictions of the previous discussion used the modified Drucker-Prager yield surface and plastic potential. Because the parameters μ and β are allowed to depend on the mean stress, the surfaces are not conic. The shapes of the surfaces in the plane Π normal to the trisectrix $\sigma_1 = \sigma_2 = \sigma_3$ are, however, circular because they do not depend on the third stress invariant. More realistic surfaces do not have a circular shape in plane Π (see Figure 5.12). Consequently, the normals to the yield surface and the plastic potential (orientation of the plastic rate of deformation) for a given stress state strongly depend on the choice of surface, which, in turn, influences the bifurcation analysis results.

We showed in Section 5.5.1 that the complete bifurcation analysis can be applied to any yield surface and plastic potential. Molenkamp (1985) has explicitly compared several models that combine Coulomb or Lade-Duncan yield surfaces and Coulomb, Lade-Duncan, or von Mises (circular cylinder) plastic potential surfaces. As shown in Figure 5.12, the normals to a Lade-Duncan surface and to a Coulomb surface differ strongly near axisymmetric stress states. Consequently, the difference in bifurcation results between the models is greater near these stress states. For example, for models with smooth yield surface and plastic potential, the bifurcation is predicted in the softening regime near the axisymmetric compression and extension stress states, and in the hardening regimes for intermediate stress states. This is similar to the previous result obtained with a Drucker-Prager model. For models using a Coulomb yield surface, the bifurcation is predicted in the hardening regime for any stress state. Molenkamp (1985) also showed that there are slight differences for the band orientation angle predicted with the different models.

5.5.4 Yield Vertex Models

In the elastic-plastic models that have been discussed thus far, the direction of the inelastic strain increment (i.e., the ratio of components) is fixed with respect to the normal to the plastic potential. Consequently, the direction is fixed by the current state of stress and inelastic deformation and does not depend on the direction of the stress increment. This is illustrated in Figure 5.20a for the bilinear models, which include the most common elastic-plastic types. For any stress increments $\dot{\sigma}$ making a positive inner product with the normal to the yield surface $\mathbf{Q}$, i.e., $\mathbf{Q} : \dot{\sigma} > 0$, the direction of the inelastic part of the rate of deformation $\mathbf{D}^p$ is the same. Furthermore, only the projection of $\dot{\sigma}$ on $\mathbf{Q}$ contributes to $\mathbf{D}^p$. For stress increments directed tangent to or within the yield surface, i.e., $\mathbf{Q} : \dot{\sigma} \leq 0$, the response is purely elastic and $\mathbf{D}^p = 0$. For the four-linear models, the situation

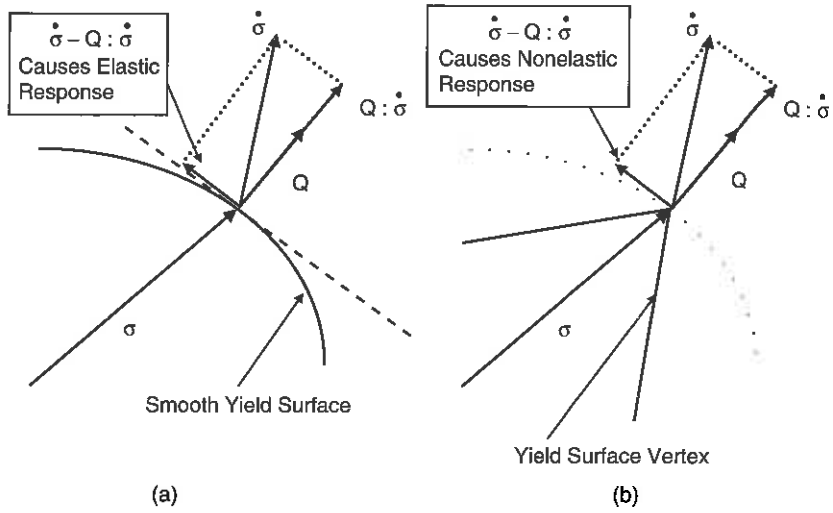

Figure 5.20 ▶ Wider range of stress increments causes inelastic deformation at a yield surface vertex (b) than for a smooth yield surface (a).

is identical unless the current stress is at the intersection of two yield surfaces. At the intersection, the same considerations applied to the bilinear models pertain to each separate yield surface.

Many models based on microstructural mechanisms of inelastic deformation predict that the current yield surface has a vertex at the current stress point (as illustrated in Figure 5.20b) and that the response direction of $\mathbf{D}^p$ varies continuously with the direction of $\dot{\sigma}$. Indeed, Hill (1967) has argued that this is an essential feature of composites and polycrystalline materials or any of materials for which the microstructural mechanisms of inelastic deformation are orientation dependent. Rudnicki and Rice (1975) suggested a conceptual model of this type for low-porosity rock in which the inelasticity results primarily from frictional sliding on fissure surfaces and the extension of microcracks (Figure 5.21). An idealized microcrack with unit normal $\mathbf{n}$ is shown in Figure 5.21a. This microcrack contributes to the inelastic deformation when the shear stress in some direction $\mathbf{s}$, τ_{ns} equals the compressive normal stress σ_{nn} multiplied by a local coefficient of friction μ_l:

$$\tau_{ns} = \mu_l \, \sigma_{nn}. \tag{5.122}$$

This condition defines a surface in the stress space (Figure 5.21b). Each material point is assumed to comprise microfissures of all possible orientations. For a given program of loading, yield will occur first on one or more favorably oriented microfissures; then, as loading proceeds, microfissures of other orientations will be activated. This process is shown schematically for two fissure yield surfaces

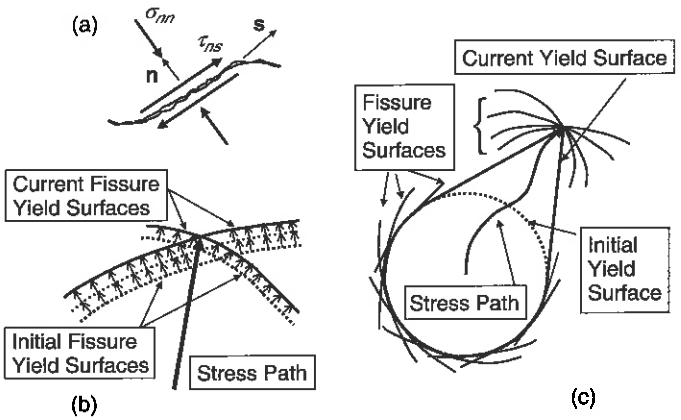

Figure 5.21 ▶ Schematic illustration of a vertex formed on the macroscopic yield surface as the inner envelope of individual fissure (microscale) yield surfaces.

in Figure 5.21b. Consequently, the macroscopic yield surface will have a vertex at the current stress point formed from the inner envelope of the fissure yield surfaces of all orientations that have been activated by that loading path (Figure 5.21c).

If the stress components entering the microfissure yield condition (5.122) are assumed to be projections of the macroscopic stresses,

$$\tau_{ns} = \frac{1}{2}(n_i s_j + n_j s_i)\sigma_{ij}, \quad \sigma_{nn} = -n_i n_j \sigma_{ij}, \tag{5.123}$$

where σ_{ij} is the macroscopic stress tensor (positive in tension), then the model is an extension of the slip theory of Batdorf and Budiansky (1949; 1954). An alternative model, proposed by Taylor (1938a,b) for the response of metals, assumes that the strain of each microelement is identical to the macroscopic strain but, in general, the local stress will not be in equilibrium with the macroscopic stress. In addition, there are many more complex models that account for the constraint of the material surrounding the microelement (e.g., Hutchinson, 1970).

Rudnicki and Chau (1996) have investigated a related model modified from the microcrack damage model proposed by Costin (1983a,b; 1985). In this model, microcrack growth is assumed to be driven by a fictitious local tensile stress given by

$$\sigma_t = n_i \sigma_{ij} n_j + f' g(a) n_i \overline{\sigma}_{ij} n_j, \tag{5.124}$$

where σ_{ij} are components of stress, $\overline{\sigma}_{ij}$ is the stress deviator, n_i are components of the unit normal to the microcrack, f' is a constant, and g is a function of crack length a. The function $g(a)$ is assumed to decrease for small extensions of the crack length from its initial value and then to increase. The decrease reflects the decrease of the local tensile stress as the tip of the flaw grows away from the

source, and the increase reflects the increasing importance of crack interaction as continued growth occurs. Rudnicki and Chau (1996) then calculated the strain by determining the increase in elastic compliance caused by an isolated crack of that length and orientation. They showed that this model predicts an initial yield surface that is triangular in the Π-plane and they calculated the form of the vertex predicted by the model for axisymmetric compression followed by torsion.

Studies of models predicting the formation of vertices on the yield surface (e.g., Budiansky, 1959; Hill, 1967; Hutchinson, 1970; Christoffersen and Hutchinson, 1979) indicate a structure similar to that shown in Figure 5.22. Stress increments directed within the vertex (into region ABC) cause elastic unloading and no continued nonelastic deformation for any orientation. Stress increments continuing in approximately the same direction as the current stress and directed into the region of fully active loading (into region DBE) cause continued nonelastic deformation for every microstructural orientation that has been activated by the current stress. For stress paths remaining within the fully active region, the response is approximately path independent and can be well approximated by a deformation theory of plasticity (Budiansky, 1959; Christoffersen and Hutchinson, 1979). In the remaining sectors, ABD and CBE, the response is fully nonlinear in the sense that the direction (ratio of components) of $\mathbf{D}^P$ depends on the direction of the stress increment.

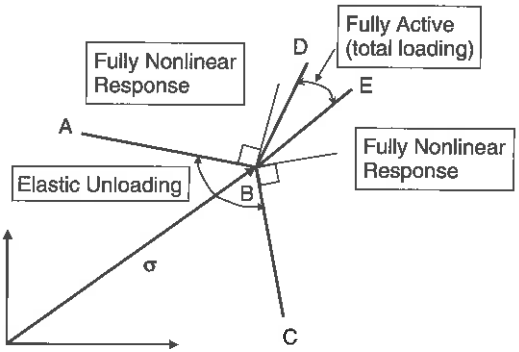

Figure 5.22 ▶ Structure of a yield surface indicating the ranges of stress increments for elastic unloading, fully active loading, and fully nonlinear behavior.

We have already alluded to the significance of vertex formation for the prediction of localization by bifurcation: the kinematic condition (5.47) constrains the difference of the deformation fields inside and outside the band to be a combination of simple shear and uniaxial deformation relative to the orientation of the band. If the homogeneous deformation field before band formation is significantly different from simple shear and uniaxial deformation, for example, as in axisymmetric compression, then formation of the band involves an abrupt change in the stress path and the response to the portion of the stress increment tangent to the yield

surface is governed by the elastic response. To compensate for the stiff elastic response, $G \gg H$, the critical value of the hardening modulus needed to permit bifurcation must be strongly negative (Rudnicki and Rice, 1975). If, however, the yield surface has a vertex at the current stress, then the portion of the stress increment that is normal to the stress (and would be tangent to a smooth yield surface through the same point) is governed by a modulus much smaller than the elastic modulus and, thus, facilitates the occurrence of bifurcation (Figure 5.20).

Of course, experimental evidence can never be definitive on the existence of a vertex: measurements of finite precision cannot distinguish between a vertex and a sharply rounded but smooth yield surface. Nevertheless, given the inevitable imperfections in any real material, the more practical issue is whether the inelastic strain increment vector is essentially independent of the direction of the stress increment, as predicted by a smooth yield surface theory, or whether it follows the stress increment, as predicted for a vertex (or sharply rounded notch). Experiments that systematically vary the direction of the stress increment and measure the direction of the inelastic strain increment provide information on this issue (Hecker, 1976). Apparently, the only experiments of this type on rocks are those of Olsson (1992) on Tennessee marble. He subjected hollow cylinders of Tennessee marble to axisymmetric compression followed by cyclic loading in torsion and measured the direction of the inelastic strain rate increment. He found that the angular variation of the strain-rate vector exceeded that predicted by a smooth yield surface model and, hence, implied the existence of a vertex.

Because of the complexity of the microstructural models predicting vertex formation and continuous variation of the stiffness of response with the direction of $\mathbf{D}^P$, precise evaluation of the bifurcation condition is difficult. To approximate the response at a vertex, Rudnicki and Rice (1975) introduced an additional inelastic modulus, H_1 (denoted h_1 in Rudnicki and Rice [1975]), to govern stress increments tangent to the yield surface (they introduced this modulus only for the deviatoric portion of stress increments because the hydrostatic portion of the stress affects all fissure orientations in the same way). The significance of H_1 can be illustrated by specializing the constitutive relation (5.110) to the case of incompressible deformation ($K \to \infty$, $\beta = 0$) and biaxial loading (only σ_{11} and σ_{22} are nonzero). In this case, the modulus H governs inelastic shearing at 45° to the geometric axes

$$\frac{1}{2}(D_{11} - D_{22}) = \frac{1}{2G}\left(\frac{\dot{\sigma}_{11} - \dot{\sigma}_{22}}{2}\right) + \frac{1}{2H}\left(\frac{\dot{\sigma}_{11} - \dot{\sigma}_{22}}{2}\right), \tag{5.125}$$

and H_1 governs inelastic shear deformation parallel to the geometric axes

$$D_{12} = \frac{\dot{\sigma}_{12}}{2G} + \frac{\dot{\sigma}_{12}}{2H_1}. \tag{5.126}$$

For this special case, the role of H_1 is significant if bifurcation involves an abrupt change from continued biaxial deformation to shear. The constitutive relations,

(5.125) and (5.126), and the version used by Rudnicki and Rice (1975) are members of a class of models that can be described as noncoaxial and are discussed more fully in the next section. When the elastic contributions to equations (5.125) and (5.126) are neglected, they have same form as those used by Hill and Hutchinson (1975) and Biot (1965) for plane strain loading of an incompressible, orthotropic material. More specifically, the moduli H and H_1 correspond to μ^* and μ respectively, of Hill and Hutchinson (1975). An explicit expression for a modulus corresponding to H_1 can also be obtained from the generalization by Mehrabadi and Cowin (1978) of Spencer's (1964) theory for the planar deformation of ideal granular materials. In addition, H_1 is an example of what is called an "out of plane" modulus by Vardoulakis and Graf (1985) and Desrues and Chambon (2002).

Storen and Rice (1975) showed that the introduction of H_1 was equivalent to the use of a deformation theory of plasticity (also see Hutchinson and Neale, 1978; 1981) and that, at least in the pressure-independent, incompressible case, H_1 could be interpreted as a secant modulus for shear. Deformation theory is essentially a nonlinear elastic theory and cannot accurately model the response of elastic-plastic materials for the full range of loadings. Nevertheless, as discussed in connection with Figure 5.21 and as noted by Budiansky (1959), deformation theory will be a good approximation to the response at a vertex for small deviations from straight-ahead loading. Furthermore, it has long been observed that predictions of buckling failures using deformation theory are more in accord with observations than those based on flow (or incremental theories) that distinguish between loading and unloading (see Christoffersen and Hutchinson, 1979, for a brief summary).

The effect of a yield surface vertex is to facilitate the occurrence of localization, particularly for deformation states such as axisymmetric compression for which shear band formation involves an abrupt change from the previous pattern of deformation. For these cases, the value of the critical hardening is predicted to be very negative for smooth yield surface models. The calculations of Rudnicki and Rice (1975), using the deformation-theory approximation of response at a vertex, suggest that the magnitude of the (negative) hardening modulus is reduced by a factor of roughly H_1/G. For $H_1 \ll G$, as expected, this reduction causes the predicted localization to be much closer to peak stress and, thus, more in accord with observations. Unfortunately, however, H_1 cannot be measured from conventional experiments. Olsson (1995) used compression–torsion tests on Tennessee marble to measure the modulus corresponding to H_1. Interpretation of the experiments was complicated by time-dependent effects and reduction of elastic (unloading) moduli by damage, but Olsson (1995) did infer a reduction of roughly 50% in the value of this modulus from its elastic value. Alternatively, the value of the modulus, as well as the fully nonlinear response at a vertex, could in principal, be calculated from a microstructural model. But apparently no calculations of the type done by Hutchinson (1970) for polycrystalline metals have been done for geomaterials.

The different predictions of the onset of localization from smooth yield surface (flow) theories, deformation theories, and corner theories is relevant not only to

failure of geomaterials in the laboratory but also to the development of faults in tectonic settings. Studies of the stability of a geological two-layer system consisting of a frictional, elastic-plastic layer overlying a viscous substratum (Leroy and Triantafyllidis, 1996; Triantafyllidis and Leroy, 1994, 1997) have shown that use of a deformation theory promotes earlier occurrence of localized deformation corresponding to faulting by comparison with the results for a smooth yield surface flow theory. Application of the results to a folded section of the Campos basin, offshore Brazil, shows the use of the deformation theory is necessary to explain the observed buckling.

5.5.5 Noncoaxial Models

As mentioned in the preceding section, at the incipient localization, the principal directions of the stress rate tensor inside the band may undergo an abrupt change and generally do not correspond to the principal directions of the stress tensor. The localization generally induces a rotation of the principal directions inside the incipient band. For example, in an idealized axisymmetric compression test (i.e., without imperfections inherent to an actual experiment), the principal directions of the stress and stress rate tensors are fixed and coincide during the homogeneous deformation, but this coaxiality is lost when localization occurs.

The constitutive relations for the elastic-plastic models with smooth yield surfaces discussed previously were isotropic (because both the elastic was isotropic and the plastic responses depended only on stress invariants and scalar hardening parameters). Consequently, a *pure* rotation of principal stress directions (i.e., without change of stress invariants) will not induce a plastic strain and the tangential stiffness (the stiffness that links the stress rate to the rate of deformation) is an elastic stiffness. Moreover, when a plastic response does occur, the principal directions of the plastic rate of deformation are identical to the principal stress directions and not influenced by the stress rate directions. For these reasons, such models are called coaxial.

Models with a vertex, discussed in the preceding section, introduce a dependence of the strain rate on the stress rate but they are generally too complex to use in bifurcation analyses. Another approach is to incorporate directly into the constitutive relation the effect of rotation of the principal stress directions on the inelastic strain rate in order to reflect anisotropy that develops due to the history of the deformation (e.g., Rudnicki and Rice, 1975). We exclude here initially anisotropic materials (structural anisotropy) and consider only deformation-induced anisotropy. Because microcracks, which are primarily responsible for inelastic deformation in brittle rocks, generally have preferential orientations, their crack evolution is strongly dependent on the direction of the stress increment. Consequently, during a (pure) rotation of principal stress directions, the tangential stiffness is typically softer than the elastic stiffness. For these reasons, bifurcation analyses are dependent on the anisotropy of the model (Hill and Hutchinson, 1975; Rudnicki 1977a; 2002).

Anisotropy can be introduced into the elastic (Bigoni and Loret, 1999) or plastic response (or both). The use of kinematic hardening (e.g., Sulem et al., 1999; Vardoulakis and Sulem, 1995) is a simple way to introduce anisotropy into the plastic response. Neither the use of kinematic hardening nor elastic anisotropy introduces a dependence of the inelastic strain increment direction on the stress increment. Within the framework of incrementally multilinear or nonlinear laws, some models are also nonisotropic. Indeed, a major motivation for development of some of these models is to improve the prediction of deformation band occurrence by bifurcation analysis (e.g., Desrues and Chambon, 2002). The importance of anisotropy in such models controls the bifurcation results (e.g., see Tamagnini et al., 2000, for a review).

In general, noncoaxial laws permit additional freedom to model rock behavior. However, the determination of some moduli from experiments on rocks can be difficult because it requires performing tests in which the principal stress directions rotate during the loading. This is not possible with classical axisymmetric tests but can be done with nonconventional tests, such as the hollow cylinder torsion test or simple shear box. Because of the difficulty of performing tests in which the principal stress axes rotate, another strategy is to calibrate the modulus of the constitutive tensor using the appearance of shear bands in classic tests. Because the modulus expressing the noncoaxial aspect of the constitutive relation plays an important role in the incipient localization, experimental observations of the localization (onset of localization, deformation band orientation) can be used to calibrate these moduli for specific stress paths (axisymmetric compression or extension, plane stress) (Vardoulakis and Graf, 1985; Desrues and Chambon, 2002).

5.6 Pore Fluid Effects

Pore fluid effects for the simple deformation state comprising uniaxial deformation and simple shear were discussed in Section 5.3.4. In summary, the results indicated that the condition for localization takes the same form as for the non–fluid-infiltrated solid in the limits of drained (constant pore pressure) and undrained (constant fluid mass) response. But, as first shown by Rice (1975) for a dilatant material, infinitesimal spatial perturbations begin to grow exponentially in time when the localization condition in terms of the drained response is met before the condition in terms of the undrained response. If the material is compacting but still frictional (in the sense that the yield stress in shear increases with increasing compressive mean stress), instability in terms of the undrained response will typically precede localization predicted in terms of the drained response. An extension of Rice (1975) analysis to include evolution of the background, homogeneous deformation solution (Garagash and Rudnicki, 2000) suggests some modification of these results, but they remain valid in the limit of infinitesimal perturbation

wavelengths. Here we follow the analysis of Rudnicki (2000) to show that the linearized perturbation analysis predicts similar results for arbitrary deformation states, at least for incrementally linear behavior. For simplicity, we restrict attention to small strains and consider only small perturbations from completely uniform deformation. Runesson et al. (1998) have presented an analysis of localization for undrained conditions for finite strains. Generalizations of the present analysis to finite strains can be adapted from the treatments of Rudnicki (1983), Runesson et al. (1996), or Coussy (1995).

The constitutive relation for drained (no change in pore pressure) response is assumed to have the same form as equation (5.52):

$$\dot{\sigma} = \mathbf{L} : \mathbf{D}, \tag{5.127}$$

where $(\mathbf{L} : \mathbf{D})_{ij} = L_{ijkl}\mathbf{D}_{kl}$. If $\mathbf{L}$ can be inverted, equation (5.127) can be written as

$$\mathbf{D} = \mathbf{K} : \dot{\sigma}, \tag{5.128}$$

where $\mathbf{K}$ and $\mathbf{L}$ are mutual inverses with components satisfying

$$L_{ijkl}K_{klmn} = \frac{1}{2}(\delta_{im}\delta_{jn} + \delta_{in}\delta_{jm}) \tag{5.129}$$

and δ_{ij} is the Kronecker delta. The components of the incremental compliances K_{ijkl} and the moduli L_{ijkl} are symmetric with respect to interchange of the first two indices and the last two indices, i.e., $L_{ijkl} = L_{jikl}$ and $L_{ijkl} = L_{ijlk}$, but for geomaterials, they are not, as noted earlier, typically symmetric with respect to interchange of the first and last pairs, i.e., $L_{ijkl} \neq L_{klij}$.

When the solid is saturated with a fluid that can be described in terms of a single scalar pore pressure (see Cleary, 1978, for a discussion of other possibilities), a term involving the rate of change of the pore pressure must be appended to equation (5.128):

$$\mathbf{D} = \mathbf{K} : \dot{\sigma} + \mathbf{A}\dot{p}. \tag{5.130}$$

Alternatively equation (5.130) can be written as

$$\dot{\sigma} = \mathbf{L} : \mathbf{D} - \alpha\dot{p}, \tag{5.131}$$

where $\alpha = \mathbf{L} : \mathbf{A}$. The introduction of the pore pressure as an additional field variable requires an ancillary constitutive equation. This is conveniently taken to be a relation for the rate of change of fluid mass content per unit (reference) volume of porous solid $m = \rho v$ where ρ is the density of homogeneous pore fluid and v is apparent void volume fraction. For arbitrarily compressible constituents, $\dot{m}$ can be expressed in terms of the rate of strain and pore pressure change

$$\frac{\dot{m}}{\rho} = \mathbf{R} : \mathbf{D} + \eta\dot{p} \tag{5.132}$$

or in terms of the stress rate and pore pressure change by substituting equation (5.130) into equation (5.132):

$$\frac{\dot{m}}{\rho} = \mathbf{R} : \mathbf{K} : \dot{\sigma} + (\mathbf{R} : \mathbf{A} + \eta)\dot{p}. \tag{5.133}$$

In equations (5.130), (5.131), and (5.132), $\mathbf{A}$, α, and $\mathbf{R}$ are symmetric because of the symmetry of $\mathbf{D}$ and $\dot{\sigma}$.

For undrained response, the fluid mass in material elements is constant, the right side of equation (5.132) is zero, and the pore pressure is given by

$$\dot{p} = -\eta^{-1}\mathbf{R} : \mathbf{D} \tag{5.134}$$

or equivalently, in terms of the stress from equation(5.133)

$$\dot{p} = \frac{-\mathbf{R} : \mathbf{K} : \dot{\sigma}}{\eta + \mathbf{R} : \mathbf{A}}. \tag{5.135}$$

Substitution of equation (5.134) into equation (5.131) gives

$$\dot{\sigma} = \mathbf{L}^u : \mathbf{D}, \tag{5.136}$$

where the undrained incremental moduli are given by

$$\mathbf{L}^u = \mathbf{L} + \eta^{-1}\mathbf{R}\alpha \tag{5.137}$$

Similarly, substitution of equation (5.135) into equation (5.130) yields

$$\mathbf{D} = \mathbf{K}^u : \dot{\sigma}, \tag{5.138}$$

where the undrained incremental compliance tensor is given by

$$\mathbf{K}^u = \mathbf{K} - (\eta + \mathbf{R} : \alpha)^{-1}\mathbf{A}\mathbf{R} : \mathbf{K}. \tag{5.139}$$

The condition for localization, either equation (5.56) or (5.57), can be evaluated in terms of the drained equation (5.127) or the undrained equation (5.136) moduli. If the drained moduli are used, the condition is

$$\det(m_{ij}) = 0, \tag{5.140}$$

where $\mathbf{m} = \mathbf{n} \cdot \mathbf{L} \cdot \mathbf{n}$. If the undrained moduli are used, the condition is

$$\det(m^u_{ij}) = 0, \tag{5.141}$$

where $\mathbf{m}^u = \mathbf{n} \cdot \mathbf{L}^u \cdot \mathbf{n}$. Equation (5.137) relates $\mathbf{m}^u$ to $\mathbf{m}$:

$$\mathbf{m}^u = \mathbf{m} + \eta^{-1}\mathbf{r}\mathbf{a}, \tag{5.142}$$

where $\mathbf{r} = \mathbf{n} \cdot \mathbf{R}$ and $\mathbf{a} = \alpha \cdot \mathbf{n}$. The condition (5.141) can be related to equation (5.140) by expanding the determinant to get

$$\det(m^u_{ij}) = m + \eta^{-1}\mathbf{r} \cdot \mathbf{k} \cdot \mathbf{a}, \qquad (5.143)$$

where $\mathbf{k}$ is the matrix of cofactors of $\mathbf{m}$, related to its inverse by $\mathbf{m}^{-1} = \mathbf{k}/m$ and $m = \det(m_{ij})$. The earlier discussion of the layer problem examined by Rice (1975) suggests that equation (5.141) may be met before or after equation (5.140) depending on the nature of the constitutive relation and, in particular, the inelastic volumetric deformation. If equation (5.140) is met before equation (5.141), Rice's (1975) analysis also suggests that undrained homogeneous deformation is unstable, in the sense that small spatial perturbations will grow exponentially in time. In this case, the condition (5.141) may be irrelevant since strongly inhomogeneous deformation may develop well before it is met.

5.6.1 Diffusive Instability

To analyze the stability of undrained homogeneous deformation, fluid mass conservation must be combined with the other field equations and an additional constitutive equation relating the fluid mass flux to gradients in pore pressure must be specified. Fluid mass conservation (in the absence of sources) is given by

$$\dot{m} + \nabla \cdot (\rho \mathbf{q}) = 0, \qquad (5.144)$$

where $\mathbf{q}$ is the volume flow rate per unit area of porous solid and ρ is the fluid mass density. Fluid mass flow is assumed to be related to the pressure gradient by Darcy's law

$$\mathbf{q} = -\mathcal{K} \cdot \nabla p, \qquad (5.145)$$

where $\mathcal{K}$ is a symmetric permeability tensor (more frequently expressed as the ratio of an intrinsic permeability, with dimensions of length squared, to the fluid viscosity). Substitution of equation (5.145) into equation (5.144) yields

$$\dot{m} = \rho \nabla \cdot \mathcal{K} \cdot \nabla p, \qquad (5.146)$$

where the fluid density has been assumed to be spatially uniform.

For simplicity, we assume, as in Rice (1975), that perturbations from undrained homogeneous deformation are small enough so that incremental constitutive parameters are the same for the uniform and perturbed fields. If this is not the case, additional inhomogeneous terms would enter the right sides of the equations. As in equation (5.60), these terms involve the differences of the constitutive parameters multiplied by the strain rate and pore pressure rate in the uniform field. Forming the difference of equation (5.131), using equation (5.47), and substituting into the equation for continuing equilibrium at band formation equation (5.50), yields

$$\mathbf{m} \cdot \mathbf{g} - \mathbf{a}\Delta\dot{p} = 0, \qquad (5.147)$$

where $\Delta\dot{p}$ is the difference between the pore pressure rates in the uniform and perturbed fields. The kinematic restriction on the perturbed strain-rate field equation (5.47) suggests that Δp depends on distance $\mathbf{n}\cdot\mathbf{x}$ perpendicular to the orientation of a planar band and, hence, can be decomposed into Fourier components of the form $\exp(i\lambda\mathbf{n}\cdot\mathbf{x})$, where $i=\sqrt{-1}$. This type of deformation mode has also been discussed for sands by Vardoulakis (1996). Because both sides of equation (5.146) are zero for the unperturbed (homogeneous, undrained) field, the difference fields also satisfy equation (5.146). Using the Fourier decomposition on the right side and assuming the permeability is uniform yields

$$\Delta\dot{m} = -\rho\kappa\,\Delta p, \tag{5.148}$$

where $\kappa = \lambda^2\,\mathbf{n}\cdot\mathcal{K}\cdot\mathbf{n}$. Forming the difference of equation (5.132) and substituting into equation (5.148) yields

$$\mathbf{r}\cdot\mathbf{g} + \eta\Delta\dot{p} + \kappa\Delta p = 0. \tag{5.149}$$

The vector $\mathbf{g}$ can be eliminated from equation (5.147) by writing the inverse of $\mathbf{m}$ as $\mathbf{k}/m$, where $\mathbf{k}$ is the matrix of cofactors and $m = \det(m_{ij})$. Substituting the result into equation (5.149) and using equation (5.143) yields

$$\eta\det(m^u_{ij})\Delta\dot{p} + m\kappa\Delta p = 0. \tag{5.150}$$

This is a linear ordinary differential equation for the time evolution of the perturbed pressure field. The solutions change from exponentially decaying to exponentially growing as m passes through zero from positive to negative values. Because the vanishing of m is the condition for localization in terms of the drained incremental moduli (equation [5.140]), this condition controls the growth rate of spatial perturbations as in the layer analysis of Rice (1975).

The coefficient of $\Delta\dot{p}$ will vanish when the condition for localization is met in terms of the undrained moduli equation (5.141). (The suggestion of Rudnicki [2000] that the relation of the vanishing of this coefficient with the condition for undrained localization depends on the symmetry of $\mathbf{k}$ and the relation of $\mathbf{a}$ to $\mathbf{r}$ is incorrect.)

5.6.2 Application to an Elastic-Plastic Relation

This section specializes the analysis of the preceding section to a particular form of elastic-plastic (bilinear) constitutive relation discussed in Section 5.5.2. The strain rate for plastic loading is given by equation (5.84). Thus, the tensor $\mathbf{K}$ in equation (5.128) is given by

$$\mathbf{K} = \mathbf{M} + \frac{1}{H}\mathbf{P}\mathbf{Q}, \tag{5.151}$$

where in equation (5.84) $\alpha = 1$ for inelastic loading. The inverse of $\mathbf{K}$, $\mathbf{L}$ in equation (5.127), is given by

$$\mathbf{L} = \mathbf{E} - \frac{\mathbf{p}\,\mathbf{q}}{H + \mathbf{Q} : \mathbf{E} : \mathbf{P}}, \tag{5.152}$$

where $\mathbf{E} = \mathbf{M}^{-1}$ is the tensor of elastic moduli, $\mathbf{p} = \mathbf{E} : \mathbf{P}$ and $\mathbf{q} = \mathbf{E} : \mathbf{Q}$.

Substitution of equation (5.152) into the localization condition (5.55) yields equation (5.92), which we write here as

$$\left\{\mathbf{n} \cdot \mathbf{E} \cdot \mathbf{n} - h^{-1}\mathbf{u}\mathbf{v}\right\} \cdot \mathbf{g} = 0, \tag{5.153}$$

where $h = H + \mathbf{Q} : \mathbf{E} : \mathbf{P}$, $\mathbf{u} = \mathbf{n} \cdot \mathbf{p} = \mathbf{n} \cdot \mathbf{E} : \mathbf{P}$ and $\mathbf{v} = \mathbf{n} \cdot \mathbf{q} = \mathbf{n} \cdot \mathbf{E} : \mathbf{Q}$. The critical value of h causing the determinant of the coefficient matrix to vanish is

$$h_c^d = \mathbf{v} \cdot \mathbf{F} \cdot \mathbf{u}, \tag{5.154}$$

where $\mathbf{F} = (\mathbf{n} \cdot \mathbf{E} \cdot \mathbf{n})^{-1}$ and the right eigenvector is proportional to $\mathbf{F} \cdot \mathbf{u}$ (Rice, 1976) and equation (5.94). The corresponding critical value of the hardening modulus is $H_c^d = h_c^d - \mathbf{Q} : \mathbf{E} : \mathbf{P}$ (equation [5.95]).

Using equation (5.152) in equation (5.147) and multiplying through by $\mathbf{F}$ yields

$$\mathbf{g} - h^{-1}(\mathbf{F} \cdot \mathbf{u})(\mathbf{v} \cdot \mathbf{g}) = \mathbf{F} \cdot \mathbf{a}\Delta\dot{p} \tag{5.155}$$

Forming the dot product of equation (5.155) from the left with $\mathbf{v}$ and using equation (5.154) yields the solution for

$$\mathbf{v} \cdot \mathbf{g} = \frac{\mathbf{v} \cdot \mathbf{F} \cdot \mathbf{a}}{(1 - h_c^d/h)}\Delta\dot{p}. \tag{5.156}$$

Substituting back into equation(5.155) yields the solution for

$$\mathbf{g} = \Delta\dot{p}\left\{\mathbf{F} + \frac{(\mathbf{F} \cdot \mathbf{u})(\mathbf{v} \cdot \mathbf{F})}{(h - h_c^d)}\right\} \cdot \mathbf{a}, \tag{5.157}$$

where the expression in braces is $\mathbf{m}^{-1}$. An ordinary differential equation for Δp results from substituting this expression into equation (5.149)

$$(h - h_c^d)\kappa\Delta p + \Delta\dot{p}\left\{[\eta + \mathbf{r} \cdot \mathbf{F} \cdot \mathbf{a}](h - h_c^d) + (\mathbf{r} \cdot \mathbf{F} \cdot \mathbf{u})(\mathbf{v} \cdot \mathbf{F} \cdot \mathbf{a})\right\} = 0. \tag{5.158}$$

The constitutive relation used by Rudnicki and Rice (1975) in their study of localization and discussed in Section 5.5.2 has the form of equation (5.84), but the yield function and plastic potential depend only on the first and second stress invariants. In this case, $\mathbf{P}$ and $\mathbf{Q}$ are given by equations (5.108) and (5.106), respectively. If the elasticity is assumed to be isotropic equation (5.109), then

$$\mathbf{F} = \frac{1}{G}\left\{\mathbf{I} - \frac{K + G/3}{K + 4G/3}\mathbf{n}\mathbf{n}\right\}, \tag{5.159}$$

where $\mathbf{I}$ is the identity tensor

$$\mathbf{p} = G\mathbf{N} + \beta K\mathbf{I} \tag{5.160a}$$

$$\mathbf{q} = G\mathbf{N} + \mu K\mathbf{I} \tag{5.160b}$$

$$\mathbf{Q} : \mathbf{E} : \mathbf{P} = G + \mu\beta K \tag{5.160c}$$

and $\mathbf{N}$ is the normalized deviatoric stress tensor, defined following equation (5.110).

Rudnicki (1984a; 1985) has extended the form of the constitutive relation (5.84) to include pore fluid effects. He assumes isotropic poroelasticity for the elastic strain increments and inelastic strain increments given by the second term of equation (5.84) with the stress replaced by the effective stress $\sigma + p\mathbf{I}$. As already noted, much experimental evidence is consistent with this form, and Rice (1977) has argued that it is appropriate for inelasticity arising from microcracking and frictional slip on surfaces with small real areas of contact. For isotropic poroelasticity, the proper form of the effective stress is $\sigma + pb\mathbf{I}$ where b is the Biot coefficient (see Chapter 1). Under the same conditions for which $\sigma + p\mathbf{I}$ is the form of the effective stress for inelastic deformation, Rice (1977) has also argued that the inelastic increment of the apparent void volume fraction (equal to $\dot{m}/\rho$) is equal to the inelastic volume strain increment. Under these circumstances, the tensor $\mathbf{A}$ in equation (5.130) and α in equation (5.131) are given by

$$\mathbf{A} = b(1/3K)\mathbf{I} + H^{-1}\mathbf{P}\mu \tag{5.161a}$$

$$\alpha = b\mathbf{I} + \frac{\mathbf{p}\mu(1-b)}{H + G + \mu\beta K} \tag{5.161b}$$

The tensor $\mathbf{R}$ and the coefficient η entering equation (5.132) are given by

$$\mathbf{R} = b\mathbf{I} + \frac{\mathbf{q}\beta(1-b)}{H + G + \mu\beta K} \tag{5.162a}$$

$$\eta = \frac{b(1-bB)}{KB} + \frac{\beta\mu(1-b)^2}{H + G + \mu\beta K}, \tag{5.162b}$$

where B is the Skempton coefficient (Chapter 1). The rate of change of pore pressure during undrained deformation (equation [5.135]) is given by

$$\dot{p} = -\frac{1}{(b/BK) + H^{-1}\beta\mu}\left\{b(1/3K)\mathbf{I} + H^{-1}\beta\,\mathbf{Q}\right\} : \dot{\sigma}. \tag{5.163}$$

The compliance tensor for undrained deformation (equation [5.139]) can be formed from these results:

$$\mathbf{K}^u = \mathbf{M} - Bb(1/3K)\mathbf{I}\mathbf{I} + \frac{1}{H_{\text{und}}}\left\{\overline{\mathbf{P}} + \frac{1}{3}(1-B)\beta\mathbf{I}\right\}\left\{\overline{\mathbf{Q}} + \frac{1}{3}(1-B)\mu\mathbf{I}\right\}. \tag{5.164}$$

where $H_{\text{und}} = H + BK\beta\mu/b$ and $\overline{\mathbf{P}}$ and $\overline{\mathbf{Q}}$ are the deviatoric parts of $\mathbf{P}$ and $\mathbf{Q}$, respectively. The contribution to the inelastic strain rate, the last term in equation (5.164), is identical in form to that for drained deformation (equation [5.84]), with H replaced by H_{und}, β replaced by $(1 - B)\beta$, and similarly for μ. If the expression for the compliance is specialized to pure shear, the result is exactly analogous to that of Rice (1975): the undrained response is identical in form to that for drained response but with H replaced by H_{und}. Because B, K, and b^{-1} are positive, H_{und} is greater or less than H depending on the sign of $\beta\mu$, in a manner identical to the dependence on the sign of $\beta\mu$ in Rice (1975). For isotropic elasticity, the elastic contribution for undrained response also has the same form as drained response with K, the elastic bulk modulus for drained deformation replaced by K_u, the value for undrained deformation (Chapter 1, equation [1.40]), where

$$K_u = K/(1 - bB). \tag{5.165}$$

Consequently, results for localization for drained response, e.g., expressions (5.153) and (5.154), also apply for undrained response with these substitutions. It follows that for a constitutive relation of this form, there is no need for a separate analysis of the undrained response. In particular, the critical value of h_u for undrained response is $h_u = \mathbf{v}^u \cdot \mathbf{F}^u \cdot \mathbf{u}^u$ and the corresponding critical value of H (not H_{und}) is given by

$$\begin{aligned} H_c^u \;=\; & H_c^d - \frac{K_u B}{b(K_u + 4G/3)(K + 4G/3)} \\ & \times \{b(\mathbf{n}\cdot\mathbf{u}) + (1-b)(K + 4G/3)\,\text{tr}\,P\} \\ & \times \{b(\mathbf{n}\cdot\mathbf{v}) + (1-b)(K + 4G/3)\,\text{tr}\,\mathbf{Q}\}, \end{aligned} \tag{5.166}$$

where H_c^d is given following equation (5.154)

A lengthy but straightforward calculation reveals that equation (5.158) can be written in the simple form

$$(H - H_c^d)\kappa\Delta p + \Delta\dot{p}\frac{b}{K_u B}\frac{(K_u + 4G/3)}{(K + 4G/3)}\left\{H - H_c^u\right\} = 0. \tag{5.167}$$

Thus, the equation has the same form as the result for the layer (Section 5.3.4): the coefficient of the first term changes sign (from positive to negative) when H passes through the critical value for localization for drained response and the coefficient of the second changes sign when H passes through the critical value for localization for undrained response.

These expressions can also be used to examine the role of the compressibilities of the individual solid and fluid constituents. If the solid constituents are incompressible, the results simplify considerably. In particular, $b = 1$, $\alpha = \mathbf{R} = \mathbf{I}$, and $\mathbf{a} = \mathbf{r}$ in equation (5.142). The compressibility of the pore fluid enters only through the Skempton coefficient B (see Chapter 1). If both the solid and fluid constituents

are incompressible, then $B = 1$. In this limit, the bulk modulus is eliminated from equation (5.164) and so is β. Consequently, both the elastic and inelastic components of the strain rate are effectively incompressible. Furthermore, μ is eliminated from equation (5.164). Therefore, any dependence of the yield function on mean stress for drained response is exactly compensated by changes in pore pressure during undrained response. Thus, the undrained response is incompressible and does not depend on the mean stress. For such a solid, shear bands are predicted to occur 45° from the principal axes, at least if $\overline{\mathbf{P}} = \overline{\mathbf{Q}}$. Runesson et al. (1996) obtain this result by direct calculation for undrained deformation of a porous elastic-plastic solid with an incompressible pore fluid (although, as already noted, a separate analysis for undrained response is unnecessary). The result pertains, however, only to solid constituents that are also incompressible. Although Runesson et al. (1996) do not explicitly state that the solid constituents are incompressible, they use $\sigma + p\mathbf{I}$ as the effective stress for both inelastic and elastic deformation. This form is consistent with linear poroelasticity only when the solid constituents are incompressible.

5.7 Experimental and Field Observations

5.7.1 Localization in Granular Soils

Although the pioneer paper on bifurcation analysis of Rudnicki and Rice (1975) focused on brittle rocks, since the 1970s a large number of laboratory experiments on sand specimens have been devoted to the characterization of strain localization. Sand behavior can be briefly summarized as frictional without cohesion, with a rigidity considerably smaller than that of rocks, and a strong dependence on initial porosity. In addition to the porosity, localization in sand specimens is influenced by the confining pressure, the size and shape of both grains and specimen, and the anisotropy of the granular deposit. Several detailed overviews about observations of strain localization in sand can be found in the literature (e.g., see Vardoulakis and Sulem, 1995; Desrues, 1998, for recent reviews).

Experimental Techniques

Sand specimens are generally contained in a rubber membrane that separates the sand from a confining fluid. Before enclosure within the membrane, the specimens are prepared inside a mold and the method of sand deposition controls the initial density. In an axisymmetric test, the specimen is cylindrical and a fluid pressure is applied to the lateral surface via the membrane. The specimen is shortened by the loading device (compression test) or extended (extension test). In a compression test, the most compressive principal stress is axial and the two other principal stresses are equal. For an extension test, the least compressive principal stress is axial.

For studies of localization, the plane strain test, often called the biaxial test (Arthur et al., 1977; Vardoulakis et al., 1978; Desrues, 1984; Tatsuoka et al., 1986; Finno et al., 1997), is generally preferred to the axisymmetric geometry. In such a test, the three principal stresses are different (Figure 5.23). The specimen is prismatic, a fluid pressure is applied on lateral surfaces (direction 1), the deformation is restrained in direction 2, and the specimen is shortened in direction 3. When strain localization occurs, the normal to the plane of the band is generally perpendicular to the direction 2 (direction of the intermediate principal stress). If the device used to prevent the deformation in direction 2 is transparent (glass platens), then the specimen can be observed during the test and the displacement field of the specimen's face measured. For example, Desrues (1984) used the false-relief stereophotogrammetry method and Tatsuoka et al. (1990) the laser speckle method to measure the incremental displacement of material points of the specimen's face from photographs taken at two loading steps. The displacement field map can be used to detect the initiation and propagation of strain localization bands.

Specimen Loading Response and Localization

The two types of tests just discussed are considered rheological tests. If the specimen is deformed homogeneously, the response represents material behavior and can be analyzed in terms of the evolution of stress versus strain. A nominal stress versus strain curve can be obtained simply by dividing the axial force by the cross-

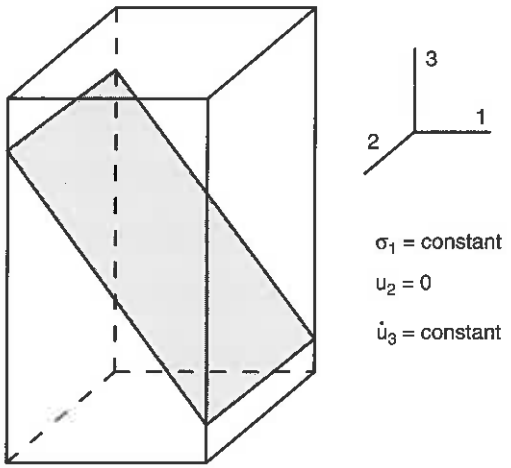

Figure 5.23 ▶ Schematic of a plane strain test (biaxial test). The vertical displacement is imposed with a constant speed (direction 3, most compressive principal stress), the lateral confinement is constant (direction 1, least compressive principal stress), and the displacement in direction 2 is restrained (intermediate principal stress direction). When strain localization occurs, the normal to the plane of the band is generally perpendicular to the direction of the intermediate principal stress.

sectional area of the specimen and the shortening by the height. The question of the homogeneity of the strain field is, however, fundamental. Nonhomogeneous deformation of the specimen can strongly affect the response and lead to errors in inferring the material response (e.g., Drescher and Vardoulakis, 1982). Nonhomogeneous deformation can also affect the initiation of strain localization. One common cause of inhomogeneities is friction between the specimen and the load caps, but this can be reduced by using lubricated and enlarged platens and by appropriately choosing the slenderness ratio (ratio of vertical to horizontal sizes) of the specimen.

As long as the strain field is more or less homogeneous, the specimen behavior is representative of sand behavior. When strain localization occurs, the specimen response reflects the combined behavior of the material inside and outside the localized zone. This aspect is illustrated in Figure 5.24 for two types of material response. The solid curves represent the material response, whereas the dotted curves represent the response of the specimens. One of the solid lines represents a continuous strain hardening behavior, whereas the second shows strain hardening up to a peak stress and then a slight softening. The material and specimen response diverge when the strain localization occurs. The strong specimen softening is caused by the localization (i.e., to the softening inside the deformation band). Of course, the portion of the material behavior curves after localization takes place cannot be observed, at least in the same test. Note also that initially homogeneous deformation may give way to diffuse nonhomogeneous deformation (bulging, barreling) before the appearance of a localized deformation mode, especially in axisymmetric compression tests.

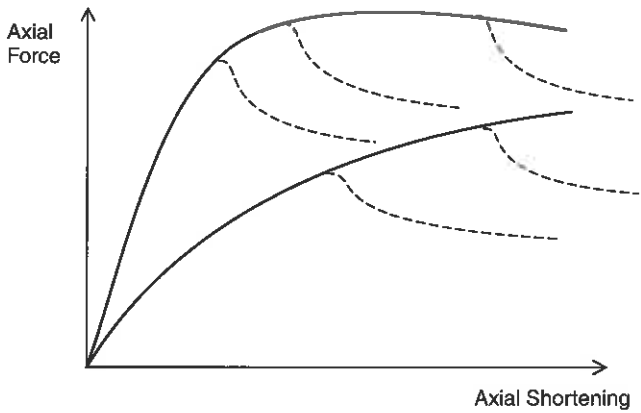

Figure 5.24 ► Typical evolution of the axial force versus axial shortening during a compression test performed on a sand specimen. The solid lines represent the response of specimens strained homogeneously. Dotted lines represent the strength softening of the specimens when strain localization occur (postlocalized response).

Results of a biaxial test performed with a Hostun RF sand specimen are presented in Figure 5.25 (Desrues, 1984). Photographs of the specimen were taken at several steps of the specimen shortening and analyzed by the false-relief stereophotogrammetry method. The strain field is diffuse and reasonably homogeneous in the initial loading between steps 1 and 2. The initiation of localization is clearly observed between steps 3 and 4, but the band does not cross the specimen completely. Specimen softening occurs only when a band crosses the entire specimen. Then, the upper part of the specimen slides over the lower part along the shear band.

The onset of localization is influenced by the specimen state. For a given initial porosity, the onset of localization occurs at larger axial strain with larger confining

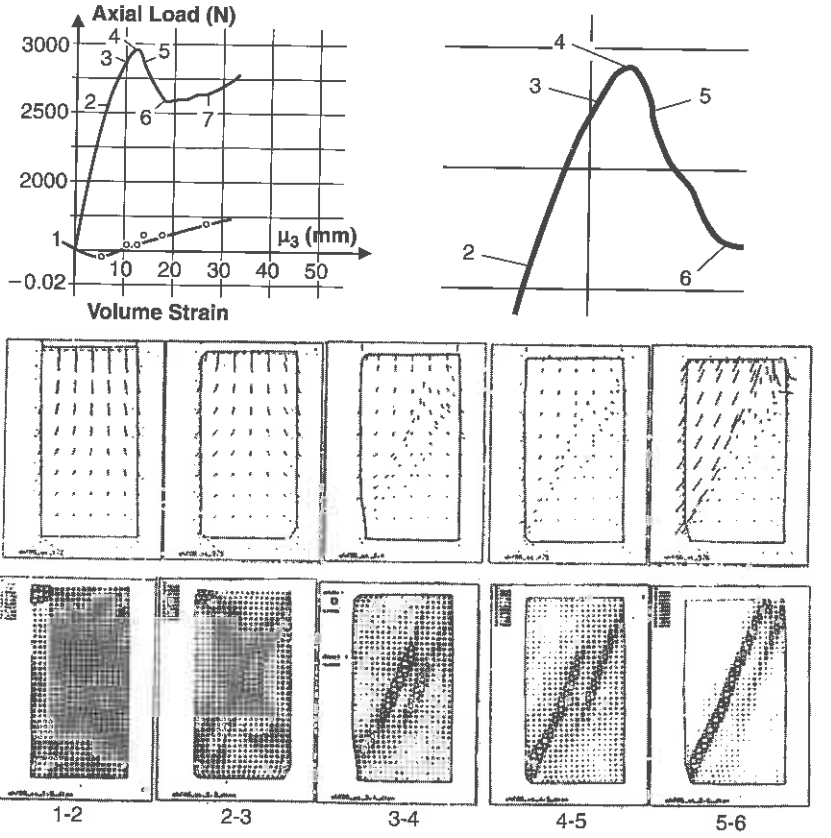

Figure 5.25 ▶ Biaxial compression test result on a Hostun RF sand specimen. (top) Photographs (1-7) were taken at several steps of the loading. (middle) Between each step, the incremental displacement field is measured and (bottom) the shear strain field (the difference between the major and minor principal strains) is computed. (Courtesy of J. Desrues.)

stress; for a given confining pressure, the onset occurs for a smaller axial strain in a dense sand sample than in a loose sample (e.g., Hammad, 1991). Localization generally occurs at larger strains in an axisymmetric test than a biaxial test.

Shear Band Orientation and Pattern

The orientation of deformation band depends strongly on the direction of principal stresses in the material. Several theories have been proposed to predict this orientation (e.g., see Bardet, 1990, for a review).

The Mohr-Coulomb prediction assumes that the failure occurs when the largest Mohr stress circle touches the failure envelope and that the deformation band is then parallel to the surface corresponding to the tangent point. The orientation of the band (the angle between the normal to the band and the direction of the most compressive principal stress) is then given by

$$\theta_C = \pi/4 + \varphi/2, \tag{5.168}$$

where φ is generally called the *friction angle* and $\tan(\varphi)$ is the slope of the failure envelope in the plane (σ_n, τ_n), where σ_n and τ_n are the normal and shear tractions on a material plane, respectively. For a cohesionless material, φ is defined by $\sin(\varphi) = (\sigma_1 - \sigma_3)/(\sigma_1 + \sigma_3)$, where σ_1 and σ_3 are the greatest and least compressive principal stresses at failure, respectively.

The prediction by Roscoe (1970) states that the deformation band is parallel to the surface of zero extension rate for the homogeneous strain rate state before failure. The angle of the band is then expressed by

$$\theta_R = \pi/4 + \psi/2, \tag{5.169}$$

where ψ is the *dilatancy angle* defined by $\sin(\psi) = -(\dot{\varepsilon}_1 + \dot{\varepsilon}_3)/(\dot{\varepsilon}_1 - \dot{\varepsilon}_3)$ and $\dot{\varepsilon}_1$ and $\dot{\varepsilon}_3$ are the most compacting and most extensive principal strain rate before failure, respectively. The Roscoe angle θ_R is generally smaller than the Mohr-Coulomb angle θ_C by about 15° (Arthur et al., 1977; Tatsuoka et al., 1990).

Arthur et al. (1977) has also proposed an ad hoc expression that combines the Roscoe and Mohr-Coulomb predictions:

$$\theta = \pi/4 + (\varphi + \psi)/4. \tag{5.170}$$

Note that the preceding predictions (5.168), (5.169), and (5.170) do not involve the intermediate value of the principal stresses or strain rates. Consequently, predictions for axisymmetric and biaxial tests will be identical.

The orientations of deformation bands in biaxial tests are generally observed to lie between θ_R and θ_C (e.g., Bardet, 1990, from results of teams of Arthur, Vardoulakis, and Desrues). Band orientation depends on many microstructural factors such as grain shape and angularity, grain size distribution, and mean grain

size. Many authors have observed that the band angle decreases with the mean grain size in many types of sands and is closer to θ_C for fine sands and to θ_R for coarse sands (Arthur and Dunstan, 1982; Vermeer, 1990; Yoshida and Tatsuoka, 1997). However, microstructural parameters differ for each sand, and grain size distribution could have a larger influence on the band orientation than the mean grain size (Viggiani et al., 2001).

The pattern of deformation bands in sand samples is influenced by the specimen shape and the amount of displacement of the specimen ends allowed by the load caps; that is, the caps may be free to translate laterally or constrained to be coaxial. Typical patterns observed (e.g., Desrues, 1998) during biaxial tests are illustrated in Figure 5.26. When the slenderness ratio of the specimen (the ratio of height to width) is about 2 or more and the free lateral displacement of a load cap is possible, a simple deformation band (or eventually two parallel bands) occurs in most cases and the band intersects a corner of the specimen. If the lateral translation of the load caps is restrained, conjugate bands generally occur. This can be understood in terms of kinematic compatibility of the specimen displacement field with the displacements of the specimen ends. If the slenderness ratio is small and a simple band cannot cross the specimen from one lateral surface to the other, one or more additional bands occur. A second band can be seen as a reflection of the first with respect to the rigid load cap. More complex patterning can also be observed in the axisymmetric test if coaxiality of the load caps is imposed. The patterning remains more or less axisymmetric but comprises a central cone and, outside it, several conjugate pairs of bands in V shapes oriented radially (Desrues et al., 1996).

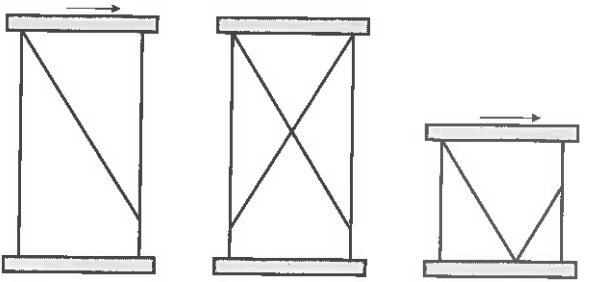

Figure 5.26 ▶ Schematic of patterns observed in sand specimens after a plane strain compression. (a) A simple band when the lateral translation of an end cap is free. (b) Two conjugate bands when the end caps are coaxial. (c) Two reflected bands when the specimen is short.

Thickness and Volume Change Inside Shear Band

Strain localization in sands can be observed with X-ray methods. X-ray radiography (Roscoe, 1970; Scarpelli and Wood, 1982; Vardoulakis and Graf, 1985; Nemat-Nasser and Okada, 2001) or computer tomography (Desrues et al., 1996;

Mandl, 1988) can detect volume change associated with strain localization. Indeed, X-ray attenuation through sand masses is controlled by the porosity in the sand (as long as the distribution of grain mineralogy is homogeneous). Dilatancy (compaction) inside the band induces a smaller (higher) attenuation of X-rays. Experimental observations show that a strong dilatancy with respect to the average porosity in the specimen occurs inside the localization band, especially in dense samples. This dilating volumetric strain is associated with shearing strain. For very loose samples, however, the porosity inside the band is close to the porosity outside the band and the sand can be slightly compacting. In a sand composed of shell remains (brittle particles), Colliat-Dangus (1986) has, however, observed compaction in a localization band, apparently associated with grain crushing at low confining pressure (0.5 MPa).

After localization, the porosity inside the band evolves to a stable value (Vardoulakis and Graf, 1985). This *critical porosity* is independent of the initial porosity of the specimen; that is, it is identical for loose samples that compact during the homogeneous straining and dense samples that dilate. For a given sand, the critical porosity (Figure 5.27) is determined by the confining pressure applied to the specimen (Mokni, 1992; Desrues et al., 1996).

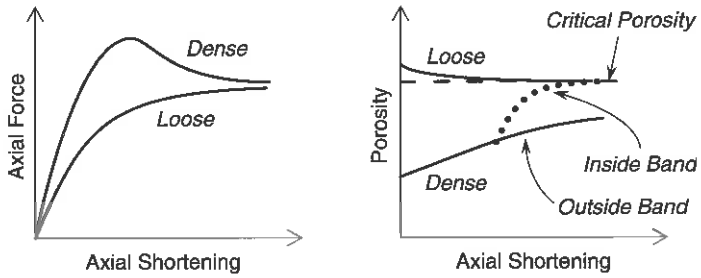

Figure 5.27 ► Idealized sample responses for a given sand and confining pressure in initially loose and dense specimens. The strengths converge after localization and the porosity inside the bands converges to a critical porosity.

The thickness of the deformation band seems essentially controlled by the size of grains in the sand but decreases slightly with increasing confining pressure. Bands are thicker for an initially loose sample than for a dense sample (Mokni, 1992). Several authors have measured the ratio between the band thickness and the mean grain size. Roscoe (1970) reported a ratio of 10, Scarpelli and Wood (1982) a ratio between 5 and 10 or more, and Mühlhaus and Vardoulakis (1987) a ratio between 13 and 18. The data from Yoshida and Tatsuoka (1997) for 10 types of granular media, shown in Figure 5.28, indicates that the ratio can vary between about 5 and 20.

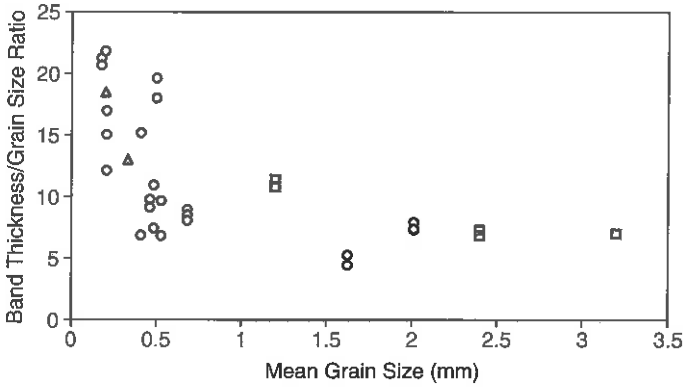

Figure 5.28 ► Observed ratio of thickness of deformation bands by the mean grain size in several sands versus the mean grain size, by Yoshida and Tatsuoka (1997) in fine and coarse sands (circles), Mokni (1992) in coarse sands (squares), and Mühlhaus and Vardoulakis (1987) in fine sands (triangles). The data vary between a ratio from about 5 to 20.

5.7.2 Experiments on Brittle Rock

In experiments on brittle rock, shear localization is generally interpreted as the formation of a fault in the specimen. Depending on the type of rock, the machine stiffness, end conditions, confining pressure and temperature, and the appearance of the fault may range from a planar surface to a gouge zone of linked cracks and comminuted material. At higher confining pressures and temperatures, characteristic of a transition to ductile behavior, localization may appear as a narrow zone of concentrated shear deformation, without fault formation, or may not occur at all. In experiments, the fault does not, of course, appear instantaneously as assumed in the bifurcation analysis. Instead, it typically begins in one location and spreads across the sample. The use of acoustic emission location systems (e.g., Lockner et al., 1992) has made possible more detailed observations of this process of initiation and propagation. In most cases, the propagation phase occurs sufficiently rapidly that it is possible to identify a definite onset of localization, and fault formation can be identified with an abrupt change in the slope of the load versus deflection curve. Furthermore, the limiting nature of the localization bifurcation (Rice, 1976) suggests that it is properly identified as the full development of a fault, rather than the first appearance of inhomogeneous deformation. The localization bifurcation is limiting in the sense that once the condition has been met it is possible to construct a localized field (albeit of infinitesimal width) even under all-round displacement boundary conditions (Rice, 1976).

Comparison of predictions with experimental observations is complicated by the presence of inhomogeneities in both material and deformation before localization. Other bifurcations, diffuse or geometric modes, will generally precede

localization (Hill and Hutchinson, 1975; Needleman, 1979; Chau and Rudnicki, 1990). The simplest of these is analogous to buckling of a thin strut or bulging of a squat cylinder. More generally, these modes are associated with the specification of traction conditions on a portion of the boundary and, in contrast to the localization condition, their onset depends on the geometry of the specimen. Natural materials are inevitably inhomogeneous on some scale, but the dimensions of samples are typically large enough that they are reasonably homogeneous. Inhomogeneity may also result from application of the boundary conditions. In some cases, localization clearly begins at the corner of the specimen where it meets the loading platen. This suggests that faulting is triggered by the stress concentration induced by the constraint of the end condition and develops by a process similar to crack propagation. In such cases, analysis with a framework of bifurcation is probably not appropriate. In many other cases, the sample deformation is sufficiently uniform and the appearance of the fault sufficiently definite that comparison with the predictions of the bifurcation theory is reasonable.

Faulting is generally observed to occur in the vicinity of peak stress and the peak stress is identified as the *strength*. The bifurcation analysis in equation (5.112) predicts, however, that localization will not occur until well after peak stress ($H < 0$) for unfavorable deformation states (e.g., axisymmetric compression or extension) but may occur before peak ($H > 0$) for a range of favorable deformation states when normality is not satisfied, as is typical for brittle rock. Despite a casual association of faulting with peak stress, a careful examination of reported observations suggests that the reality is more complex. It is, however, important to properly relate the quantities observed in the experiment to the parameters appearing in the prediction.

The bifurcation analysis described in earlier sections yields a relation among material parameters at which localization is predicted to occur and predicts the orientation of the band in terms of these parameters. For the constitutive relation used by Rudnicki and Rice (1975), equation (5.110), these are expressed by equation (5.112) (if the condition [5.115] is met) and by equation (5.113) with (5.114). The relation for the onset of localization in equation (5.112) involves the elastic constants, G and ν, and the inelastic material parameters, the hardening modulus H, the friction coefficient μ, and the dilatancy factor β; the expression for the orientation (5.114) depends only on the sum $\beta + \mu$ and the Poisson ratio ν. Although equation (5.112) is written as an expression for a critical value of the hardening modulus, H^c, all the inelastic parameters (see, e.g., Holcomb and Rudnicki, 2001) and even the elastic parameters (Sulem et al., 1999) will evolve with inelastic deformation. Thus, equation (5.112) gives the relation among the *current* values of the parameters at localization.

Importantly, the analysis predicts that both the onset of localization and the band angle depend on the stress state parameter N. N is related to the Lode angle (Hill, 1950) θ_L by

$$\sin(3\theta_L) = \sqrt{27/4}N(1 - N^2), \tag{5.171}$$

where θ_L is defined by

$$\theta_L = \frac{1}{3} \arcsin \left\{ -\frac{27}{2} \frac{\det(\bar{\sigma}_{ij})}{(3\bar{\tau})^{3/2}} \right\}. \tag{5.172}$$

Thus, the localization predictions, equations (5.112) and (5.113), depend on the third invariant of the deviatoric stress, $\det(\bar{\sigma}_{ij})$, even though the constitutive relation (5.110) depends only on the first and second stress invariants (although other constitutive relations may introduce an additional dependence on the third invariant). Unfortunately, this predicted dependence is difficult to evaluate by experiment because the vast majority of rock testing has been in axisymmetric compression ($N = 1/\sqrt{3}$), with a few results in axisymmetric extension ($N = -1/\sqrt{3}$), and very few at intermediate values. One of the only studies to systematically investigate the response over a range of values of N is that of Mogi (1971) on Dunham dolomite using a true triaxial apparatus (one that can apply three distinct principal stresses). Figure 6 of Mogi (1971) shows a series of eight curves of stress difference (maximum minus least compressive stress) against strain (measured in the direction of maximum compression). The least compressive stress is fixed at 1.25 kbar and the intermediate principal stress increases from this value to 5.16 kbar. The values of N at failure (presumed to be faulting) can be calculated by estimating the maximum compressive stress from the graphs; they decrease from $1/\sqrt{3}$ (axisymmetric compression) to about 0 (deviatoric pure shear) with increasing intermediate principal stress. The slope of the stress strain curve at failure clearly increases with decreasing N, consistent with the prediction of equation (5.112). The mean stress also increases with decreasing N, however, and it is not possible to separate the effects of changing deviatoric stress state (decreasing N) from those of increasing mean stress. A further difficulty, discussed in more detail later, is that, except for axisymmetric stress states, the value of H (defined in terms of the curve of shear stress versus shear strain at *constant* mean stress) is not simply related to the slope of the stress strain curve.

Mogi (1971) did not report fault angles but Mogi (1967) does report them for axisymmetric compression and extension tests on Westerly granite, Dunham dolomite, and Solnhofen limestone. Figure 5.29 shows results from all the tests summarized in Table 2 of Mogi (1967) in which failure angles are given. Also shown are results from a series of biaxial tests on Dunham dolomite summarized in Table 3 of Mogi (1967). Unfortunately, there are only a few results for extension and compression tests at the same mean stress for a given rock type. (Note that if the failure angles in extension and compression are observed at the same mean stress or if the constitutive parameters are assumed to be independent of mean stress, then evaluating equation [5.113] for $N = 1/\sqrt{3}$ and for $N = -1/\sqrt{3}$ makes it possible to determine the value of ν and of the sum $\beta + \mu$ at failure.) Nevertheless, for each rock type, the failure angles for extension are considerably greater than those for compression in accordance with the prediction of equation (5.113). For both the extension and compression tests the failure angle decreases with increasing

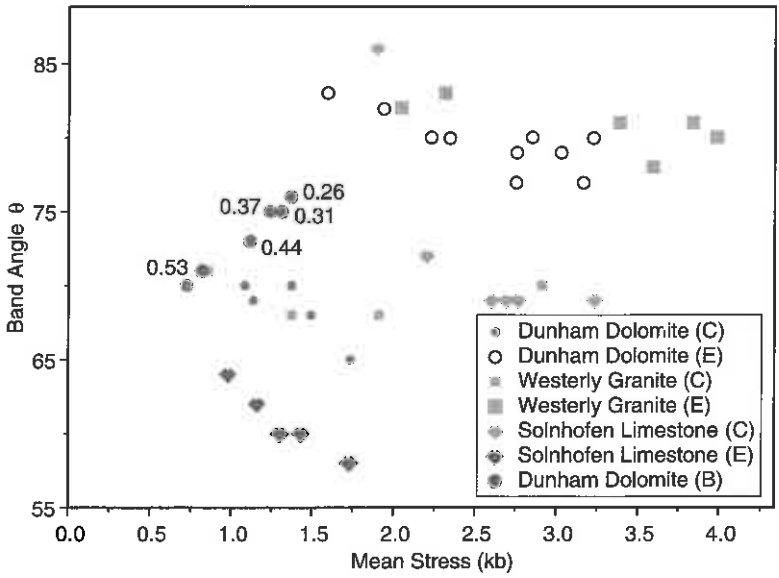

Figure 5.29 ▶ Band angle (between most compressive principal stress direction and the normal to the band) against mean stress from data from Mogi (1967). Open symbols are from extension tests (E), closed from compression tests (C), and crossed circles from biaxial tests (B). Different shapes indicate different rock types.

mean stress, with the rate of decrease varying with test and rock type. From data of Bésuelle et al. (2000), Bésuelle (2001a,b) showed that both for extension and compression axisymmetric tests, the observed decrease of the failure angle with mean stress is quantitatively predicted from the observed decrease of $\beta + \mu$ at failure. In contrast, the failure angle in the biaxial tests increases with mean stress but the values of N (shown next to the data points in Figure 5.29) are also decreasing. The increase of the failure angle as N decreases from the value for axisymmetric compression toward extension is consistent with the larger angles observed and predicted in extension and with the trend equation (5.113). Figure 6 of Rudnicki and Olsson (1998), which plots the failure angles from biaxial data against N (without regard to the different mean stresses), indicates that the increase of the observed angle with N is much more rapid than predicted by equation (5.113) for fixed value of $\beta + \mu$. If the decrease in angle with mean stress observed for the axisymmetric tests is assumed to apply to the biaxial data, the increase would be even more rapid for fixed mean stress.

The most common testing configuration for rocks is axisymmetric compression (often called triaxial compression). For this configuration, equation (5.112) predicts that localization does not occur until well after peak stress (negative values of H_c that are substantial fractions of G in magnitude). Rudnicki (1977b) has argued

that the studies of Wawersik and Brace (1971) and Tapponnier and Brace (1976) on Westerly granite, Wawersik and Fairhurst (1970) and Rummel and Fairhurst (1970) on Tennessee marble, and Crouch (1970) on a sandstone clearly indicate that a fault has not developed until well past peak stress. Fredrich et al. (1989) report that localization in Carrara marble (at a confining pressure of 5 MPa) does not occur until well past peak stress, and acoustic emission measurements of Lockner et al. (1992) on Westerly granite also indicate that fault formation does not occur until after peak stress in a granite. In a sandstone, Lockner et al. (1992) observed some localization of acoustic emission events just before peak but fault formation did not occur until after peak. Santarelli and Brown (1989); Bésuelle et al. (2000) also systematically observed a loss of the homogeneity of the strain field (from multiple internal measurements on specimens) before the peak but did not state whether the band fully formed before or after peak.

For equation (5.110), the tangent modulus for axisymmetric compression (slope of axial stress versus axial strain curve) is related to the hardening modulus by Cleary and Rudnicki (1976):

$$E_{\tan}^{-1} = E^{-1} + (3H)^{-1}(1 - \mu/\sqrt{3})(1 - \beta/\sqrt{3}). \tag{5.173}$$

Because Young modulus $E > 0$, the sign of H is the same as the sign of $E_{\tan}$ as long as β and μ are less than $\sqrt{3}$, which is generally the case. Consequently, faulting in the postpeak regime of the axisymmetric compression test indicates localization with $H < 0$. Although this is consistent with the predictions of the bifurcation theory, values of H at localization are probably not so negative as predicted by equation (5.112). As discussed earlier, using a noncoaxial constitutive model or one having a vertex at the current stress point considerably reduces the magnitude of H_c and predicts that localization will occur much closer to peak stress. Parameters governing the response at a vertex cannot, however, be obtained from conventional axisymmetric compression experiments and are uncertain. Olsson's (1992; 1995) compression torsion experiments on hollow cylinders of Tennessee marble are the only ones exploring response at a vertex in rock. He finds reductions, relative to the elastic shear modulus, of up to a factor of three in the shear moduli governing increments of torsion superimposed on axisymmetric compression. This is probably not sufficient, however, to bring the predictions of localization near peak stress for axisymmetric compression.

Other models, such as the incrementally nonlinear models (see Section 5.4.5), predict a localization before a peak of the material response in axisymmetric or intermediate stress states (Chambon et al., 1994). In this last model, the slope of the stress versus strain curve is continuously positive. Some material parameters are obtained from the homogeneous behavior of specimens (before localization) tested in conventional experiments. Other parameters that cannot be obtained from these conventional tests are evaluated from the characterization of the strain localization that occurred at the end of these tests (onset of localization, band orientation), to have agreement between the bifurcation prediction and the observations.

Although a great deal of study (see Paterson [1978] for a summary) has been devoted to the effects of length to diameter ratio of specimens and end conditions on deformation and failure, effects on localization can be subtle and difficult to control. Furthermore, because the deformation is nonelastic and satisfaction of the localization condition indicates a change in type of the governing equations, assurances about the role of boundary conditions cannot be based on appeal to St. Venant's principle (Sokolnikoff, 1956).

Albert and Rudnicki (2000) conducted detailed finite element simulations of the axisymmetric compression test using a constitutive relation of the type in equation (5.110) determined by Holcomb and Rudnicki (2001) from a suite of axisymmetric tests on Tennessee marble. For a specimen aspect ratio of 2.5 they found that curves of the nominal stress (load divided by cross-sectional area) versus nominal strain (change in sample length divided by original length) were virtually independent of friction at the sample–platen interface over the entire range from perfectly bonded (infinite friction) to shear free (zero friction). The detailed distribution of stress and strain in the sample was, however, strongly affected by the friction at the ends and this contributed to differences in the onset of localization. At the center of the sample, even a small coefficient of friction (e.g., 0.01) causes an increase in the mean stress (relative to homogeneous deformation) and, consequently, the slope of the stress-strain curve is still rising at strain levels for which homogeneous response is softening. In contrast, an element at the periphery on the midline of the specimen softens more rapidly than the homogeneous response (Albert and Rudnicki [2000] show the response of this element only for the perfectly bonded case but note that results are similar for any small but finite level of friction). Similarly dramatic differences occur for elements immediately under the platen. The equivalent shear stress (J_2) decreases on the centerline of the specimen but so does the mean stress: consequently, the element ceases to deform nonelastically and essentially follows a trajectory tangent to the yield surface. In contrast, the mean stress for the element under the platen at the periphery of the specimen increases, and although it continues to deform nonelastically, the inelastic strains are small because of the inhibiting effect of the mean stress. These results are consistent with the conjecture of Olsson (2000) that conditions for localization will first be met in an outer layer of the specimen. He suggests that this may be the origin of observations of Luders bands on the surface of specimens. The acoustic emission observations of Lockner et al. (1992) also indicate that localization initiates on the periphery of the sample near the midline.

Although axisymmetric compression is the most common testing configuration for rocks, in the Earth's crust neither artificially induced nor tectonic deformations are likely to be axisymmetric. In addition, although the analysis indicates that axisymmetric deformation is relatively resistant to localization, predictions based on this state may be considerably nonconservative. In contrast to axisymmetric compression, plane strain deformation includes a plane of zero extension rates. Consequently, localization in plane strain does not involve such an abrupt change in the pattern of deformation as in the axisymmetric symmetric state, and as a

result, localization is predicted to occur more readily (at a larger, and possibly even positive, value of the critical hardening modulus H_c). Because the change in deformation pattern with localization is not so abrupt, the issue of a smooth versus corner yield surface is not so crucial (though still possibly significant). For these reasons, the plane strain state is attractive for investigating localization from the theoretical point of view. Although there are significant practical difficulties in maintaining the plane strain constraint for strong rocks, a number of plane strain tests have been conducted (Wawersik et al., 1990; Ord et al., 1991; Labuz et al., 1996) to test the prediction of Rudnicki and Rice (1975) that fault formation could occur for positive H.

Despite the apparent theoretical advantages of the plane strain test for studying localization, there are a number of less obvious difficulties. The first is that, unlike axisymmetric compression (with modest restrictions on β and μ), the sign of the tangent modulus of the stress versus strain curve may differ from that of H. Hence, observation of localization on the rising portion of the stress-strain curve does not necessarily indicate that localization has occurred with $H > 0$. The origin of this effect is the rapid increase of the mean stress caused by the out-of-plane constraint. For the constitutive relation (5.110), the tangent modulus for plane strain ($d\sigma_{33}/d\varepsilon_{33}$) is given by

$$E_{\tan}^{pl.\epsilon} = \frac{H + EP_{22}Q_{22}}{(1-\nu^2)(H/E) + P_{22}Q_{22} + P_{11}Q_{11} + \nu(P_{22}Q_{11} + P_{11}Q_{22})}, \tag{5.174}$$

where P_{ij} and Q_{ij} are defined by equation (5.106) and 1 and 2 denote the loading and plane strain directions, respectively. Clearly, the expression does not necessarily change sign when H does. Holcomb and Rudnicki (2001) have emphasized this point with an example (derived from unpublished finite element calculations of N. Higgs) for a material with a constant negative value of $H = -0.49G$, $\mu = 0.7$, and $\beta = 0$. In this example, localization is predicted to occur in plane strain but not in axisymmetric compression. Consequently, reports by Labuz et al. (1996) that localization did not occur until after the peak of the stress-strain curve for tests on Berea sandstone and by Ord et al. (1991) that localization occurred prepeak in Gosford sandstone are not definitive about the sign of H. Holcomb and Rudnicki (2001) conducted a more elaborate investigation of observations in plane strain deformation of Tennessee marble by using a suite of axisymmetric compression tests at different confining pressures to determine the constitutive relation (5.110). In particular, they determined the variations of H, β, and μ with nonelastic shear strain and mean stress. By comparing the calculated response for plane strain with that observed in the experiment they concluded that localization did occur with positive H. They did, however, find discrepancies between the calculated and observed response that appeared to be caused by the anisotropy induced by the plane strain constraint.

Another, related complication of the plane strain test is that the value of N varies during the test. For isotropic, elastic plane strain deformation,

$$N = \pm(1 - 2\nu)/\sqrt{3(1 - \nu + \nu^2)}, \tag{5.175}$$

where the $(+)$ sign is for compression and the $(-)$ for tension. Thus, $N = 0$, corresponding to pure shear, for an incompressible elastic material, $\nu = 1/2$, but $N = \pm 1/\sqrt{3}$, corresponding to axisymmetric stressing, for $\nu = 0$. In the example from Holcomb and Rudnicki (2001), just cited, N varies from 0.38 (the elastic value for $\nu = 0.2$) to slightly less than 0.2 at localization. The variation inferred from a plane strain test on Tennessee marble (Figure 11 of Holcomb and Rudnicki [2001]) is from about 0.21 (corresponding to $\nu = 0.34$) to slightly above 0.3 followed by a small decrease.

The values of N in plane strain lie between those for deviatoric pure shear ($N = 0$) and axisymmetric compression ($N = 1/\sqrt{3}$). The largest (most positive) value of H at localization is predicted by equation (5.112) to be $N = -(\beta + \mu)/3$. For positive β and μ, this lies between deviatoric pure shear and axisymmetric extension. Ideally, a thorough experimental investigation of the predictions of the bifurcation approach would involve tests over the entire range of N for several fixed values of the mean stress. More than 30 years ago, Mogi (1971) reported results using a true triaxial machine, previously discussed. Although only a few results have been reported since then, almost exclusively on weak or medium-strength rocks, Haimson and Chang (2000) have recently described an apparatus that is suitable for testing of higher strength rock and they have reported results on Westerly granite. A careful and thorough investigation of constitutive behavior and failure over a range N values would be a major impetus for constitutive and failure modeling.

5.8 Postlocalization

Bifurcation theory applied to rate-independent constitutive relations yields predictions for the onset of strain localization, an orientation of the deformation band, and the direction of the strain rate inside the band at its inception. A limitation of this analysis is that it does not constrain at all the thickness of the band. If the band width becomes increasingly narrow with ongoing deformation, a reasonable approximation is to treat the localized zone as a surface of displacement discontinuity. In this case, a constitutive relation can be specified for the traction on the surface as a function of relative displacement, displacement rate, etc. Without the thickness of the band, it is not, however, possible to analyze the progression of localized deformation within a zone of finite width or the transition to a surface of relative displacements. Furthermore, the absence of a length scale in the

constitutive model for problems with large strain gradients will cause numerical simulations to depend strongly (and spuriously) on the mesh size. The energy dissipation in the solid after localization is controlled by the band thickness, and as will be shown in the following analytical study (Section 5.8.1) applied to the layer problem introduced at the beginning of the chapter, the thickness of the band controls the global response of the layer. The thickness of the localization band also has important implications for permeability in field applications (e.g., stability of faults, oil production). Localization bands can represent zones where the permeability can be greater or less than that of the surrounding material and the global permeability of the rock mass is influenced by the thickness of these zones.

The inability to predict the thickness of the band arises from the lack of a length-scale parameter in the classic rate-independent constitutive models. Both rate-dependent constitutive models and rate-independent models with an internal length scale have been used to study the postlocalization response of a continuum. Rate dependence may reflect the observed or inferred response of the material or, in some cases, may be introduced artificially, from a mathematical or computational point of view, simply to regularize the localization problem (e.g., Loret and Prevost, 1990). Rate dependence will introduce a length scale directly in dynamic problems or, indirectly, from the requirement of an initial inhomogeneity, in quasi-static problems. In rate-independent models, this length scale is introduced directly into the constitutive relation and reflects the microstructure of the material. Examples of such models applied to a layer problem are presented in Sections 5.8.2 and 5.8.3. In particular, we consider a model with a microstructure and a local formulation and a model with a nonlocal formulation.

5.8.1 Thickness of the Band

The simple analysis in this subsection illustrates the strong dependence of solutions for the rate-independent constitutive model on the band thickness. Consider again the layer of thickness h described in Section 5.3, subjected to a shear boundary displacement U in the x direction. The onset of localization occurs when the tangent modulus $H_{\tan}$ vanishes and is assumed to occur in a band of thickness t ($t < h$, Figure 5.30). For a standard elastic-plastic (bilinear) constitutive model, the tangent modulus is different for elastic unloading and continued plastic loading. Consequently, the material outside the band unloads elastically and the material inside the band loads plastically. Because localization occurs at peak stress, the shear stress decreases when the band is initiated and $H_{\tan}$ is negative in the band for this geometry. Moreover, one assumes here an abrupt decrease of $H_{\tan}$ after the localization (see Figure 5.30).

The constitutive relation can be expressed by

$$\text{outside the band}: \; d\tau^{\text{out}} = G\, d\gamma^{\text{out}} \quad (\text{if } d\gamma^{\text{out}} < 0) \tag{5.176a}$$

$$\text{inside the band}: \; d\tau^{\text{band}} = H_{\tan}(\gamma)\, d\gamma^{\text{band}} \quad (\text{if } d\gamma^{\text{band}} > 0). \tag{5.176b}$$

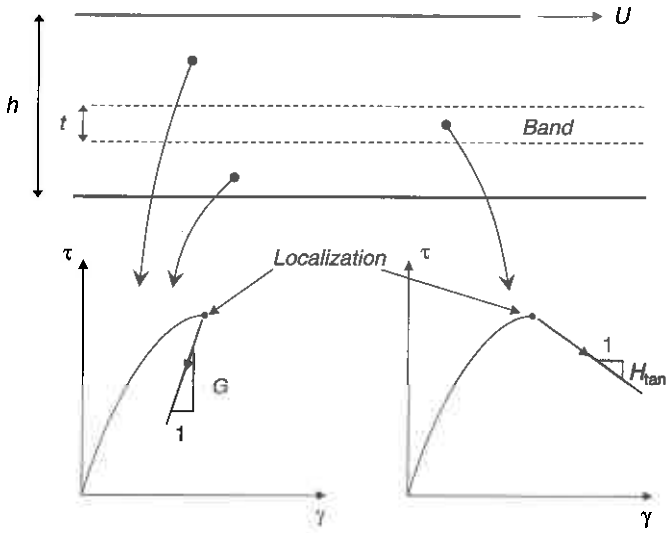

Figure 5.30 ▸ The material inside the band loads plastically and the material outside the band unloads elastically.

The equilibrium of the shear stress increment inside and outside the band (see also equations [5.2] in Section 5.3) is expressed by

$$\frac{\partial(d\tau^{\text{out}})}{\partial y} = 0 \qquad \frac{\partial(d\tau^{\text{band}})}{\partial y} = 0, \tag{5.177}$$

and the increment of shear stress at the interfaces of the band is continuous

$$d\tau^{\text{out}} = d\tau^{\text{band}}. \tag{5.178}$$

If we assume, for simplicity, that the tangent modulus after localization is constant [$H_{\text{tan}}(\gamma) = H_{\text{tan}}$], then substitution of equation (5.176) in equation (5.177) requires that the strain be homogeneous inside and outside the band and have a discontinuity at the interface. Because of equation (5.178), the shear strain increments inside and outside of the band are linked by

$$H_{\text{tan}}\, d\gamma^{\text{band}} = G\, d\gamma^{\text{out}}. \tag{5.179}$$

Finally, the increment of boundary displacement dU at the top of the layer is

$$dU = \int_0^h d\gamma\, dy = (h-t)\, d\gamma^{\text{out}} + t\, d\gamma^{\text{band}}$$

$$dU = \frac{1}{G}\left[h + t\,\frac{G - H_{\text{tan}}}{H_{\text{tan}}}\right] d\tau. \tag{5.180}$$

Figure 5.31 shows the importance of the band thickness t in controlling the overall response of the layer. As t becomes larger and approaches h, the layer loads plastically everywhere and the incremental layer response is $dU = h\,d\tau/H_{\tan}$. As t decreases to the limiting value $t_u = h\,H_{\tan}/(H_{\tan} - G)$, for which $dU = 0$, it is not possible to increase the boundary displacement quasi-statically, even with a displacement-controlled loading. A dynamic solution could be obtained by retaining the inertia terms in the equation of motion. In numerical solutions, this strong dependence of the layer response on the assumed band thickness results in a pathological mesh size dependence of the postlocalization problem. Note also that the layer response depends neither on the position of the band nor on the number of layers so long as their total thickness is t. This illustrates the nonuniqueness of the boundary value problem after bifurcation.

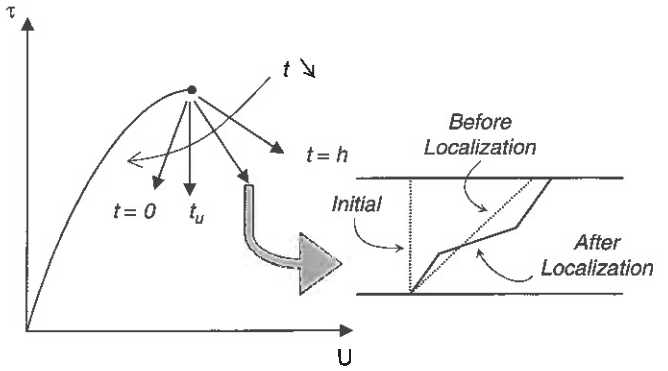

Figure 5.31 ▶ Layer responses after localization for different values of localization band thickness. The displacement field u_x is plotted for three steps of the layer loading, in cases where $t_u < t < h$.

5.8.2 A Model with Microstructure

The scale effect in localization, namely, the band thickness, is linked to a material internal scale for geological materials (i.e., grain size, crystal size). Models with microstructure can be introduced from the kinematic description of a continuum established by Mindlin (1964). Two scales are considered, a macro scale that corresponds to the classical kinematics of a continuum and a micro scale that represents the kinematics at a grain scale. The macro kinematics are described by the macro strain and macro rotation; the micro kinematics are described by a micro strain and a micro rotation. The micro kinematics can be different from the macro kinematic. This seems reasonable when one considers the deformation in a granular assemblage: the macro deformation in the assemblage results in several types of mechanisms at the micro scale, such as deformation inside grains,

deformation at the interface between grains, and microcracks. The Cosserat continuum (Cosserat, 1909) is a particular case of the present kinematic description in which the micro strain vanishes. This description seems appropriate for the study of localization in sand: the grains are more or less rigid and can rotate and translate (e.g., Mühlhaus and Vardoulakis, 1987; Vardoulakis and Sulem, 1995). The second gradient models assume that the micro kinematics is identical to the macro kinematics (e.g., Frantziskonis and Vardoulakis, 1992; Fleck and Hutchinson, 1997; Chambon et al., 2001). With respect to classic models, the second-gradient models have the advantage that not only the first gradient but also the second gradient of the displacement is introduced in the energy formulation; the second-gradient term becomes significant when the strain gradient is high, as in strongly nonhomogeneous problems and in strain localization bands. The models discussed in this subsection are local because of the introduction of dual terms of the micro kinematic variables with respect to the energy. The equilibrium and boundary conditions are modified to account for the dual terms. In contrast, some second-gradient models are nonlocal (see Section 5.8.3).

Kinematic Variables

Consider again the problem of the layer in which a displacement u_x exists in a direction x parallel to the layer and depends on the coordinate y normal to the layer. The macro displacement gradient is $\Psi = \partial u_x/\partial y$, which is equal in the present case to the shear strain γ. The kinematics of a model with structure at the micro scale is described by a micro kinematic gradient ψ. The micro deformation gradient (the second gradient) is defined as $\chi = \partial\psi/\partial y$. Here, we limit the analysis to the small strains and a quasi-static case.

Following the expressions for potential energy given by Mindlin (1964) for the elastic case and for the internal energy density given by Germain (1973) in more general cases, we can express the increment of internal energy density corresponding to an increment of deformation in terms of the macro strain increment, the difference between the micro kinematic gradient increment and the macro displacement gradient increment, and the micro deformation gradient increment:

$$\begin{aligned} \delta w^i &= \delta w^i(\delta\gamma, \delta\psi - \delta\Psi, \delta\chi) \\ &= \tau\,\delta\gamma + \eta\,(\delta\psi - \delta\Psi) + \mu\,\delta\chi, \end{aligned} \tag{5.181}$$

where the dual terms are τ, the classic shear stress; η, a *relative stress*; and μ a *double stress* associated with the second gradient.

For a purely second-gradient model, $\psi = \Psi$ and, in this case, the expression for the increment of internal work density simplifies to

$$\begin{aligned}\delta w^i &= \tau\frac{\partial(\delta u_x)}{\partial y}+\mu\frac{\partial^2(\delta u_x)}{\partial y^2}\\ \delta w^i &= \frac{\partial}{\partial y}(\tau\,\delta u_x)-\frac{\partial\tau}{\partial y}\delta u_x\\ &\quad+\frac{\partial}{\partial y}\left(\mu\frac{\partial(\delta u_x)}{\partial y}\right)+\frac{\partial^2\mu}{\partial y^2}\delta u_x-\frac{\partial}{\partial y}\left(\frac{\partial\mu}{\partial y}\delta u_x\right).\end{aligned}\tag{5.182}$$

The internal work increment in the whole layer (for a unit width) is the negative of the integral with respect to y from zero to h of the energy density:

$$\delta W^i=\int_0^h\left(\frac{\partial\tau}{\partial y}-\frac{\partial^2\mu}{\partial y^2}\right)\delta u_x\,dy-\left[\left(\tau-\frac{\partial\mu}{\partial y}\right)\delta u_x+\mu\frac{\partial(\delta u_x)}{\partial y}\right]_0^h.\tag{5.183}$$

This expression motivates the expression for the increment of work of external forces (body forces are neglected here) as

$$\delta W^e=t_0\,\delta u_x(0)+t_h\,\delta u_x(h)+T_0\left.\frac{\partial(\delta u_x)}{\partial y}\right|_0+T_h\left.\frac{\partial(\delta u_x)}{\partial y}\right|_h,\tag{5.184}$$

where t is the (classic) surface force per unit area and T is the surface double force per unit area. The presence of a nonzero double force at the surface introduces boundary effects.

Equilibrium Equations

The equilibrium equations can be deduced from the requirement that the sum of the increments of internal and external work inside the layer is zero. A more complete demonstration should use the theorem of virtual work (Germain, 1973). Inside the layer, the following equation must be satisfied at each point:

$$\frac{\partial\tau}{\partial y}-\frac{\partial^2\mu}{\partial y^2}=0\tag{5.185}$$

and at the bottom and top boundaries of the layer, respectively,

$$\begin{aligned}\tau-\frac{\partial\mu}{\partial y}&=-t_0 \qquad & \mu&=-T_0\\ \tau-\frac{\partial\mu}{\partial y}&=t_h & \mu&=T_h.\end{aligned}\tag{5.186}$$

The first term of the equilibrium equation (5.185) is identical to the classic models; the additional term is the gradient of the double stress. In addition, there is a condition on the double stress that must be satisfied at the boundaries.

Constitutive Relations

The relation between classic terms, stress, and strain can be expressed with usual constitutive laws. The physical meaning of the relation concerning the additional terms is probably not yet clear and needs further investigation. We assume a simple incremental law that neglects links between stress and the second gradient and between the double stress and strain. We adopt the bilinear relation between the increments of shear stress and shear strain used in Section 5.8.1 and a linear relation between the increments of double stress and the second gradient, identically to the choice of Chambon et al. (1998). Such a relation can be formulated in an extended elasto-plastic framework with two independent potentials, one that depends on the stress and a second that depends on the double stress (in the present case the double stress is always in its elastic domains):

$$\begin{aligned} d\tau &= G\, d\gamma \quad \text{if} \quad d\gamma < 0 \\ d\tau &= H_{\tan}\, d\gamma \quad \text{if} \quad d\gamma > 0 \\ d\mu &= A\, d\chi. \end{aligned} \tag{5.187}$$

The modulus A describes the influence of the strain gradient on the material response via the double stress; it is expected to be positive. Although, in general, this modulus may evolve with the state of the material, for simplicity and due to lack of information, we take it to be constant. Similarly, the shear modulus G, assumed here to be constant, could decrease with plastic loading due to material degradation.

Solutions in the Layer

The formulation just described is used to determine the response of a layer with an embedded localization band. In this solution, the material is loading plastically inside the band and unloading elastically outside. Four interfaces need to be introduced: the bottom of the layer $y = 0$, the bottom and the top of the band $y = b$ and $y = b+t$, respectively, and the top of the layer $y = h$. To neglect boundary effects, the double stress at the layer boundaries is assumed to be zero and its continuity is required at each side of the two boundaries of the band. Moreover, at the borders of the band, where an elastic zone meets a plastic zone, the strain rate vanishes. Note that the layer solution without a band (i.e., layer plastically or elastically deformed everywhere) is the homogeneous solution (the strain rate is constant over the band). Integrating equation (5.185) and using equation (5.186) leads to the requirement that the following incremental equations should be satisfied everywhere in the layer:

$$d\tau - \frac{\partial(d\mu)}{\partial y} = dt_h = -dt_0. \tag{5.188}$$

Using equation (5.187) in equation (5.188) gives

$$K\frac{\partial(du_x)}{\partial y} - A\frac{\partial^3(du_x)}{\partial y^3} = dt_h, \tag{5.189}$$

where $K = G$ outside the band and $K = H_{\tan}$ inside. For incipient localization, the initial field is homogeneous and then so is $H_{\tan}$. Then equation (5.189) can be written

$$K\,du_x - A\frac{\partial^2(du_x)}{\partial y^2} = dt_h\,y + K\,c. \tag{5.190}$$

A solution of equation (5.190) can be found with the form $du_x = du\,e^{\lambda y}$. If $H_{\tan} < 0$, then the solution inside the band can be written

$$du_x = a^b \sin(\omega y) + b^b \cos(\omega y) + dt_h/H_{\tan}\,y + c^b, \tag{5.191}$$

with $\omega = (-H_{\tan}/A)^{1/2}$, and outside the band

$$du_x = a^o \sinh(\lambda y) + b^o \cosh(\lambda y) + dt_h/G\,y + c^o, \tag{5.192}$$

with $\lambda = (G/A)^{1/2}$. The parameters a, b, and c are determined by the boundary conditions; the two last terms of equations (5.191) and (5.192) represent the solution for a classic model (see Section 5.8.1), whereas the two terms in sines and cosines regularize the solution (no discontinuity of the first and second displacement gradients). This solution shows that a band can exist only if $H_{\tan} < 0$, which corresponds to the onset of localization for the classic model. Moreover, the thickness of the band is determined by the constitutive moduli of the law and depends on the layer thickness (Chambon et al., 1998). Nevertheless, the band thickness tends rapidly toward the intrinsic value

$$t = 2\sqrt{-\frac{A}{H_{\tan}}}\left[\pi - \operatorname{atan}\left(\sqrt{-\frac{H_{\tan}}{G}}\right)\right] \tag{5.193}$$

when the layer thickness is not too small in comparison (i.e., greater than about 1.5 times band thickness). The position of the band is determined by the boundary conditions and is centered in the layer. A displacement field is plotted in Figure 5.32. The number of bands (assumed to be one here) is, however, not imposed and solutions with more than one band are possible. Thus, uniqueness of the solution does not exist after the localization.

As far as the band thickness is concerned, it has to be smaller than the layer thickness. If the moduli $H_{\tan}$ or A are too high, then this condition cannot be satisfied and localization is not possible. For example, if the evolution of the tangent modulus is continuous at the stress peak, the predicted thickness of the band just after the stress peak is infinite, which is unrealistic. Localization will be possible

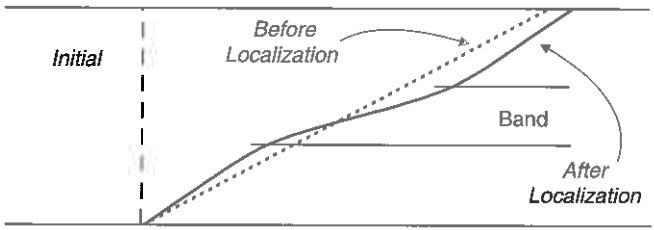

Figure 5.32 ▶ Displacement field u_x plotted for three steps of the layer loading, with a second-gradient model.

during the subsequent loading of the layer if the tangent modulus decreases. The onset of localization with the second-gradient model is predicted to occur after that of the classic model and depends on the size of the layer.

5.8.3 A Model With Nonlocal Effects

Nonlocal models represent another strategy for obtaining a band thickness. In such models, the constitutive relation at a point inside the solid is influenced not only by the material state at this point, as expressed, for example, by the plastic strain, but also by the state in a finite neighborhood of the point (an averaged plastic strain). The size of the zone of averaging introduces an internal length. Most nonlocal elasto-plastic models are a perturbation of classic models. Terms describing the material degradation are defined with a nonlocal relation while the classic expression of the yield surface (see also equation [5.81]) is retained:

$$F(\sigma_{ij}, q) = 0, \tag{5.194}$$

where q is a state variable that tracks the history of the deformation. In the classic model, q is generally a function of the local plastic strain γ^p; in nonlocal models q becomes a function of the nonlocal plastic strain $\bar{\gamma}^p$. For example, Bažant et al. (1987) and Bažant and Lin (1988) have proposed the expression

$$q = q(\bar{\gamma}^p) \quad \text{with} \quad \bar{\gamma}^p(x) = \frac{1}{V_r}\int_V \alpha(s-x)\,\gamma^p(s)\,dV, \tag{5.195}$$

where α is a weighting function and V_r is defined by

$$V_r = \int_V \alpha(s-x)\,dV. \tag{5.196}$$

A bell function around the current point is generally adopted for α and the shape of the function determines the internal length of the model. A similar approach was previously adopted for damage models (e.g., Bažant and Pijaudier-Cabot, 1988), for which the term of stiffness degradation is defined by a nonlocal relation. In such

cases, the classic equilibrium equations are conserved but the boundary conditions can be difficult to formulate.

In other nonlocal elasto -plastic models, Vardoulakis and Aifantis (1991) and de Borst and Mühlhaus (1992) have expressed q as a function of the local plastic strain and its Laplacian:

$$q = q(\gamma^p, \nabla^2\gamma^p) = q(\gamma^p + l^2\nabla^2\gamma^p). \tag{5.197}$$

Such a choice, in which l is a characteristic length, represents an approximation (by Taylor series) of expression (5.195) for the averaged plastic strain (Bažant et al., 1987; Vardoulakis and Aifantis, 1991). Schreyer (1990) has taken q to be a function of the plastic strain and its gradient and a parameter k that also has a length dimension:

$$q = q\left(\gamma^p + \left[k\,\nabla\gamma^p\right)\right]^2\Big). \tag{5.198}$$

Solutions in the Layer

Using equation (5.197) to analyze the layer problem, the constitutive relation can be expressed, via the consistency condition on the yield limit (Vardoulakis and Aifantis, 1991; de Borst and Mühlhaus, 1992), by

$$\begin{aligned} &\text{for elastic unloading} \quad d\tau = G\,d\gamma = G\,d\gamma^e \\ &\text{for plastic loading} \quad d\tau = H\,d\gamma^p - c\,\frac{\partial^2\,(d\gamma^p)}{\partial y^2}, \end{aligned} \tag{5.199}$$

where G is an elastic modulus and H and c are plastic moduli that can depend on the plastic strain and its Laplacian. Note that, unlike the classic models, the second relation corresponds to a constitutive relation that is a differential equation in terms of increments of stress and total strain.

To solve the layer problem, we assume that the material behavior outside the band is elastic (the first relation in equation [5.199]) and it is plastic inside the band (the second relation in equation [5.199]). At the interfaces of the band, equilibrium must be satisfied and the strain field must be continuous:

$$d\tau^o = d\tau^b \quad \text{and} \quad d\gamma^b = 0. \tag{5.200}$$

Inside and outside the band, the equilibrium equation must be satisfied:

$$\frac{\partial\,(d\tau)}{\partial y} = 0. \tag{5.201}$$

Outside the band, the strain is constant. Inside the band, the solution has the form of sines or cosines only if $H < 0$, which corresponds to the bifurcation condition

of a classical elasto-plastic model. In such a case, the strain increment inside the incipient band can be expressed as

$$d\gamma = a^b \cos(\omega y) + b^b \sin(\omega y) + d\tau \left(\frac{1}{G} + \frac{1}{H} \right), \tag{5.202}$$

with $\omega = \sqrt{-H/c}$.

The parameters a^b and b^b are determined by the continuity condition of the strain at the two interfaces of the band. The thickness of the band is determined by the supplementary condition of no plastic flow at the interfaces, introduced by Vardoulakis and Aifantis (1991):

$$\frac{\partial (d\gamma^p)}{\partial y} = 0. \tag{5.203}$$

This results in a band thickness of

$$t = 2\pi \sqrt{\frac{-c}{H}}. \tag{5.204}$$

Comparison of the Two Enriched Models

The displacement field of the solution for the nonlocal model is close to the solution for the model with microstructure presented in Section 5.8.2. For both, the displacement field is harmonic inside the band, but for the nonlocal model the thickness of the band does not depend on the elastic modulus. A major difference between the two solutions is that the field is not necessarily homogeneous in the elastic patches with the model with microstructure because of the condition on the double stress at the interfaces of the band. Figure 5.33 illustrates the two solutions for the same band thickness, which means the same thickness of the zone of plastic softening. It is interesting that the band thickness does not appear to be the same for the two solutions shown in Figure 5.33, and superficial observation of the displacement field could result in overestimating the band thickness for the solution of the model with microstructure. This poses an interesting problem for practical determination of the band thickness in situ or inside a specimen.

For models with microstructure and nonlocal models, the first possible onset of a localization band corresponds to the bifurcation onset with a classic model. However, the thickness of the band at this onset is infinite (e.g., Vardoulakis and Aifantis, 1991; Chambon et al., 2001), at least if one adopts a law with a continuous evolution of tangent modulus, and decreases after this onset. Consequently, the enriched models suggest that the onset of localization could be delayed by the size effect.

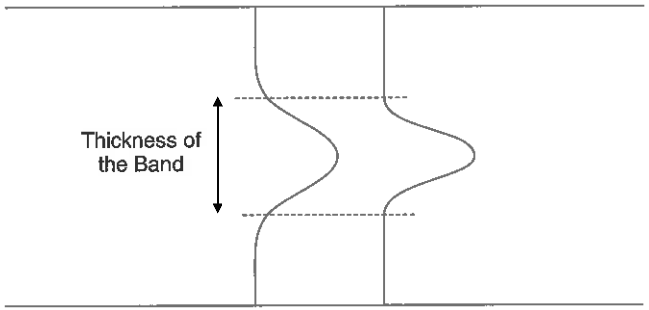

Figure 5.33 ▶ Shear strain field after localization in the layer for a local second-gradient model (left) and a nonlocal second-gradient model (right). The constitutive parameters are chosen to predict an identical band thickness. The elastic response outside the band with the nonlocal model is homogeneous, whereas it is nonhomogeneous for the local model because of the existence of a nonvanishing double stress at the interfaces of the band.

Bibliography

Albert, R.A., and Rudnicki, J.W. Non-uniformity of stress and deformation in axisymmetric finite element models of Tennessee marble. In *Pacific Rocks 2000*, J. Girard, M. Liebman, C. Breeds, and T. Doe, eds., pp. 999–1006. Balkema, Rotterdam, 2000. Proc. Fourth North Am. Rock Mech. Symp. NARMS 2000, Seattle, Washington, 31 July–3 August 2000.

Arthur, J.R.F., and Dunstan, T. Rupture layers in granular media. In *IUTAM Conf. on Deformation and Failure in Granular Materials*, Vermeer, P.A., and Luger, H.J., eds., pp. 453–459. Delft. Balkema, Rotterdam, 1982.

Arthur, J.R.F., Dunstan, T., Al-Ani, Q.A.J.L., and Assadi, A. Plastic deformation and failure in granular media. *Géotechnique* 27(1): 53–74, 1977.

Aydin, A., and Johnson, A.M. Analysis of faulting in porous sandstones. *J. Struct. Geol.* 5: 10–31, 1983.

Bardet, J.P. A comprehensive review of strain localization in elastoplastic soils. *Comput. Geotech.* 10(1): 163–188, 1990.

Batdorf, S.B., and Budiansky, B. A mathematical theory of plasticity based on the concept of slip. Technical Note 1971, N. A. C. A., 1949.

Batdorf, S.B., and Budiansky, B. Polyaxial stress strain relations of a strain-hardening metal. *J. Appl. Mech.* 21: 323–326, 1954. Transactions of ASME, vol 76.

Baud, P., Schubnel, A., and Wong, T.-f. Dilatancy, compaction and failure mode in Solnhofen limestone. *J. Geophys. Res.* 105: 19289–19303, 2000.

Bažant, Z., and Lin, F.-B. Non-local yield limit degradation. *Int. J. Numer. Meth. Engng.* 26(8): 1805–1823, 1988.

Bažant, Z., Lin, F.-B., and Pijaudier-Cabot, G. Yield limit degradation: Nonlocal continuum model with local strain. In *Computational Plasticity. Models, Software and Applications*, D.R. Owen, E. Hinton, and E. Oñate, eds., pp. 1757–1780. Pineridge Press, Swansea, 1987.

Bažant, Z., and Pijaudier-Cabot, G. Nonlocal continuum damage, localization instability and convergence. *J. Appl. Mech.* 55(2): 287–293, 1988.

Benallal, A., and Comi, C. Localization analysis via a geometrical method. *Int. J. Solids Struct.* 33(1): 99, 1996.

Benallal, A., and Comi, C. Material instabilities in inelastic saturated porous media under dynamic loadings. *Int. J. Solids Struct.* 39(13–14): 3693–3716, 2002.

Bésuelle, P. Compacting and dilating shear bands in porous rock: Theoretical and experimental conditions. *J. Geophys. Res.* 106(B7): 13435–13442, 2001a.

Bésuelle, P. Evolution of strain localization with stress in a sandstone: Brittle and semi-brittle regimes. *Phys. Chem. Earth, Part A* 26(1-2): 101–106, 2001b.

Bésuelle, P., Desrues, J., and Raynaud, S. Experimental characterisation of the localization phenomenon inside a Vosges sandstone in a triaxial cell. *Int. J. Rock Mech. Min. Sci.* 37(8): 1223–1237, 2000.

Bigoni, D., and Hueckel, T. Uniqueness and localization—I. Associative and non-associative elastoplasticity. *Int. J. Solids Struct.* 28(2): 197–213, 1991.

Bigoni, D., and Loret, B. Effects of elastic anisotropy on strain localization and flutter instability in plastic solids. *J. Mech. Phys. Solids* 47: 1409–1436, 1999.

Biot, M.A. *Mechanics of Incremental Deformations*. John Wiley, New York, 1965.

Borre, G., and Maier, G. On linear versus non linear flow rules in strain localization **analysis**. *Meccanica* 24: 36–41, 1989.

Brace, W.F. Brittle fracture of rocks. In *State of Stress in the Earth's Crust*, W.R. Judd, ed., pp. 111–174. Elsevier, Amsterdam, 1964.

Budiansky, B. A reassessment of deformation theories of plasticity. *J. Appl. Mech.* pp. 259–264, 1959.

Chambon, R. Bifurcation par localization en bande de cisaillement, une approche avec des lois incrémentalement non linéaires. *J. Méc. Théor. Appl.* 5(2): 277–298, 1986.

Chambon, R. Bases théoriques d'une loi de comportement incrémentale consistante pour les sols. *Groupe C.O.S.M., Rapport de Recherche*, 1989.

Chambon, R., and Caillerie, D. Existence and uniqueness theorems for boundary value problems involving incrementally non linear models. *Int. J. Solids Struct.* 36: 5089–5099, 1999.

Chambon, R., Caillerie, D., and El Hassan, N. One-dimensional localisation studied with second grade model. *Eur. J. Mech. A/Solids* 17(47): 637–656, 1998.

Chambon, R., Caillerie, D., and Matsushima, T. Plastic continuum with microstructure, local second gradient theories for geomaterials: localization studies. *Int. J. Solids Struct.* 38 (46–47): 8503–8527, 2001.

Chambon, R., Crochepeyre, S., and Desrues, J. Localization criteria for non-linear constitutive equations of geomaterials. *Mech. Cohesive-Frictional Mater.* 5: 61–82, 2000.

Chambon, R., Desrues, J., and Tillard, D. Shear modulus identification versus experimental localization data. In *Localisation and Bifurcation Theory for Soils and Rocks*, R. Chambon, J. Desrues, and I. Vardoulakis, eds., pp. 101–111. Balkema, Rotterdam, 1994.

Chau, K.T., and Rudnicki, J.W. Bifurcations of compressible pressure-sensitive materials in plane strain tension and compression. *J. Mech. Phys. Solids* 38: 875–898, 1990.

Chester, F.M., Evans, J.P., and Biegel, R.L. Internal structure and weakening mechanisms of the San Andreas fault. *J. Geophys. Res.* 98: 771–786, 1993.

Christoffersen, J., and Hutchinson, J.W. A class of phenomenological corner theories of plasticity. *J. Mech. Phys. Solids* 27(5/6): 465–487, 1979.

Cleary, M.P. Elastic and dynamic response regimes of fluid-impregnated solids with diverse microstructures. *Int. J. Solids Struct.* 14: 795–819, 1978.

Cleary, M.P., and Rudnicki, J.W. Initiation and propagation of dilatant rupture zones in geological materials. In *The Effects of Voids on Material Deformation*, S.C. Cowin, ed., vol. 16, pp. 13–30. ASME Appl. Mech. Div., 1976. Proc. Symp. Effects of Voids on Material Deformation, Salt Lake City, Utah, 14 June 1976.

Colliat-Dangus, J.L. *Comportement des Matériaux Granulaires sous Fortes Contraintes. Influence de la Nature Minéralogique du Matériau Etudié.* Ph.D. diss. University of Grenoble, France, 1986.

Cosserat, E., and Coserat, F. *Théorie des Corps Déformables.* Hermann, Paris, 1909.

Costin, L.S. A microcrack damage model for brittle rock. Technical Report SAND83-1590, Sandia National Laboratories, Albuquerque, New Mexico, 1983a.

Costin, L.S. A microcrack model for the deformation and failure of brittle rock. *J. Geophys. Res.* 88: 9485–9492, 1983b.

Costin, L.S. Damage mechanics in the post failure regime. *Mech. Mat.* 4: 149–160, 1985.

Coussy, O. *Mechanics of Porous Continua.* Wiley, New York, 1995.

Crouch, S.L. Experimental determination of volumetric strains in failed rock. *Int. J. Rock Mech. Min. Sci.* 7: 589–603, 1970.

Darve, F., and Labanieh, S. Incremental constitutive law for sands and clays. Simulation of monotonic and cyclic tests. *Int. J. Numer. Anal. Meth. Geomech.* 6: 243–275, 1982.

De Borst, R., and Mühlhaus, H.-B. Gradient-dependent plasticity: Formulation and algorithmic aspects. *Int. J. Numer. Meth. Engng.* 35: 521–539, 1992.

Desrues, J. *La Localization de la Déformation dans les Matériaux Granulaires*. Ph.D. diss University of Grenoble, France, 1984.

Desrues, J. Localization patterns in ductile and brittle geomaterials. In *Material Instabilities in Solids*, R. de Borst and E. van der Giessen, eds., pp. 137–158. Wiley, New York, 1998.

Desrues, J., and Chambon, R. Shear bands analysis and shear moduli calibration. *Int. J. Solids Struct.* 39: 3757–3776, 2002.

Desrues, J., Chambon, R., Mokni, M., and Mazerolle, F. Void ratio evolution inside shear bands in triaxial sand specimens studied by computed tomography. *Géotechnique* 46(3): 529–546, 1996.

Dieterich, J.H. Modeling of rock friction, 1, experimental results and constitutive equations. *J. Geophys. Res.* 84: 2161–2168, 1979a.

Dieterich, J.H. Modeling of rock friction, 2, simulation of preseismic slip. *J. Geophys. Res.*, 84: 2169–2175, 1979b.

DiGiovanni, A.A., Fredrich, J.T., Holcomb, D.J., and Olsson, W.A. Micromechanics of compaction in an analogue reservoir sandstone. In *Pacific Rocks 2000, Proceed. Fourth North Am. Rock Mech. Symp.*, J. Girard, M. Liebman, C. Breeds, and T. Doe, eds., pp. 1153–1158. Balkema, Rotterdam, 2000.

DiMaggio, F.L., and Sandler, I.S. Material model for granular soils. *ASCE: J. Engng. Mech. Div.* 97: 935–950, 1971.

Drescher, A., and Vardoulakis, I. Geometric softening in triaxial tests on granular material. *Géotechnique* 32(4): 291–303, 1982.

Drucker, D.C., and Prager, W. Soil mechanics and plasticity analysis or limit design. *Quart. Appl. Math.* 10(2): 157–165, 1952.

Finno, R.J., Harris, W.W., Mooney, M.A., and Viggiani, G. Shear bands in plane strain compression of loose sand. *Géotechnique* 47(1): 149–165, 1997.

Fleck, N.A., and Hutchinson, J.W. Strain gradient plasticity. *Advances Appl. Mech.* 33: 295–361, 1997.

Frantziskonis, G., and Vardoulakis, I. On the micro-structure of the surface effects and related instabilities. *Eur. J. Mech. A/Solids* 11(1): 21–34, 1992.

Fredrich, J.T., Evans, B., and Wong, T.-f. Micromechanics of the brittle to plastic transition in Carrara marble. *J. Geophys. Res.* 94(B4): 4129–4145, 1989.

Garagash, D., and Rudnicki, J.W. Stability of undrained deformation of fluid-saturated dilating/compacting solids (abstract). In *Dwentieth Int. Cong. Theor. Appl. Mech.* Chicago, IL, Aug. 27–Sept. 2 2000.

Germain, P. La méthode des puissances virtuelles en mécanique des milieux continus, première partie: Théorie du second gradient. *J. Méc.* 12(2): 235–274, 1973.

Hadamard, J. *Leçons sur la Propagation des Ondes et les Equations de l'Hydrodynamique*. Hermann, Paris, 1903.

Haimson, B., and Chang, C. A new true triaxial cell for testing mechanical properties of rock, and its use to determine rock strength and deformability of Westerly granite. *Int. J. Rock Mech. Min. Sci.* 37(1-2): 285–296, 2000.

Hammad, W.I. *Modélisation Non Linéaire et Etude Expérimentale des Bandes de Cisaillement dans les Sables*. Ph.D. diss. University of Grenoble, France, 1991.

Han, C., and Vardoulakis, I.G. Plane strain compression experiments on water-saturated fine-grained sand. *Géotechnique* 41: 49–78, 1991.

Hecker, S. S. Experimental studies of yield phenomena in biaxially loaded metals. In *Constitutive Equations in Viscoplasticity: Computational and Engineering Aspects*, J.A. Stricklin and K.J. Saczulski, eds., pp. 1–33. ASME, New York, 1976. Appl. Mech. Div. Vol. 20.

Hill, R. *The Mathematical Theory of Plasticity*. Oxford Engineering Science Series. Oxford, London, 1950.

Hill, R. A general theory of uniqueness and stability in elastic-plastic solids. *J. Mech. Phys. Solids* 6: 236–249, 1958.

Hill, R. Some basic principles in the mechanics of solids without a natural time. *J. Mech. Phys. Solids* 7: 209–225, 1959.

Hill, R. Bifurcation and uniqueness in non-linear mechanics of continua. In J.R.M. Radok, ed., *Problems of Continuum Mechanics*, pp. 155–164. Society Indust. Appl. Math., Philadelphia, 1961a.

Hill, R. Discontinuity relations in mechanics of solids. In I.N. Sneddon and R. Hill, eds., *Progress in Solid Mechanics*, pp. 245–276. North-Holland, Amsterdam, 1961b.

Hill, R. Uniqueness in general boundary-value problems for elastic or inelastic solids. *J. Mech. Phys. Solids* 9: 114–130, 1961c.

Hill, R. Acceleration waves in solids. *J. Mech. Phys. Solids* 10: 1–16, 1962.

Hill, R. The essential structure of constitutive laws for metal composites and polycrystals. *J. Mech. Phys. Solids* 15: 79–95, 1967.

Hill, R., and Hutchinson, J.W. Bifurcation phenomena in the plane tension test. *J. Mech. Phys. Solids*, 23: 239–264, 1975.

Holcomb, D.J., and Rudnicki, J.W. Inelastic constitutive properties and shear localization in Tennessee marble. *Int. J. Numer. Anal. Meth. Geomech.* 25: 109–129, 2001.

Hubbert, M.K., and Rubey, W.W. Role of fluid pressure in the mechanics of overthrust faulting I: Mechanics of fluid-filled porous solids and its application to overthrust faulting. *Geolog. Soc. Am. Bull.* 70: 115–166, 1959.

Hueckel, T., and Maier, G. Incremental boundary value problems in the presence of coupling of elastic and plastic deformations: a rock mechanics oriented theory. *Int. J. Solids Struct.* 13: 1–15, 1977.

Hutchinson, J.W. Elastic-plastic behavior of polycrystalline metals and composites. *Proc. Royal Soc. London A* 319: 247–272, 1970.

Hutchinson, J.W., and Neale, K.W. Sheet necking—II. time-independent behavior. In *Mechanics of Sheet Metal Forming*, D.P. Koistinen and N.-M. Wang, eds., pp. 127–150. Plenum Publishing Corporation, 1978.

Hutchinson, J.W., and Neale, K.W. Finite strain J2 deformation theory. In D.E. Carlson and R.T. Shield, eds., *Proc. IUTAM Symp. Finite Elasticity*, pp. 237–247. Martinus Nijhoff Publishers, 1981.

Issen, K.A. The influence of constitutive models on localization conditions for porous rock. *Engng. Fract. Mech.*, 69(17): 1891–1906, 2002.

Issen, K.A., and Rudnicki, J.W. Conditions for compaction bands in porous rock. *J. Geophys. Res.* 105(B9): 21529–21536, 2000.

Issen, K.A., and Rudnicki, J.W. Theory of compaction bands in porous rock. *Phys. Chem. Earth, Part A* 26(1–2): 95–100, 2001.

Jaeger, J. C., and Cook, N.G.W. *Fundamentals of Rock Mechanics*, 2nd ed. John Wiley, New York, 1969.

Koiter, W.T. Stress-strain relations, uniqueness and variational theorems for elastic-plastic materials with a singular yield surface. *Quart. Appl. Math.* 11: 350–353, 1953.

Kolymbas, D. An outline of hypoplasticity. *Arch. Appl. Mech.* 61: 143–151, 1991.

Labuz, J.F., Dai, S.-T., and Papamichos, E. Plane-strain compression of rock-like materials. *Int. J. Rock Mech. Min. Sci.* 33(6): 573–584, 1996.

Lade, P.V. Elasto-plastic stress-strain theory for cohesionless soil with curved yield surface. *Int. J. Solids Struct.* 13: 1019–1035, 1977.

Lade, P.V., and Duncan, J.M. Elasto-plastic stress-strain theory for cohesionless soil. *ASCE: J. Geotech. Engng. Div.* 101(GT10): 1037–1053, 1975.

Larsson, R., and Axelsson, K. A slip line model based on plastic localization and discontinuous approximation. In *Numerical Methods in Geotechnical Engineering*, I.M. Smith, ed., Balkema, Rotterdam, 1994.

Leroy, Y.M., and Triantafyllidis, N. Stability of a frictional, cohesive layer on a viscous substratum: Variational formulation and asymptotic solution. *J. Geophys. Res.* 101: 17, 795–817, 811, 1996.

Lockner, D.A., Byerlee, J.D., Kuksenko, V., Ponomarev, A., and Sidorin, A. Observations of quasistatic fault growth from acoustic emissions. In *Fault Mechanics and Transport Properties of Rocks*, B. Evans and T.-f. Wong, eds., pp. 3–31. Academic Press, San Diego, CA, 1992.

Lockner, D.A., and Madden, T.R. A multiple-crack model of brittle fracture 1. non-time-dependent simulations. *J. Geophys. Res.* 96(B12): 19623–19642, 1991a.

Lockner, D.A., and Madden, T.R. A multiple-crack model of brittle fracture 2. time-dependent simlulations. *J. Geophys. Res.* 96(B12): 19643–19654, 1991b.

Logan, J.M., Dengo, C.A., Higgs, N.G., and Wang, Z.Z. Fabrics of experimental fault zones: Their development and relationship to mechanical behavior. In *Fault Mechanics and Transport Properties in Rocks.*, B. Evans and T.-f. Wong, eds., pp. 33–67. Academic Press, New York, 1992.

Loret, B., and Prevost, J.H. Dynamic strain localization in elasto- (visco-) plastic solids, Part 1. General formulation and one dimensional examples. *Comput. Meth. Appl. Mech. Engng* 83: 247–273, 1990.

Lubliner, J. *Plasticity Theory*. Macmillan, New York, 1990.

Mandel, J. Généralisation de la théorie de plasticité de W.T. Koiter. *Int. J. Solids Struct.* 1: 273–295, 1965.

Mandel, J. Conditions de stabilité et postulat de Drucker. In *Rheology and Soil Mechanics*, J. Kravtchenko and P.M. Sirieys, eds., pp. 58–68. Springer, Berlin, 1966a.

Mandel, J. *Cours de Mécanique des Milieux Continus*. Gauthier-Villars, Paris, 1966b.

Mandl, G. *Faulting in Brittle Rocks*. Elsevier, 1988.

Mandl, G., de Jong, L.N.J., and Maltha, A. Shear zones in granular material. *Rock Mech.* 9: 95–144, 1977.

Marciniak, Z., and Kuczynski, K. Limit strains in the processes of stretch-forming sheet metal. *Int. J. Mech. Sci.* 9: 609–620, 1967.

Marone, C., Raleigh, C.B., and Scholz, C.H. Frictional behavior and constitutive modeling of simulated fault gouge. *J. Geophys. Res.* 95: 7007–7025, 1990.

Martin, R.J., III. Pore pressure stabilization of failure in Westerly granite. *Geoph. Res. Lett.* 7: 404–406, 1980.

Matsuoka, H., and Nakai, T. A new failure criterion for soils in three-dimensional stresses. In *IUTAM Conf. on Deformation and Failure in Granular Materials*, P.A. Vermeer and H.J. Luger, eds., pp. 253–263. Delft, Balkema, Rotterdam, 1982.

McGarr, A., Spottiswoode, S.M., Gay, N.C., and Ortlepp, W.D. Observations relevant to seismic driving stress, stress drop, and efficiency. *J. Geophys. Res.* 84(B5): 2251–2261, 1979.

Mehrabadi, M.M., and Cowin, S.C. Initial planar deformation of dilatant granular materials. *J. Mech. Phys. Solids* 26: 269–284, 1978.

Menéndez, B., Zhu, W., and Wong, T.-f. Micromechanics of brittle faulting and cataclastic flow in Berea sandstone. *J. Struct. Geol.* 18(1): 1–16, 1996.

Mindlin, R.D. Micro-structure in linear elasticity. *Arch. Rat. Mech. Anal.* 4: 50–78, 1964.

Mogi, K. Effect of the intermediate principal stress on rock failure. *J. Geophys. Res.* 72: 5117–5131, 1967.

Mogi, K. Effect of the triaxial stress system on the failure of dolomite and limstone. *Tectonophysics* 11: 111–127, 1971.

Mokni, M. *Relation entre Déformations en Masse et Déformations Localisées dans les Matériaux Granulaires.* Ph.D. diss. University of Grenoble, France, 1992.

Mokni, M., and Desrues, J. Shear localization measurements in undrained plane-strain biaxial tests on Hostun RF sand. *Mech. Cohesive-Frictional Mater.* 4: 419–441, 1999.

Molenkamp, F. Comparison of frictional material models with respect to shear band initiation. *Géotechnique* 35: 127–143, 1985.

Mròz, Z. Non-associated flow laws in plasticity. *J. Méc.* 2: 21–42, 1963.

Mühlhaus, H.-B., and Vardoulakis, I. The thickness of shear band in granular materials. *Géotechnique* 37(3): 271–283, 1987.

Needleman, A. Non-normality and bifurcation in plane strain tension and compression. *J. Mech. Phys. Solids* 27: 231–254, 1979.

Needleman, A. Material rate dependence and mesh sensitivity in localization problems. *Comput. Meth. Appl. Mech. Engng* 67: 69–87, 1987.

Nemat-Nasser, S., and Okada, N. Radiographic and microscopic observation of shear bands in granular materials. *Géotechnique* 51(9): 753–765, 2001.

Nguyen, Q.S., and Bui, H.D. Sur les matériaux élastoplastiques à écrouissage positif ou négatif. *J. Méc.* 13(2): 321–342, 1974.

Nur, A., and Byerlee, J.D. An exact effective stress law for elastic deformation of rock with fluids. *J. Geophys. Res.* 76: 6414–6419, 1971.

Nur, A., and Walder, J. Time-dependent hydraulics of the earth's crust. In *The Role of Fluids in Crustal Processes*, pp. 113–127. National Academy Press, Washington, D.C., 1990.

Olsson, W.A. The formation of a yield-surface vertex in rock. In *Proc. 33rd U.S. Symp. Rock Mech.*, J. R. Tillerson and W.R. Wawersik, eds., pp. 701–705. Balkema, Rotterdam, 1992.

Olsson, W.A. Development of anisotropy in the incremental shear moduli for rock undergoing inelastic deformation. *Mech. Mat.* 21: 231–242, 1995.

Olsson, W.A. Theoretical and experimental investigation of compaction bands in porous rock. *J. Geophys. Res.* 104(B4): 7219–7228, 1999.

Olsson, W.A. Origin of Lüders' bands in deformed rock. *J. Geophys. Res.* 105: 5931–5938, 2000.

Ord, A., Vardoulakis, I., and Kajewski, R. Shear band formation in Gosford sandstone. ***Int. J. Rock Mech. Min. Sci.*** 28(5): 397–409, 1991.

Ottosen, N.S., and Runesson, K. Properties of discontinuous bifurcation solutions in elasto-plasticity. *Int. J. Solids Struct.* 27(4): 401–421, 1991.

Pan, J. Perturbation analysis of shear strain localization in rate sensitive materials. *Int. J. Solids Struct.* 19(2): 153–164, 1983.

Pan, J., and Rice, J.R. Rate sensitivity of plastic flow and implications for yield-surface vertices. *Int. J. Solids Struct.* 19(11): 973–987, 1983.

Paterson, M.S. *Experimental Rock Deformation, The Brittle Field.* Springer, Berlin, 1978.

Perrin, G., and Leblond, J.B. Rudnicki and Rice's analysis of strain localization revisited. *J. Appl. Mech.* 60(4): 842–846, 1993.

Pierce, D., Shih, C.F., and Needleman, A. A tangent modulus method for rate dependent solids. *Comput. Struct.* 5(18): 875–887, 1984.

Pollard, D.D., and Aydin, A. Progress in understanding jointing over the past century. *Geolog. Soc. Am. Bull.* 100: 1181–1204, August 1988.

Prager, W. *Introduction to the Mechanics of Continua.* Ginn and Company, Boston, 1961, reprinted by Dover, 1973.

Raleigh, C.B., Healy, J.H., and Bredehoeft, J.D. An experiment in earthquake control at Rangely, Colorado. *Science* 191: 1230–1237, 1976.

Raniecki, B., and Bruhns, O.T. Bounds to bifurcation stresses in solids with non-associated plastic flow law at finite strain. *J. Mech. Phys. Solids* 29(2): 153–172, 1981.

Reynolds, O. On the dilatancy of media composed of rigid particles in contact, with experimental illustrations. In *Papers on Mechanical and Physical Subjects*, volume 2, pp. 203–216. Cambridge University Press, New York, 1901.

Rice, J.R. On the stability of dilatant hardening for saturated rock masses. *J. Geophys. Res.* 80 (11): 1531–1536, 1975.

Rice, J.R. The localization of plastic deformation. In *Theoretical and Applied Mechanics*, W.T. Koiter, ed., pp. 207–220. North-Holland Pub. Comp., Delft, 1976. Proc Fourteenth Int. Cong. Theor. Appl. Mech.

Rice, J.R. Pore pressure effects in inelastic constitutive formulations for fissured rock masses. In *Advances in Civil Engineering through Engineering Mechanics*, pp. 360–363. Am. Soc. Civil Engineers, New York, 1977.

Rice, J.R. Unpublished notes, 1981.

Rice, J.R. Fault stress states, pore pressure distributions, and the weakness of the San Andreas fault. In *Fault Mechanics and Transport Properties of Rocks*, B. Evans and T.-f. Wong, eds., pp. 475–503. Academic Press, San Diego, CA, 1992.

Rice, J.R., and Cleary, M.P. Some basic stress diffusion solutions for fluid-saturated elastic porous media with compressible constituents. *Rev. Geophys. Space Phys.* 14: 227–241, 1976.

Rice, J.R., and Rudnicki, J.W. A note on some features of the theory of the localization of deformation. *Int. J. Solids Struct.* 16: 597–605, 1980.

Rice, J.R., and Ruina, A. Stability of steady frictional slipping. *J. Appl. Mech.* 50: 343–349 1983.

Roscoe, K.H. The influence of strain in soil mechanics. *Géotechnique* 20(2): 129–170, 1970 The Tenth Rankine Lecture.

Rudnicki, J.W. The effect of stress-induced anisotropy on a model of brittle rock failure as localization of deformation. In *Energy Resources and Excavation Technology*, F.-D. Wang and G.B. Clark, eds., pp. 3B4-1–3B4-8. 1977a. Proc. Eighteenth U.S. Symp. Rock Mech., Keystone, Colorado, 22–24 June 1977.

Rudnicki, J.W. The inception of faulting in a rock mass with a weakened zone. *J. Geophys. Res.* 82: 844–854, 1977b.

Rudnicki, J.W. A formulation for studying coupled deformation—pore fluid diffusion effects on localization of deformation. In *Geomechanics, Proc. Symp. Mech. Rocks, Soils, and Ice*, S. Nemat-Nasser, ed., Vol. 57, pages 35–44. Am. Soc. Mech. Engineers, New York, 1983.

Rudnicki, J.W. A class of elastic-plastic constitutive laws for brittle rock. *J. Rheol.* 28(6): 759–778, 1984a.

Rudnicki, J.W. Effects of dilatant hardening on the development of concentrated shear deformation in fissured rock masses. *J. Geophys. Res.* 89: 9259–9270, 1984b.

Rudnicki, J.W. Effect of pore fluid diffusion on deformation and failure of rock. In *Mechanics of Geomaterials*, Z.P. Bažant, ed., pp. 315–347. IUTAM William Prager Symposium on Mechanics of Geomaterials: Rocks, Concretes, Soils, September 11–15, 1983, Northwestern University Evanston, Illinois, John Wiley, 1985.

Rudnicki, J.W. Diffusive instabilities in dilating and compacting geomaterials. In *Multiscale Fracture and Deformation in Materials and Structures—The James R. Rice Sixtieth Anniversary Volume*, T.-J. Chuang and J.W. Rudnicki, eds., pp. 159–182. Kluwer Academic Publishers, Dordrecht, The Netherlands, 2000.

Rudnicki, J.W. Conditions for compaction and shear bands in a transversely isotropic material. *Int. J. Solids Struct.* 39(13–14): 3471–3756, 2002.

Rudnicki, J.W., Alarcon, M.A., Finno, R.J., Viggiani, G., and Mooney, M.A. Coupled deformation-pore fluid diffusion effects on the development of localized deformation in fault gouge. In *Prediction and Performance in Rock Mechanics and Rock Engineering*, G. Barla, ed., pp. 1261–1268. Balkema, Rotterdam, 1996. Proc. ISRM Int. Symp. Prediction and Performance in Rock Mech. Rock Engng., EUROCK'96, September 2–5, 1996, Torino, Italy.

Rudnicki, J.W., and Chau, K.T. Multiaxial response of a microcrack constitutive model for brittle rock. In *Tools and Techniques in Rock Mechanics*, M. Aubertin, F. Hassani, and H. Mitri, eds., pp. 1707–1714. Balkema, Rotterdam, 1996. Proc. NARMS'96, 2nd North Am. Rock Mech. Symp., ISRM Regional Conference, June 19–21, 1996.

Rudnicki, J.W., and Chen, C.-H. Stabilization of rapid frictional slip on a weakening fault by dilatant hardening. *J. Geophys. Res.* 93: 4745–4757, 1988.

Rudnicki, J.W., and Olsson, W.A. Reexamination of fault angles predicted by shear localization theory. *Int. J. Rock Mech. Min. Sci.* 35: 512–513, 1998. Extended abstract.

Rudnicki, J.W., and Rice, J.R. Conditions for the localization of deformation in pressure-sensitive dilatant materials. *J. Mech. Phys. Solids* 23: 371–394, 1975.

Ruina, A.L. *Friction Laws and Instabilities: A Quasi-Static Analysis of Some Dry Frictional Behavior*. Ph.D. diss. Div. Engng., Brown University, 1980.

Ruina, A.L Slip instability and state variable friction laws. *J. Geophys. Res.* 88: 10359–10370, 1983.

Rummel, F., and Fairhurst, C. Determination of the post-failure behavior of brittle rock using a servo-controlled testing machine. *Rock Mech.* 2: 189–204, 1970.

Runesson, K., Larsson, R., and Sture, S. Localization in hyperelasto-plastic porous solids subjected to undrained conditions. *Int. J. Solids Struct.* 35: 4239–4255, 1998.

Runesson, K., Peric, D., and Sture, S. Effect of pore fluid compressibility on localization in elastic-plastic porous solids under undrained conditions. *Int. J. Solids Struct.* 35: 4239–4255, 1996.

Santarelli, F.J., and Brown, E.T. Failure of three sedimentary rocks in triaxial and hollow cylinder compression test. *Int. J. Rock Mech. Min. Sci.* 26(5): 401–413, 1989.

Scarpelli, G., and Wood, D.M. Experimental observations of shear band patterns in direct shear tests. In *IUTAM Conf. on Deformation and Failure in Granular Materials*, P.A. Vermeer and H.J. Luger, eds., pp. 493–499. Delft, Balkema, Rotterdam, 1982.

Scholz, C.H. *The Mechanics of Earthquakes and Faulting*. Cambridge University Press, Cambridge, 1990.

Schrefler, B.A., Sanavia, L., and Majorana, C.E. A multiphase medium model for localization and post localization simulation in geomaterials. *Mech. Cohesive-Frictional Mater.* 1: 95–114, 1996.

Schreyer, H.L. Analytical solutions for nonlinear strain-gradient softening and localization. *J. Appl. Mech.* 57(3): 522–528, 1990.

Sewell, M.J. A yield-surface corner lowers the buckling stress of an elastic-plastic plate under compression. *J. Mech. Phys. Solids* 21: 19–45, 1973.

Shanley, F.R. Inelastic column theory. *J. Aeronaut. Sci.* 14(5): 261–267, 1947.

Shawki, T.G., and Clifton, R.J. Shear band formation in thermal viscoplastic materials. *Mech. Mat.* 8(1): 13–43, 1989.

Sokolnikoff, S. *Mathematical Theory of Elasticity*, 2nd ed. McGraw-Hill, 1956.

Spencer, A.J.M. A theory of the kinematics of ideal soils under plane strain condtions. *J. Mech Phys. Solids* 12: 337–351, 1964.

Storen, S., and Rice, J.R. Localized necking in thin sheets. *J. Mech. Phys. Solids* 23: 421–441 1975.

Sulem, J., Vardoulakis, I., Papamichos, E., Oulahna, A., and Tronvall, J. Elasto-plastic modelling of Red Wildmoor sandstone. *Mech. Cohesive-Frictional Mater.* 4(3): 215–245, 1999.

Tamagnini, C., Viggiani, G., and Chambon, R. A review of two different approaches to hypoplasticity. In *Constitutive Modelling of Granular Materials*, D. Kolymbas, ed., pp. 107–145 Springer, Berlin, 2000.

Tapponnier, P., and Brace, W.F. Development of stress-induced microcracks in Westerly granite *Int. J. Rock Mech. Min. Sci.* 13: 103–112, 1976.

Tatsuoka, F., Nakamura, S., Huang, C.-C., and Tani, K. Strength anisotropy and shear band direction in plane strain tests of sand. *Soils Found.* 30(1): 35–54, 1990.

Tatsuoka, F., Sakamoto, M., Kawamura, T., and Fukushima, S. Strength and deformation characteristics of sand in a plane strain compression at extremely low pressure. *Soils Found.* 26(1): 65–84, 1986.

Taylor, G. I. Plastic strain in metals. *J. Inst. Metals* 62: 307–324, 1938a.

Taylor, G.I. Analysis of plastic strain in a cubic crystal. In *Stephen Timoshenko Sixtieth Anniversary Volume*, J.M. Lessels, ed., pp. 218–224. Macmillan, New York, 1938b. Reprinted with added note in The Scientific Papers of Sir Geoffrey Ingram Taylor, Mechanics of Solids, G.K. Batchelor, ed. Vol. I, pp. 439-445. Cambridge University Press, Cambridge, 1958.

Triantafyllidis, N., and Leroy, Y.M. Stability of a frictional material layer resting on a viscous half-space. *J. Mech. Phys. Solids* 42(1): 51–110, 1994.

Triantafyllidis, N., and Leroy, Y.M. Stability of a frictional, cohesive layer on a viscous substratum: Validity of asymptotic solution and influence of material properties. *J. Geophys. Res.* 102(B9): 20551–20570, 1997.

Truesdell, C. Hypo-elasticity. *J. Rat. Mech. Anal.* 4: 83–133, 1955.

Tse, S.T., and Rice, J.R. Crustal earthquake instability in relation to the depth variation of frictional slip properties. *J. Geophys. Res.* 91: 9452–9472, 1986.

Van Eekelen, H.A.M. Isotropic yield surfaces in three dimensions for use in soil mechanics. *Int. J. Numer. Anal. Meth. Geomech.* 4: 89–101, 1980.

Vardoulakis, I. Deformation of water-saturated sand: I uniform undrained deformation and shear banding. *Géotechnique* 46: 441–456, 1996.

Vardoulakis, I., and Aifantis, E.C. A gradient flow theory of plasticity for granular materials. *Acta Mechanica* 387: 197–217, 1991.

Vardoulakis, I., Goldscheider, M., and Gudehus, G. Formation of shear bands in sand bodies as a bifurcation problem. *Int. J. Numer. Anal. Meth. Geomech.* 2: 99–128, 1978.

Vardoulakis, I., and Graf, B. Calibration of constitutive models for granular materials using data from biaxial experiments. *Géotechnique* 35(3): 299–317, 1985.

Vardoulakis, I., and Sulem, J. *Bifurcation Analysis in Geomechanics*. Blackie Academic & Professional, Glasgow, 1995.

Vermeer, P.A. The orientation of shear bands in biaxial tests. *Géotechnique* 40(2): 223–236, 1990.

Viggiani, G., Küntz, M., and Desrues, J. An experimental investigation of the relationships between grain size distribution and shear banding in sand. In *Continuous and Discontinuous Modelling of Cohesive-Frictional Materials*, P.A. Vermeer, S. Diebels, W. Ehlers, H.J. Herrmann, S. Luding, and E. Ramm, eds., pp. 111–127. Springer, Berlin, 2001.

Von Terzaghi, K. The shearing resistance of saturated soils. In *Proc. First Int. Conf. Soils Mech.*, pp. 54–56. Cambridge, Massachusetts, 1936.

Wang, C.C. A new representation theorem for isotropic functions. *Arch. Rat. Mech. Anal.* 36(I-II): 166–223, 1970.

Wawersik, W.R., and Brace, W.F. Post-failure behavior of a granite and diabase. *Rock Mech.* 3: 61–85, 1971.

Wawersik, W.R., and Fairhurst, C. A study of brittle rock fracture in laboratory compression experiments. *Int. J. Rock Mech. Min. Sci.* 7: 561–575, 1970.

Wawersik, W.R., Rudnicki, J.W., Olsson, W.A., Holcomb, D.J., and Chau, K.T. Localization of deformation in brittle rock: Theoretical and laboratory investigations. In *Proc. Int. Conf. Micromechanics of Failure of Quasi-Brittle Materials, Albuquerque, New Mexico*, pp. 115–124. Elsevier, Amsterdam, 1990.

Wong, T.-f. Shear fracture energy of Westerly granite from post-failure behavior. *J. Geophys. Res.* 87(B2): 990–1000, 1982.

Wong, T.-f., and Baud, P. Mechanical compaction of porous sandstone. *Oil Gas Sci. Techn.* 54(6): 715–727, 1999.

Wong, T.-f., and Beigel, R. Effects of pressure on the micromechanics of faulting in San Marcos gabbro. *J. Struct. Geol.* 7(6): 737–749, 1985.

Wu, F.H., and Freund, L.B. Deformation trapping due to thermoplastic instability in one-dimensional wave propagation. *J. Mech. Phys. Solids* 32: 119–132, 1984.

Yoshida, T., and Tatsuoka, F. Deformation property of shear band in sand subjected to plane strain compression and its relation to particle characteristics. In *Proc. 14th ICSMFE*, number 1, pp. 237–240. Hamburg, 1997.